



Aramco
Journal
of Technology

SUMMER 20
23

page 2 /

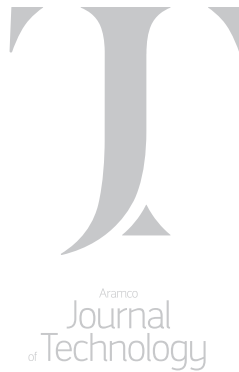
New Navigation Techniques for Untethered Downhole Robots

Dr. Huseyin R. Seren, Dr. Max Deffenbaugh, Mohamed Larbi Zeglache and Dr. Ahmed Y. Bukhamseen

page 54 /

Automatic Placement of Sidetrack Wells during Simulation Run Time

Babatope O. Kayode, Dr. Karl D. Stephen and Dr. Babatunde O. Moriwawon



The *Aramco Journal of Technology* is published quarterly by the Saudi Arabian Oil Company, Dhahran, Saudi Arabia, to provide the company's scientific and engineering communities a forum for the exchange of ideas through the presentation of technical information aimed at advancing knowledge in the hydrocarbon industry.

Management

Amin Nasser

President & CEO, Saudi Aramco

Nabeel A. Al-Jama'

Executive Vice President, HR & Corporate Services

Khalid A. Zamil

Vice President, Public Affairs

Editorial Advisors

Abdul Hameed A. Al-Rushaid

Senior Vice President, Drilling & Workover

Khalid M. Al-Abdulqader

Senior Vice President, Unconventional Resources

Waleed A. Al Mulhim

Senior Vice President, Petroleum Engineering & Development

Jumaan G. Zahrani

Senior Vice President, Northern Area Gas Operations

Ali A. Meshari

Senior Vice President, Technology Oversight and Coordination

Khaled A. Al Abdulgader

Vice President, Southern Area Drilling & Workover Operations

Omar S. Al-Husaini

Vice President, Northern Area Drilling & Workover Operations

Faisal N. Al Nughaimish

Vice President and Chief Petroleum Engineer

Khalid Y. Al-Qahtani

Vice President and Chief Engineer

Gerald M. De Nazelle

Director, Research & Development Center

Ghaithan A. Muntasheri

Director, EXPEC Advanced Research Center

Editor

William E. Bradshaw

william.bradshaw.1@aramco.com.sa

tel: +966-013-876-0498

Production Coordination

Richard E. Doughty

Corporate Publications, Aramco Americas

Design

Graphic Engine Design Studio

Austin, Texas, U.S.A.

No articles, including art and illustrations, in the *Aramco Journal of Technology* except those from copyrighted sources, may be reproduced or printed without the written permission of Saudi Aramco. Please submit requests for permission to reproduce items to the editor.

The *Aramco Journal of Technology* gratefully acknowledges the assistance, contribution and cooperation of numerous operating organizations throughout the company.

ISSN 1319-2388

© Copyright 2023 Aramco Services Company, all rights reserved.

Contents

p. **2** **New Navigation Techniques for Untethered Downhole Robots**

Dr. Huseyin R. Seren, Dr. Max Deffenbaugh, Mohamed Larbi Zeglache and Dr. Ahmed Y. Bukhamseen

p. **10** **Innovative Solid Lubricant Solution to Reduce Friction in Challenging ERD Wells**

Tulio D. Olivares, Zach Turi and Brandon Hayes

p. **17** **Reduced Polymer Loaded Fracturing Fluid for Extreme Temperature Proppant Fracturing**

Prasad B. Karadkar, Ataur R. Malik, Mohammed I. Al-Abdrabalnabi and Dr. Feng Liang

p. **30** **Global First 18.625" and 13.375" Level-2 Casing-while-Drilling Successful Deployment through Open Hole and Cased Hole Sidetracked Wellbores to Isolate Severe Unstable Zones**

Salahaldeen S. Almasmoom, Ahmed S. Refai, Faris A. Al-Qahtani and David B. Stonestreet

p. **46** **New Horizon for Downhole Scale Management toward Sustained Well Production**

Hussain A. Almajid, Ibrahim K. Al-Thwaiqib and Carlos E. Amancio Ribeiro

p. **54** **Automatic Placement of Sidetrack Wells during Simulation Run Time**

Babatope O. Kayode, Dr. Karl D. Stephen and Dr. Babatunde O. Moriwawon

p. **62** **Real-time Bit Wear Prediction and Deployment Validation in Challenging Hard and Heterogeneous Sandstones Using 3D Detailed and Simplified Physics-Based Progressive Wear Models**

Dr. Guodong (David) Zhan, William B. Contreras, Dr. Xu Huang, Reed Spencer and Dr. John Bomidi

p. **71** **Using Isotope Technology to Identify Oil and Gas Reservoir Sweet Spots**

Dr. Feng H. Lu

p. **76** **Thermal Impact on Sandstone's Physical and Mechanical Properties**

Qasim A. Sahu, Ayman R. Al-Nakhli and Dr. Rajendra A. Kalgaonkar

p. **86** **Another Record Year for Patents**

Michael Ives

New Navigation Techniques for Untethered Downhole Robots

Dr. Huseyin R. Seren, Dr. Max Deffenbaugh, Mohamed Larbi Zeghlache and Dr. Ahmed Y. Bukhamseen

Abstract /

Following the Fourth Industrial Revolution, automation of oil and gas operations became a prime target. Various efforts have been put forward to create autonomous downhole tools, which can increase the time and cost efficiency while reducing health and safety hazards. Navigation of the autonomous tools remains as one of the high barriers preventing these technologies from becoming available. This article presents two new solutions we developed for our untethered autonomous logging tool to overcome this barrier.

To increase the environmental self-awareness of downhole robots, we developed two technologies that will work together. The first technology is a low power miniaturized casing collar locator (CCL) where a millimeter-size magnetometer chip and two 1" rod magnets are employed. The second technology is based on a 1D feature matching of residual magnetic fields generated by the steel casings. Here, two magnetometers are placed on the tool with a known separation along the direction of the motion. A correlation algorithm calculates the position and speed using the magnetic field logs.

The low power miniaturized CCL is placed on a wireline tool for the proof of concept demonstration. The tool was run in a water filled test well with a depth of 1,450 ft. Decentralizers were used to keep the tool close to the casing wall. Clear peaks were observed at regular intervals. The detection depths were compared to a CCL run by a logging service company and a one to one match was observed. The 1D magnetic feature matching technology is demonstrated first by collecting residual magnetic field data from the same test well with a wireline tool. The collected signal was shifted in space, and noise is added to mimic the difference with a second magnetometer.

The matching algorithm was used to successfully find the shift between the two signals in time along the full log. This helped to estimate the speed of the tool, which is used to calculate the position. Using information from the presented technologies, along with the data from other environmental sensors, such as pressure and temperature, will provide the precise location that were not available before. The certainty will be improved by employing a Kalman filter that will integrate the sensor inputs.

As in all autonomous vehicles, increasing the environmental self-awareness of autonomous downhole tools carries a high importance for intelligent decision making, and a successful and safe operation. Technologies of surface applications, such as the global positioning system and radar, are not suitable for the downhole environment. Therefore, the new sensing technologies that we present here will accomplish these jobs for the robots operating below the surface.

Introduction

Logging and intervention in oil and gas wells have evolved from the aspects of both sensors and operations. For operations, the most important component is conveyance, which is the interface between sensors and surface systems. In most common logging and intervention configurations, conveyance ensures the safe journey of sensors and tools from the surface to the required bottom interval while maintaining an electrical and/or mechanical connection with the bottom-hole assembly (BHA).

The conveyance technique selection depends mainly on the well profile and downhole conditions. The mechanical connection is required to deploy memory and battery powered tools in the well; while surface powered and real-time logging tools require electrical connectivity through the conveyance system. Figure 1 shows the conveyance techniques, which are classified based on the case of real-time. This is referred as a tethered conveyance. For the sensors and tools that do not have a hard mechanical and/or electrical connection, the logging and intervention is referred to as untethered.

Untethered autonomous robots have reached unprecedented capabilities in the last couple of decades. They are currently used in a wide variety of environments, such as land, above and under water, air, and space, including other planets^{1,2} and asteroids³. Moreover, the use of autonomous robots is highly limited in underground use,

more specifically, in the downhole environment of oil and gas wells. Some of the challenges include: geometric constraints, harsh and inhomogeneous media, limited surface communication, locomotion, and navigation. Many times, the uniqueness of the environment prevent adoption of the existing robotic technologies and requires upgrades or completely new solutions. For example, navigation tools, such as echolocation used by submarines, or global positioning systems used by water, land, and aerial vehicles, cannot be used for downhole robots.

Navigation problems for tethered downhole tools, such as drilling tools or wireline tools, are solved to a great extent to determine the distance from the surface reference point — ground floor, Kelly bushing, or rotary table, etc. For wireline tools, they mainly rely on the wire length as measured by depth wheels that are mounted on the wireline drum. For drilling tools, they mainly rely on the tally of the BHA. When necessary, secondary depth measurements are deployed, such as cable marks, casing collar locators (CCL), natural gamma ray detection, and inertial measurements.

Magnetic field measurements are commonly used in downhole tools. For example, high accuracy magnetometers are used during directional drilling to determine the azimuth. CCLs also make use of magnetic field distortions to detect collars. These tools can either have one or more of the disadvantages of heavy weight, high energy consumption, or excessive cost. On the other hand, downhole robots need to be lightweight, low energy, and low-cost as they rely on batteries, and are expected to be more practical than their conventional counterparts.

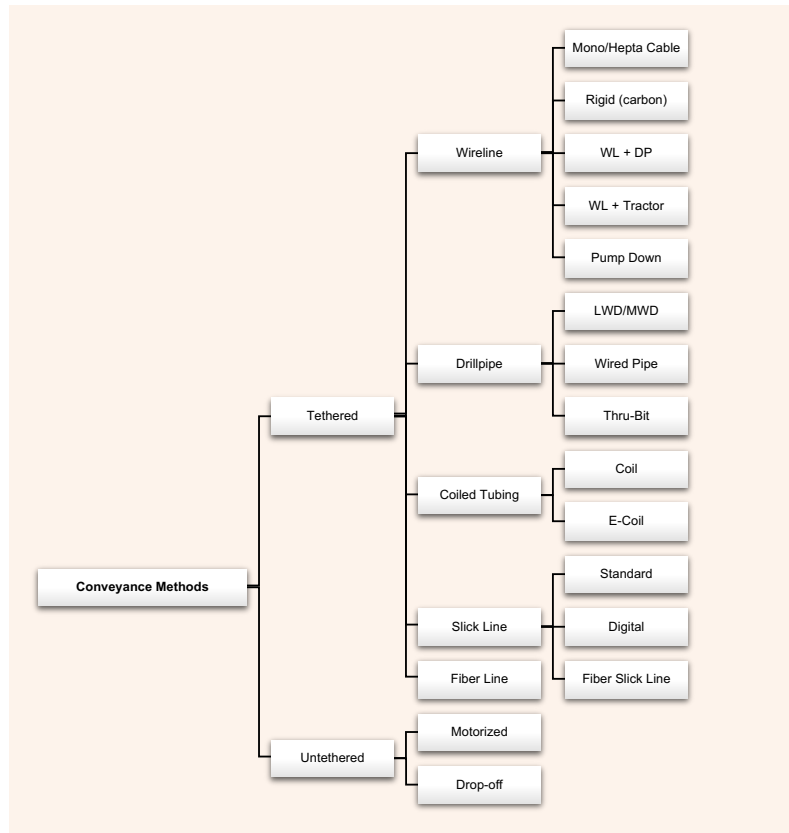
The authors have previously introduced an autonomous untethered miniaturized logging robot called sensor ball⁴⁻⁶. The palm-size robot is dropped in fluid filled wells. It falls to a desired depth where it releases a small dissolvable weight to become buoyant. Then, it returns to the surface with the logged data in its internal memory. This robot significantly reduces operation time at the well site as it doesn't need any heavy equipment such as a crane, winch, or pressure control equipment, and large crews for the supervision — besides deployment and retrieval.

What makes this robot a reliable alternative to conventional wireline and slick line surveillance is the low power electronics, miniaturized sensors, and actuators. One of the challenges of the sensor ball, and therefore, any similar untethered autonomous robots, is the depth determination. Feasibility study and implementation were conducted for two techniques that work in tandem. The first is a low power miniaturized CCL. The second is a 1D feature matching of residual magnetic fields generated by the ferromagnetic casings, such as carbon steel.

Miniature CCL

A typical CCL relies on two cylindrical magnets with the repelling poles (north-to-north or south-to-south) facing each other. This geometry creates a symmetry plane where the normal magnetic field component on

Fig. 1 The classification of conveyance methods.



the plane becomes near zero. Therefore, relatively small disturbances to the symmetric magnetic field distribution can be detected. Across casing collars, the increased metal thickness will cause deflection to magnetic flux. Conventionally, strong and heavy magnets are used together with a coil in the symmetry plane measuring the induced voltages by the varying magnetic field.

For the sensor ball, the CCL design is miniaturized where a millimeter-size magnetometer chip and two 1" long, 5/16" diameter Nd-Fe-B rod magnets are employed. The magnets are separated by 2½" and the magnetometer is centered in between them with one principal axis aligned with the polarization direction of the rod magnets. The effects of several design parameters were studied, including magnet length, distance between the magnets, and the magnetic permeability of the casing material⁷.

The performance of the miniaturized CCL is evaluated by integrating it into a wireline tool, Figs. 2 and 3, and comparing the results with a commercial CCL log from a test well. The CCL logs are collected from a test well completed with a 6½" internal diameter steel casing.

The results are summarized in Fig. 4. The logs were collected first without the magnets, which reveals a rich residual magnetic field variation due to the steel

Fig. 2 The magnetometer circuit integration on the wireline tool.

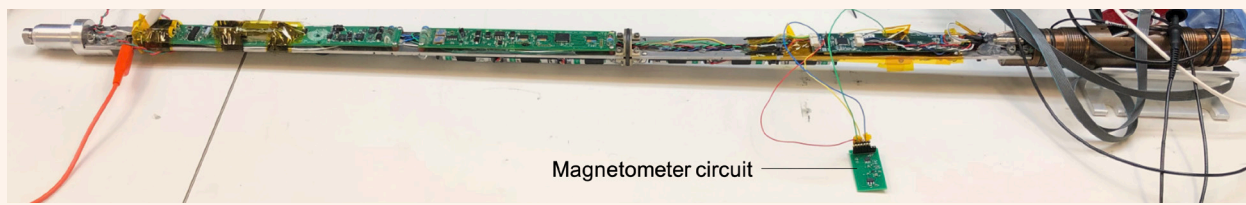
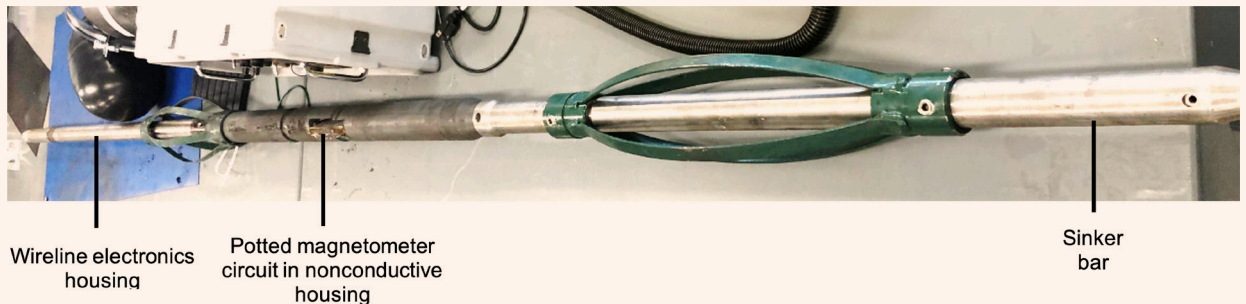


Fig. 3 The wireline tool used for testing the miniaturized CCL.



casings, Fig. 4a. Then, the magnets were placed, and the logs were collected in three offset distances of the tool from the wall of the casing, i.e., 2", 1", and ½". The miniature CCL log results are presented in Figs. 4b, 4c, and 4d. The results show that the performance strongly depends on the sensor offsets from the casing wall. As the distance to the inner casing wall increases, the collected field data closely correlates to the residual magnetic field data collected without the magnets. This indicates that the contribution from the permanent magnets in this case is insignificant. Subsequently, large peaks are observed as the tool is closer to the casing inner wall. Applying a thresholding filter to the collected log at the closest distance provided accurate collar location, Fig. 4e, compared to the commercial tool's log, Fig. 4f. Therefore, designing the untethered tool so that it travels as close as possible to the casing inner wall can provide clear CCL outputs even with a miniaturized design as presented. Although, additional strategies are needed if the tool location cannot be properly controlled along the well profile.

As an alternative to the miniature CCL, the residual magnetic field data has been investigated. Often, the residual magnetic field exhibits a fast change around the collars; however, they are not always clearly distinguishable. Applying various filters, e.g., a differential filter, the detection accuracy can be improved. Moreover, as the joint length and separation distance between collars are known, stronger predictions can be made by looking at the time separation of the detected residual peaks.

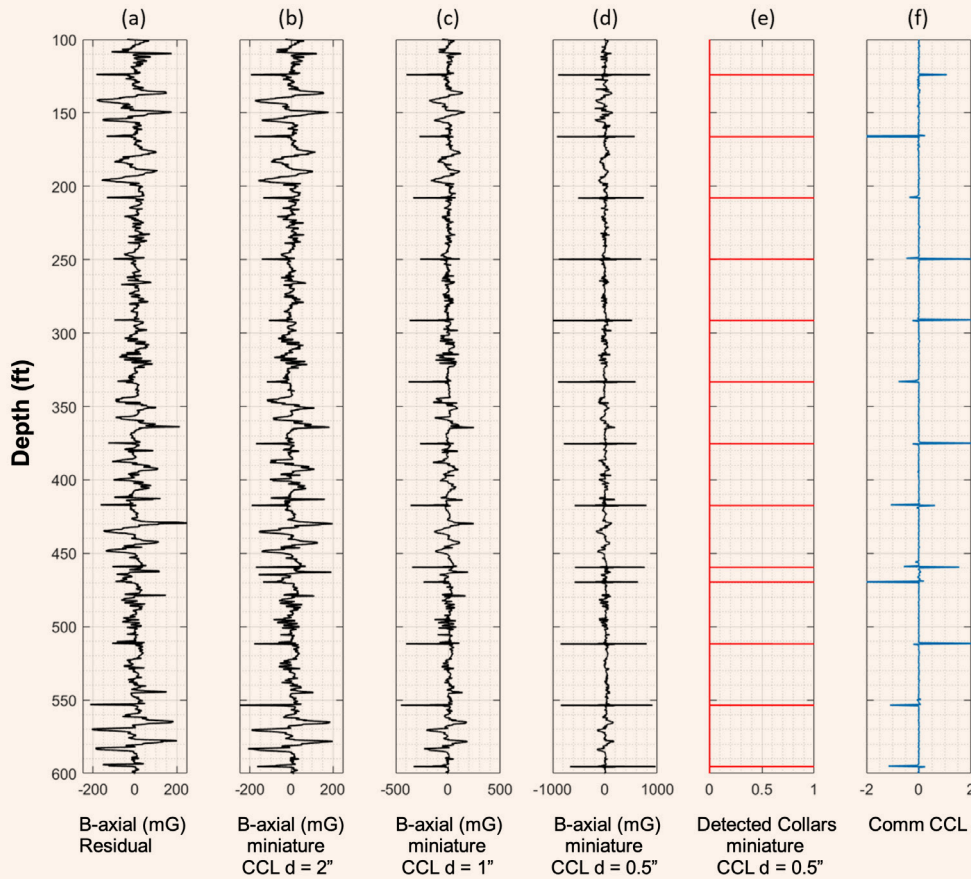
Magnetic Odometer

As previously discussed, the miniature CCL data quality depends on the offset distance of the robot from the casing inner wall, which may produce false negatives or false positives. This brings the need for additional sensing techniques for improved collar detection and depth control. For this purpose, using a CCL together with an odometer was suggested by Santos and Meggiolaro (2015)⁸, however, this can be useful only for wheeled robots that have a good grip on the casing wall.

Here, the proposed solution is a magnetic odometer, which can be used in steel cased wells by any downhole tool⁹. The magnetic odometer relies on the measurement of the residual magnetic field inside the wells using two magnetometers with a known offset along the wellbore axis, Fig. 5a. As the tool travels along the well, two time series data of the residual magnetic field of the well are acquired, Fig. 5b. The two sensors sample the same magnetic field pattern with a time delay depending on the tool speed in both downward and upward motion. The average velocity of the tool can be estimated from the known distance between the two sensors and calculated time difference between their collected signals found using a 1D feature search algorithm.

The algorithm used to find the speed and displacement is summarized in Fig. 6. The calculation starts by selecting a sample of the data from the first magnetometer, which is used as a search feature, or reference data. The window length is selected such that it contains distinctive features, e.g., oscillations, within the

Fig. 4 The miniature CCL test results with comparison to a commercial log. (Only a section is displayed for clear visualization.) (a) Residual magnetic field of the well; (b-d) miniature CCL output at indicated distances from the wall; (e) Processed miniature CCL data showing binary detection of collars; and (f) Commercial CCL data.



window. Then, another window with the same length is applied on the data from the second magnetometer. The sample signals are first conditioned, i.e., bias removal and normalization, to eliminate the differences caused by the sensor calibration. Then, a figure of merit (FOM) for similarity is found by time integration of the absolute difference between the sampled signals. A small FOM value indicates high similarity between the signals. The FOM calculation is repeated by shifting the window on the second data set.

The time shift is limited to a maximum expected value to reduce the computation cost. For example, if the slowest expected tool speed is 0.1 ft/s and the distance between the sensors is 1 ft, the maximum time shift is limited to 10 seconds. Therefore, a time shift value that represents the best FOM is found for the selected reference window and speed, and displacement can be calculated that will provide an average over the windowed time. The process continues by shifting the reference window to update the speed and displacement until the end of the log.

This technique is demonstrated by using the residual magnetic field data from the test well and simulating

the motion of a tool with two magnetometers on board. First, the distance between the magnetometers is assumed to be 1 ft. Then, a speed profile is used, such that the speed changes between 0.5 ft/s and 1.5 ft/s sinusoidally with 200 seconds periodicity. The displacement (or depth) of the tool based on this speed profile is calculated as in the gray curve in Fig. 7a. The magnetic fields that would be observed by the two magnetometers are found if the tool followed this hypothetical displacement curve in the test well. Finally, the algorithm is used to find the estimated trajectories and understand the effect of various conditions. Figures 7a and 7b show the effect of the magnetic signal noise on the estimated trajectory and resulting relative error rate, respectively.

The inset of the Fig. 7b shows sample signals with the added gaussian noise where the top curve has a signal-to-noise ratio (SNR) of 10, and the bottom curve has an SNR of 1. As expected, the higher SNR results in better depth prediction, such that the relative error rates were found as 30% and 1% after 900 ft travel for the SNRs of 1 and 10, respectively. Another important parameter is the sampling rate. The performance of the

Fig. 5 (a) The concept of the magnetic odometer showing the residual magnetic field of the casing, and the two magnetometers placed on the robot; and (b) Example time series data collected by each magnetometer.

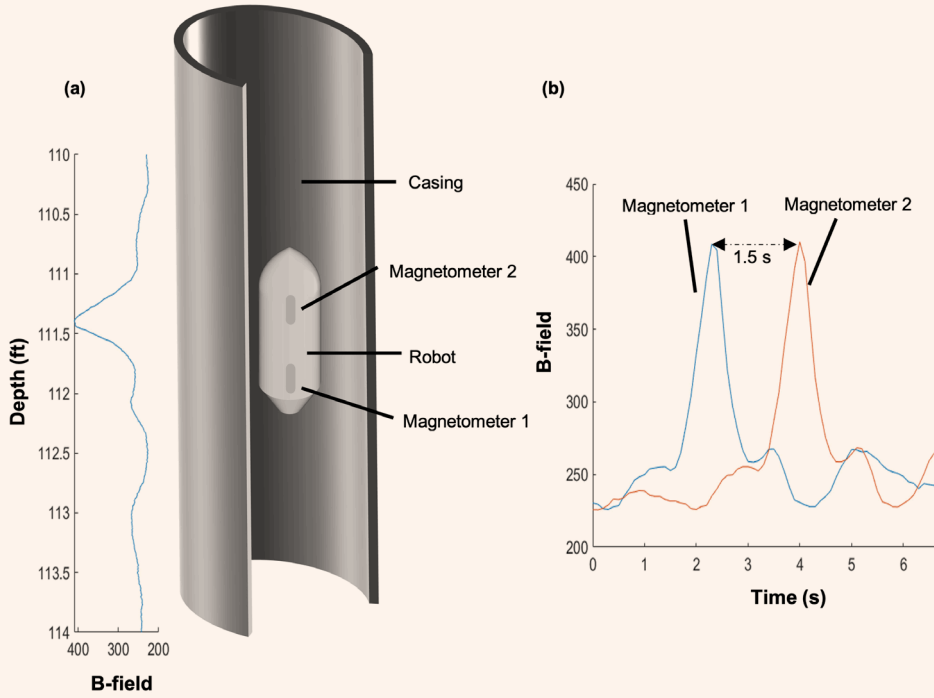


Fig. 6 The algorithm for speed and displacement of the tool using magnetometers.

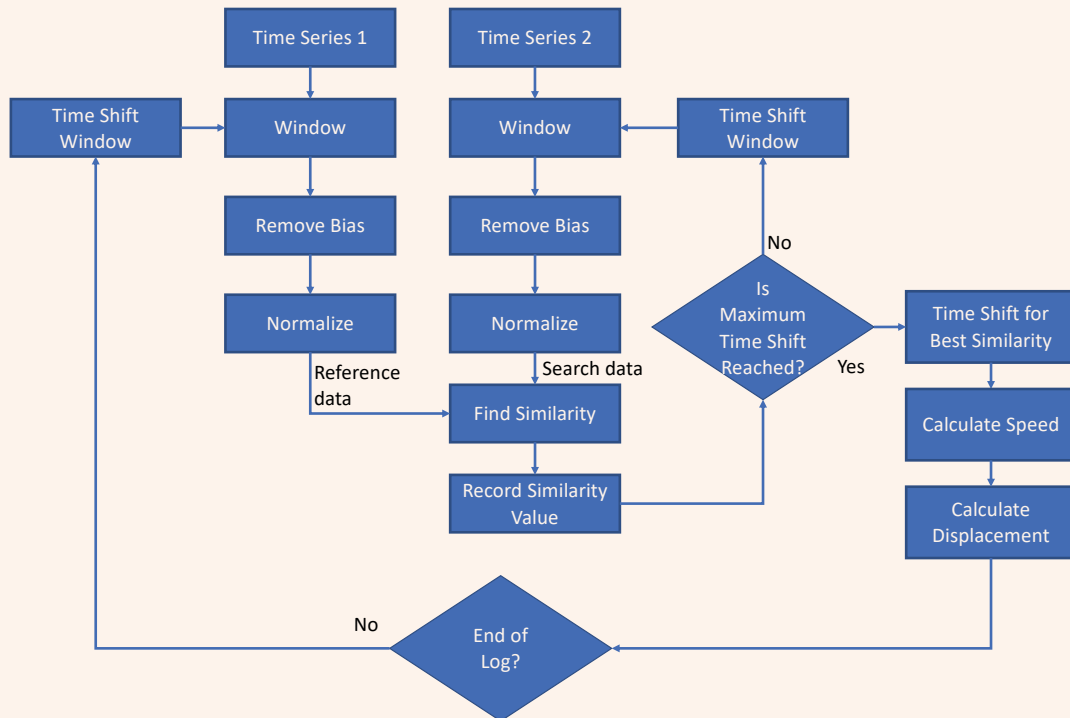
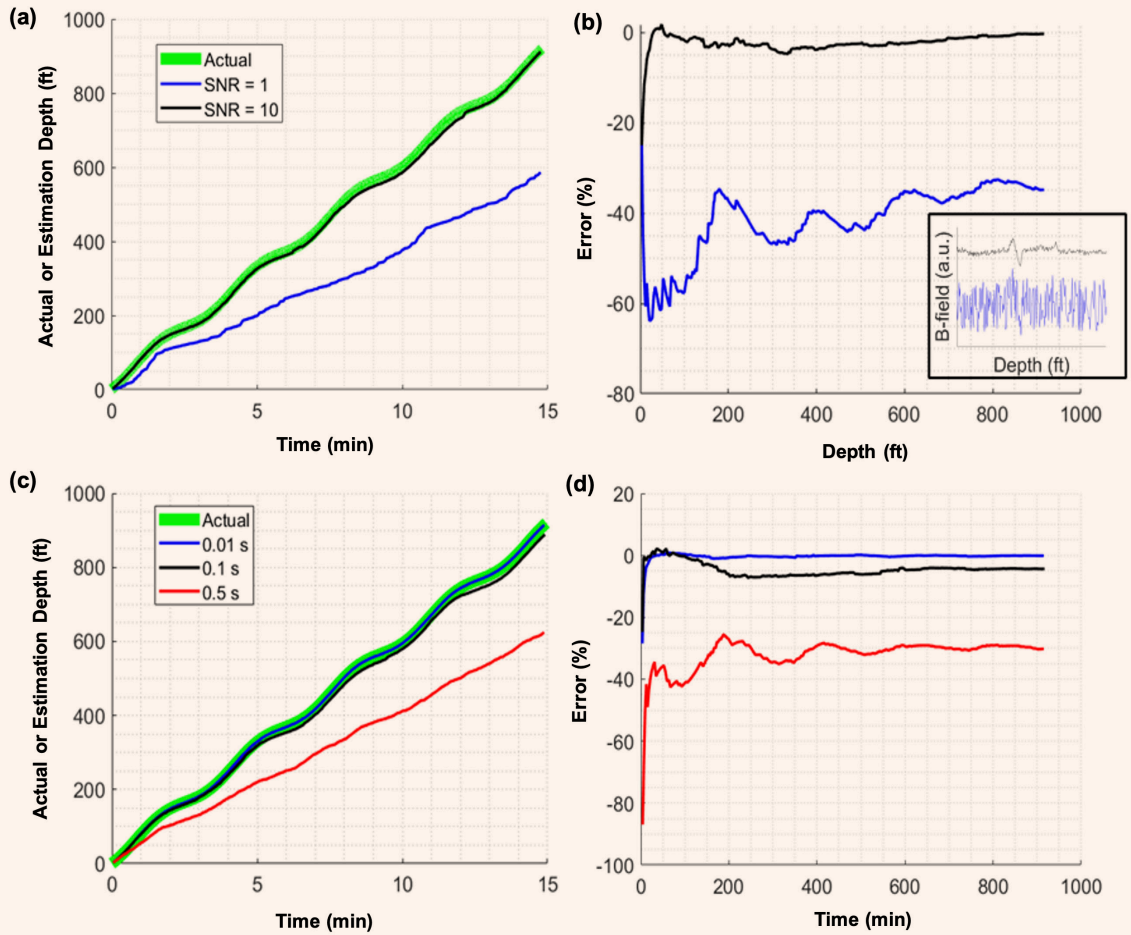


Fig. 7 (a) The actual and measured depth profiles as a function of SNR; (b) The relative calculated depth errors as a function of SNR. The inset shows a sample section of the magnetic field data for each SNR; (c) The actual and measured depth profiles as a function of the sampling period; and (d) The relative calculated depth errors as a function of the sampling period.



technique was tested for the magnetic field sampling periods of 0.01 second, 0.1 second, and 0.5 seconds. Like the accelerometer-based displacement estimation, high sampling frequency helps to increase the accuracy.

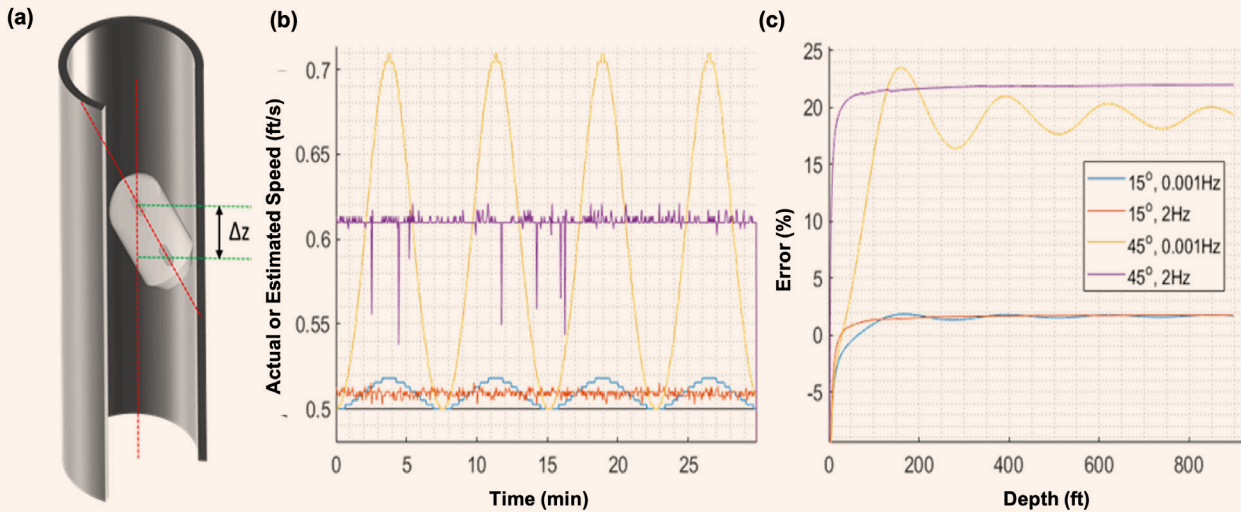
Consequently, the odometer-based displacement estimation typically requires less sampling since it calculates displacement by integrating speed over time once as opposed to twice during the integration in the accelerometer-based estimation technique. The relative errors were found as less than 0.1% for the 0.01 second sampling, whereas it became 2.5% and 31% for the 0.1 second and 0.5 second sampling periods, respectively. This result can also be interpreted as such that the trajectory estimation improves when the tool moves slower for any sampling frequency.

One disadvantage of the described magnetic odometer is that it assumes the displacement happens along the axis of the magnetometers. This assumption is mostly true for the downhole tools whose length is several times longer than the borehole diameter. For freely moving short tools such as the sensor ball, the angle between

the tool's vertical axis and the cylindrical wellbore's major axis may vary due to the well inclination and wobbling of the tool, Fig. 8a¹⁰.

To understand the effect of the wobbling amplitude and frequency, the simulation was repeated assuming a constant tool speed of 0.5 ft/s, and a second sampling period of 0.01. The trajectories and magnetic field data for each magnetometer were found based on wobble amplitudes of 15°, and 45°, and wobbling frequencies of 0.001 Hz and 2 Hz. Figure 8b shows that the higher wobbling amplitudes cause the algorithm to overestimate the speed. This is because during wobbling, the apparent distance between the two magnetometers become shorter than their actual distance. The apparent distance is the projection of the length between the magnetometers on the borehole axis, which is illustrated as Δz in Fig. 8a. The wobbling frequency does not largely affect the error rate. The error rates for 15° wobbling amplitude were found to be approximately 2%, whereas for 45° they were approximately 20%, Fig. 8c.

Fig. 8 (a) The untethered downhole robot moving at an angle with respect to the borehole axis; (b) The actual (black line) and estimated speeds, and (c) The relative error in estimated depth for various wobbling amplitudes and frequencies.



Discussion and Conclusions

The depth detection of autonomous, non-wheeled, and non-motorized robots for downhole sensing is a challenging task as compared to other types of downhole robots and conveyance methods. The proposed research work provides a reliable alternative to exploit downhole sensor data and convert time series into depth series. The magnetic CCL design is optimized for relatively small autonomous robots to detect casing collars as the tool travels along the inner wall of the casing and tubing strings. This is complemented by sensing the residual magnetic field using a simple magnetic odometer.

A fit for purpose algorithm is used to analyze both magnetometers' data to detect response similarities, i.e., estimate the speed and location of the tool along the borehole. All techniques presented here utilize the magnetic fields and have varying sensitivities to the orientation of the robot with respect to the casing. The miniature CCL works better as it becomes closer to the casing wall. Using residual magnetic fields for collar detection or for magnetic odometer require alignment with the borehole axis. These can be accomplished by the mechanical design of the robot¹¹. Additionally, centralizers or decentralizers can provide the necessary alignments with the casing without the need for active position control; however, the risk of robot being immobilized downhole increases with those approaches.

It's quite certain that no one single sensing type can provide accurate depth for untethered robots. This means data from various sensors should be used together. Sensor fusion techniques, e.g., Gaussian filters, Bayesian filters, etc., are commonly employed in robotic localization using probabilistic methods. For example, the depth calculation using a magnetic odometer can

be corrected every time a casing collar is detected with high probability.

This can prevent the accumulated error due to integration of the speed. Another addition could be using an accelerometer and/or gyroscope to understand linear acceleration and wobbling of the robot along with the Earth's gravity vector. This data can be used to eliminate or correct the wrong speed and depth measurements.

Acknowledgments

This article was presented at the Middle East Oil and Gas Show and Geosciences Conference and Exhibition, Manama, Kingdom of Bahrain, February 19-21, 2023.

References

1. Maurette, M.: "Mars Rover Autonomous Navigation," *Autonomous Robots*, Vol. 14, Issue 2, March 2005, pp. 199-208.
2. Serricchio, F., San Martin, A.M., Brugarolas, P. and Casoliva, J.: "The Mars 2020 Perseverance Navigation Filter," article presented at the AAS/AIAA Astrodynamics Specialist Conference, Big Sky, Montana, August 9-12, 2021.
3. Elvis, M.: "Let's Mine Asteroids — for Science and Profit," *Nature*, Vol. 485, Issue 7400, May 2012, p. 549.
4. Deffenbaugh, M., Ham, G.D., Alvarez, J.O., Bernero, G., et al.: "Method and Device for Obtaining Measurements of Downhole Properties in a Subterranean Well," U.S. Patent No. 10,900,551, January 2021.
5. Buzi, E., Seren, H.R., Deffenbaugh, M., Bukhamseen, A., et al.: "Sensor Ball: Autonomous, Intelligent Logging Platform," OTC paper 51149, presented at the Offshore Technology Conference, virtual and Houston, Texas, August 16-19, 2021.
6. Seren, H.R., Buzi, E., Al-Maghrabi, L., Ham, G., et al.:

- “An Untethered Sensor Platform for Logging Vertical Wells,” *IEEE Transactions on Instrumentation and Measurement*, Vol. 67, Issue 4, December 2017, pp. 798-805.
7. Seren, H.R. and Deffenbaugh, M.: “Miniaturized Casing Collar Locator for Small Downhole Robots,” *IEEE Sensors Letters*, Vol. 6, Issue 4, April 2022, pp. 1-4.
 8. Santos, H.F.L. and Meggiolaro, M.A.: “Probabilistic Robotics Applied to Self-Localization Inside Oil Wells of an Autonomous System,” paper presented at the 25th ABCM International Congress of Mechanical Engineering, Rio de Janeiro, Brazil, December 6-11, 2015.
 9. Seren, H.R. and Deffenbaugh, M.: “Determining a Location of a Tool in a Tubular,” U.S. Patent Application No. 17/254,555, 2021.
 10. Seren, H.R., Buzi, E. and Deffenbaugh, M.: “Autonomous Well Logging Robot with Passive Locomotion,” paper presented at the 21st International Conference on Control, Automation and Systems (ICCAS), Jeju, Republic of Korea, October 12-15, 2021.
 11. Seren, H.R., Deffenbaugh, M. and Zeghlache, M.L.: “Orienting a Downhole Tool in a Wellbore,” U.S. Patent Application No. 17/164,067, 2021.

About the Authors

Dr. Huseyin R. Seren

*Ph.D. in Mechanical Engineering,
Boston University*

Dr. Huseyin R. Seren joined the Sensors Development Team at the Aramco America's Houston Research Center in 2015 as a Research Scientist. His focus areas are research and development of technologies for autonomous untethered downhole tools, microfabricated sensors, and electromagnetic metamaterials for applications in hydrogen production and sensing.

Huseyin received his B.S. and M.S. degrees in Electrical Engineering from Koç University,

Istanbul, Turkey, in 2007 and 2009, respectively. In 2014, he received his Ph.D. degree in Mechanical Engineering from Boston University, Boston, MA.

During Huseyin's academic life, he studied and developed micro-electromechanical system-based miniaturized spectrometers, metamaterial-based terahertz absorbers and modulators, and wireless communication platforms for miniaturized downhole sensors.

Dr. Max Deffenbaugh

*Ph.D. in Electrical Engineering,
Massachusetts Institute of
Technology*

Dr. Max Deffenbaugh joined the Aramco Americas' Houston Research Center in 2013 as a Research Engineer. He founded and leads the Sensors Development Team, who create new measurement techniques and instruments for the oil field.

Previously, Max worked for 16 years at ExxonMobil on seismic signal processing, inverse problems related to geological processes, computational rock physics, and

development of downhole sensor networks.

In 1991, he received his B.S.E. degree in Electrical Engineering from Princeton University, Princeton, NJ. Max then received his M.S. degree in 1994, and his Ph.D. degree in 1997, both in Electrical Engineering, in a joint program of the Massachusetts Institute of Technology, Cambridge, MA, and the Woods Hole Oceanographic Institution, Falmouth, MA.

Mohamed Larbi Zeghlache

*M.S. in Reservoir Engineering
and Field Development,
French Petroleum Institute*

Mohamed Larbi Zeghlache is a Senior Researcher and the well integrity logging subject matter expert working with the Production Technology Team of Saudi Aramco's Exploration and Petroleum Engineering Center – Advanced Research Center (EXPEC ARC). He previously led the well integrity logging team in the Reservoir Description and Simulation Department.

Since joining Saudi Aramco, Mohamed has been responsible for formation evaluation and well placement in Ghawar carbonates and Central Arabia clastics.

He has 22 years of experience in the oil and gas industry, and previously worked with both Schlumberger and Halliburton where he held various positions, including Wireline Field Engineer, Log Analyst, Business Development, and Technical Advisor.

Mohamed is the author of several publications and patents.

He received his M.S. degree in Reservoir Engineering and Field Development from the French Petroleum Institute (IFP), Paris, France.

Dr. Ahmed Y. Bukhamseen

*Ph.D. in Petroleum Engineering,
Stanford University*

Dr. Ahmed Y. Bukhamseen is a Petroleum Engineer working with the Production Technology Team of Saudi Aramco's Exploration and Petroleum Engineering Center – Advanced Research Center (EXPEC ARC). His extensive experience includes reservoir engineering, production operations and completions research and development. Ahmed's current research activities cover smart well completions,

production optimization, fiber optic sensing and multiphase flow metering.

He has published several technical papers and holds three patents.

Ahmed received his B.S. degree from the Colorado School of Mines, Golden, CO, and both his M.S. and Ph.D. degrees from Stanford University, Stanford, CA, all in Petroleum Engineering.

Innovative Solid Lubricant Solution to Reduce Friction in Challenging ERD Wells

Tulio D. Olivares, Zach Turi and Brandon Hayes

Abstract /

Extended reach drilling (ERD) has become increasingly more frequent in the petroleum industry as it allows access to additional reserves in oil and gas reservoirs from a single wellbore. Consequently, this has led to an increase in friction-related problems while drilling and running casing. This article describes the extensive lab testing and technical implementation of an innovative technology that utilizes a customized solid lubricant to reduce friction and help operators achieve challenging depths.

Comprehensive lab testing was conducted to tailor the required formulations of the solid lubricant and two field trials were completed to evaluate the performance. To properly conduct this evaluation, key performance indicators (KPIs) were established in both wells. A minimum torque reduction value of 10% was targeted for a treatment containing 5 pounds per barrel (ppb) of the solid lubricant. Baseline torque values were captured prior to the addition of the lubricant and were the benchmark for performance evaluation. Drilling fluid from the active pit was then enhanced with 5 ppb of the solid lubricant and sweeps were pumped downhole to reduce friction.

Two extended reach wells were identified in which water-based mud was used to drill. On Well-A, at a 79° inclination, high and erratic torque was experienced, which affected the drilling performance. A baseline torque was recorded and a sweep with 4 ppb of the solid lubricant was pumped — resulting in a 5.5% torque reduction. After drilling another stand, a second sweep was pumped with 5 ppb concentration and torque was reduced 14.7%. On Well-B, at an 84° inclination, high and erratic torque was once again experienced. The baseline torque was recorded, and the first sweep was pumped with 5 ppb of the solid lubricant: resulting in a 10.4% torque reduction.

A second sweep was immediately pumped with another 5 ppb concentration and torque was reduced by 24.3%. In both Well-A and Well-B, a pill was spotted in the open hole with 8 ppb solid lubricant concentration to assist with the liner run. These field applications successfully demonstrated the concept of this innovative technology to reduce friction and overcome torque challenges in ERD applications; thereby resulting in a drastic reduction in nonproductive time.

The industry is continuously looking for opportunities to reduce nonproductive time while drilling. This innovative solid lubricant is environmentally safe, compatible in all mud systems, and is highly effective in low concentrations to reduce friction while drilling in some of the most challenging extended reach wells. Minimizing friction and the subsequent torque issues will allow for optimal rates of penetration while drilling in these challenging conditions, and therefore reduce the overall time constructing the well.

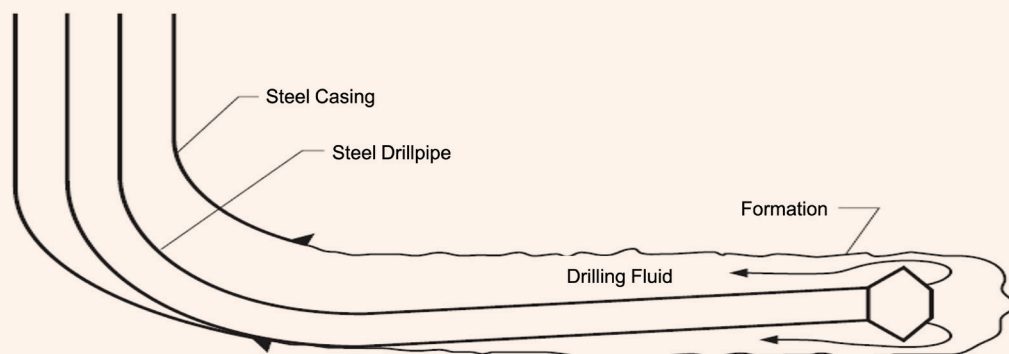
Introduction

The growing necessity for the production of oil and gas has led drilling operators to drill highly deviated and long horizontal wells to increase the reservoir contact, and therefore the subsequent production from a single wellbore. These challenging wells are becoming more and more common notwithstanding the problems linked to the drilling design and operation. Well trajectory is also significant, which should be considered as an important factor for torque and drag analysis, and for the reduction of the applied stress on the drillstring. Moreover, additional research on the recognition of torque and drag causes are still essential.

Communication between the drillstring, including the bit, bottom-hole assembly (BHA), drillpipe, and the well trajectory is the main reason for the generation of torque and drag, due to the friction between their surfaces, especially in extended reach drilling (ERD) wells. In ERD well construction, the frictional forces created between the drillstring and the wellbore wall can cause a high enough amount of torque and drag that often the mechanical limits of the drillstring are reached. When this occurs, the well can no longer be drilled without the risk of damaging or breaking the drillstring tubulars or BHA, Fig. 1.

These frictional forces are best captured in a single variable known as the coefficient of friction (COF)¹. There are several factors that affect this value, including the nature of the two surfaces that are in contact as well as in this situation, the composition of the fluid that flows between them. Certain additives, such as lubricants,

Fig. 1 A schematic of an ERD well.



can be added to this drilling fluid to lower that COF between the surfaces, and thereby reduce the overall torque and drag.

An Innovative Solid Lubricant Technology

A lubricant can be any substance that helps to lower the frictional forces between two surfaces that are in contact with one another. It can come in various forms, such as a liquid or a solid. In either case, the lubricant penetrates the space between the two surfaces and either chemically or mechanically reduces that frictional force between them. In the case of a solid lubricant, the frictional force reduction is traditionally mechanical².

In this evaluation, an environmentally safe, nonabrasive solid lubricant technology containing a blend of copolymer beads were used, Fig. 2. As such, in this case, the mechanism for lubrication is in fact mechanical and even more specifically, the frictional force reduction is caused by the spherical solids creating a standoff between the two surfaces, thereby reducing the contact force between them; similar to the way a small ball bearing would work.

Solid lubricants hold several advantages over a liquid lubricant, such as: easier handling and storage,

enhanced compatibility with different fluid systems, and they can be highly effective in low concentration applications. One of the biggest disadvantages to a liquid lubricant is the potential for incompatibility in the mud system.

Often, chemical impurities and other additives within the mud system can cause a liquid lubricant to foam or create a thick grease that can cause highly undesirable operational consequences. On the other hand, solid lubricants typically are chemically inert and are not reliant on specific mud system conditions to adequately perform. Additionally, solid lubricants are far more resilient of the harshest drilling conditions such as extremely high temperatures and pressures.

This innovative solid lubricant technology was designed to be applied in low concentrations and help reduce torque and drag while drilling, improve the ability to slide, and reduce the COF while running casing, thereby allowing for a smooth casing run. In addition to the benefits seen in the drilling performance, the use of this solid lubricant can also help reduce both drillpipe and casing wear. As the drillpipe and casing rub across the formation face during drilling operations or the casing run, the steel pipe will begin to wear away, which could eventually lead to mechanical failures. By utilizing the solid lubricant in these highly deviated sections of the wellbore, this wear can be greatly reduced as it creates a barrier between the two surfaces, and therefore reduces the abrasive contact with the formation face.

For the sake of this technology assessment, the primary focus was to evaluate the solid lubricant's ability to affect drilling performance and casing runs with the understanding that pipe wear was a secondary benefit. This technology initially underwent extensive evaluation in a laboratory setting before ultimately being put to the test in the field to determine if it could provide satisfactory results.

Laboratory Evaluation

During the extensive lab evaluation, a baseline specification was developed for the solid lubricant. Axial deformation or geometry of the solid body was evaluated

Fig. 2 An environmentally safe, nonabrasive solid lubricant technology.



Table 1 The results of the solid lubricant specification lab testing.

Test	Solid Lubricant	Baseline Specifications	Pass/Fail
Specific Gravity	1.08	1.06 – 1.30	Pass
Particle Size Distribution (microns)	200 – 1,000	100 – 1,000	Pass
Axial Deformation at 16,000 psi	9.486	8.830	Pass

to predict the safe forming limits of the solid lubricant and understand the microstructural deformation mechanism. Similarly, specific gravity and particle size distribution of the solid lubricant were measured to verify if this friction reduction technology could be pumped downhole without limitations through the bit and downhole tools.

Table 1 lists the results of the solid lubricant specification lab testing.

This lab testing provided verification that the solid lubricant would successfully pass through the downhole tools without any issues. It also helped confirm that it would hold up under the expected downhole conditions without the fear of severe degradation. Both of these criteria were important to confirm prior to field operations to ensure no operational issues, and that the solid lubricant technology would not be adversely affected by the drilling conditions.

Field Evaluation

Once the solid lubricant specifications were verified at the lab, the next phase was to test this technology at the field level. To properly evaluate it, several key performance indicators (KPIs) in the evaluation criteria were established as:

1. The solid lubricant should provide a minimum of 10% reduction in drilling torque in an extended reach well after pumping a sweep pill.
2. The solid lubricant should be field-tested as a lubricant pill in the open hole while running a liner or casing in an extended reach well, and demonstrate a smooth casing run to the bottom.
3. The addition of the solid lubricant in the drilling fluid system should be easy without any safety or operational issues, and there should be no sign of any adverse effects on the fluid system properties.
4. The above criteria needs to be accomplished in a minimum of two different extended reach wells.

To measure the friction reduction percentage while drilling the extended reach well, a drilling torque baseline was captured and then compared after the addition of the solid lubricant. Once the baseline torque was established, sweeps with varying concentrations of the solid lubricant were trialed to determine the ideal concentration to meet the mentioned KPIs. The two

wells, discussed next, were used to evaluate the performance of the solid lubricant for both torque reduction as well as for the liner run.

Well-A

The first field evaluation was in Well-A; a directionally drilled 8½" hole with 77 pounds per cubic foot (pcf) water-based drilling fluid building an angle from 1.40° to 76° with full returns. The first solid lubricant pill contained 4 ppb of the solid lubricant and a 35 bbl sweep was sent as the torque had begun to increase above the desirable limit. Once the pill had exited the bit, a 5.5% reduction, Fig. 3, in torque was calculated based upon the established baseline torque measurements. The KPI for torque reduction had been set at a minimum of 10%, therefore on this pill the KPI was not achieved.

Drilling continued with an inclination of 79.1°, and a second 35-bbl solid lubricant pill was built; this time increasing the solid lubricant concentration to 5 ppb. Once the pill exited the bit and started crossing through the annulus, a torque reduction of 14.7%, Fig. 4, was calculated based upon the newly established baseline torque reading. This value was in line with the desired KPI, and going forward, the 5 ppb concentration would be utilized for the remaining sweeps.

The hole section was then drilled to total depth and before pulling out of the hole to run the 7" liner, an open hole equivalent volume of 79 pcf solid lubricant pill was mixed with no issues using the regular rig mixing system. This pill was mixed using the active water-based drilling fluid with an addition of 8 ppb of the solid lubricant.

After performing a wiper trip and properly conditioning the hole with adequate circulation, the rig proceeded to spot the entire pill in the open hole, and the liner go-pill was efficiently placed with the above-mentioned solid lubricant concentration. The liner was successfully run to the bottom without any issues, complying with the previously established KPI.

Well-B

The second field evaluation was on Well-B, which was in a different area than the previous field evaluation. This ERD well was drilled with 77-pcf inhibited water-based drilling fluid building an angle from 11.04° to 84.04° with full returns. The first solid lubricant

Fig. 3 The first solid lubricant friction reduction pill in Well-A.

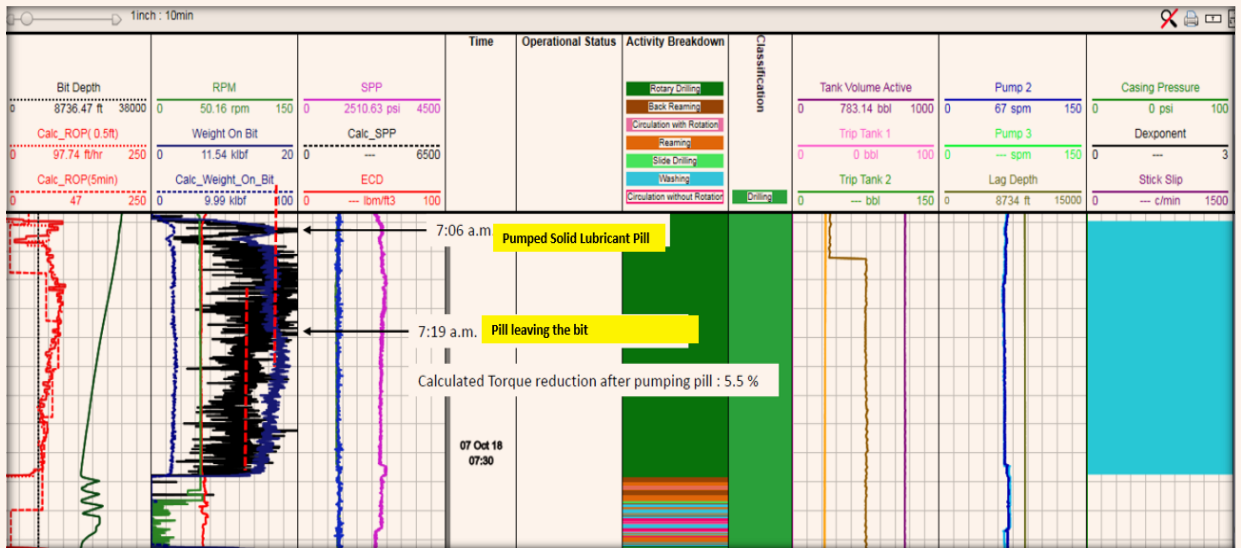
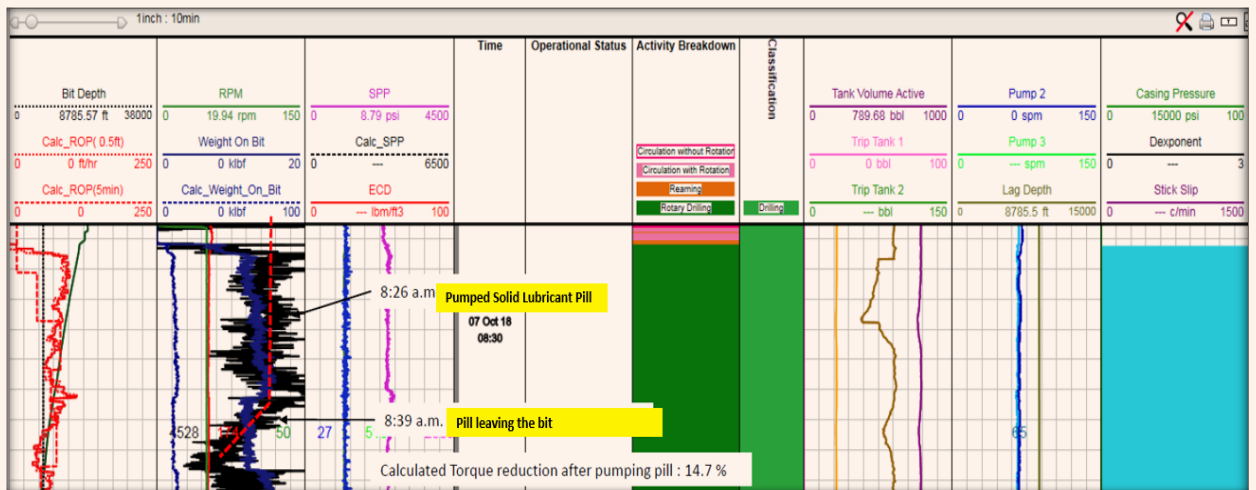


Fig. 4 The second solid lubricant friction reduction pill in Well-A.



pill was built with a 5-ppb concentration of the solid lubricant and a 20-bbl pill was pumped as a sweep. As the sweep exited the bit, a 10.4% reduction in torque was observed, Fig. 5.

As the torque began to rise, a second 20-bbl solid lubricant pill — containing the same 5-ppb concentration — was once again mixed and pumped as a sweep. This time as the sweep exited the bit, there was a calculated torque reduction of 24.3%, Fig. 6.

Finally, a third 20-bbl solid lubricant pill was pumped with a 5-ppb concentration as a sweep, which reduced the torque 10.13% once the pill exited the bit, Fig. 7. Overall, all three of the sweeps utilized on Well-B

resulted in a torque reduction greater than 10%, which met the KPI criteria for field evaluation. Through this field evaluation, it was also determined that a 5-ppb concentration of the solid lubricant was the minimum necessary concentration to yield the desired results in this particular drilling fluid system.

The directional hole was then drilled to total depth with 77-pcf inhibited water-based drilling fluid with full returns. Prior to running the 7” liner, an open hole equivalent volume of a 77-pcf liner go-pill, which contained the active water-based drilling fluid and 8 ppb of the solid lubricant, was pumped and spotted in the open hole. The liner was successfully run to

Fig. 5 The first solid lubricant friction reduction pill in Well-B.

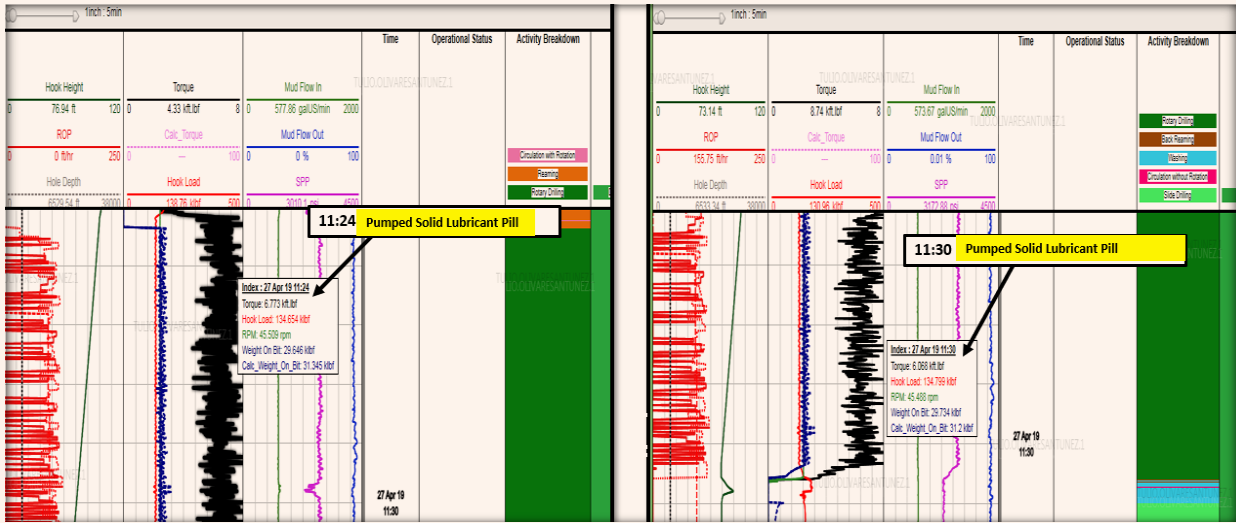
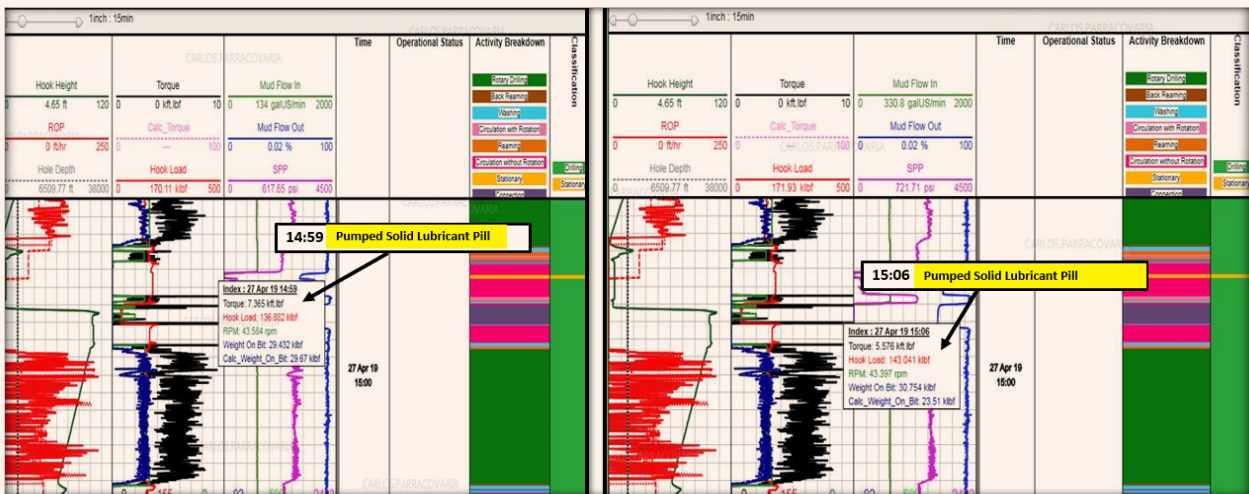


Fig. 6 The second solid lubricant friction reduction pill in Well-B.



the bottom without any issues, thereby complying with the KPI.

After the successful applications on Wells A and B, this innovative solid lubricant solution was considered to be used to assist long casing and liner runs in very tough and long horizontal conditions. The first utilizations were to run 7” and 4½” liners in horizontal sections with a length of more than 5,000 ft across limestone and carbonate formations. These pills were called the casing go-pill or liner go-pill, and were customized on a case-by-case basis depending on the specific wellbore conditions, type of well, type of drilling fluid, and several other variables.

The go-pills included concentrations of 8 ppb to 10 ppb of the innovative solid lubricant solution. The solid lubricant was easily added into the active system through the mixing tank hopper without any issues. These go-pills would then be spotted through the entirety of the open hole while tripping out in preparation to run the casing or the liner. This has allowed for a smooth operational procedure that did not require any additional equipment or rig time to accomplish. These go-pills have been implemented in more than 500 wells per year and have yielded satisfactory results in allowing for smooth and efficient casing and liner runs.

Fig. 7 The third solid lubricant friction reduction pill in Well-B.



Conclusions

1. The innovative solid lubricant technology can be utilized to efficiently reduce torque and drag in ERD wells by applying low concentration sweeps as needed. The field evaluation demonstrated that the solid lubricant technology is highly effective in these low concentrations at reducing friction while drilling in some of the most challenging extended reach wells.
2. Solid lubricants provide many benefits over a traditional liquid lubricant, including ease of handling and storage, enhanced compatibility with the fluid system, and a high resilience to the harshest drilling conditions.
3. During field evaluation, the solid lubricant pills provided a minimum of 10% torque reduction in drilling operation after pumping sweeps with a concentration of 5 ppb. The torque reduction varied between a minimum of 10.13% and up to 24.3% at the mentioned concentration.
4. The solid lubricant was successfully utilized and field-tested as a lubricant go-pill with 8 ppb concentration to assist in the 7" liner runs in ERD Wells A and B. These pills have been successfully utilized to assist in casing and liner runs by enhancing the lubricity of the drilling fluid; especially in tough wellbore conditions and long horizontal sections.
5. The addition of the solid lubricant in the drilling fluid system was simple, it did not require any additional mixing equipment, and there were no safety or operational issues.
6. During the field evaluation, the solid lubricant was mixed in two different water-based drilling fluids and the properties of the fluid system were not affected after the lubricant additions. No adverse effects or incompatibilities were noticed whatsoever.

References

1. Olivares, T., Al-Zahrani, W., Sindi, R. and Abahussain, A.: "Novel Torque Reduction Technology for Invert Emulsion Fluids in ERD Wells," paper AAE-22-FTCE-070, presented at the AAE Fluids Technical Conference and Exhibition, Houston, Texas, April 19-20, 2022.
2. Mohammadi, M.K. and Nowtarki, K.T.: "A Case Study on the Successful Application of Solids Lubricants in Directional and Horizontal Drilling Operations to Reduce Torque and Drag and Improve ROP in One of the Carbonate Oil Reservoirs," SPE paper 176475, presented at the SPE/IATMI Asia Pacific Oil and Gas Conference and Exhibition, Nusa Dua, Bali, Indonesia, October 20-22, 2015.

About the Authors

Tulio D. Olivares

*B.S. in Chemical Engineering,
Universidad Rafael Urdaneta*

Tulio D. Olivares is a Drilling Engineer working in Saudi Aramco's Drilling Technical Services Evaluation Unit of the Drilling Technical Department. He has 22 years of experience working in different supervisory, technical, and management level positions in Venezuela and Saudi Arabia with Halliburton, Chevron, and Saudi Aramco. Tulio is currently working as a drilling fluids subject matter expert.

He is the author of more than 22 Society of Petroleum Engineers (SPE) and American Association of Drilling Engineers (AADE) publications. Tulio has published three filed U.S. patents.

He received his B.S. degree in Chemical Engineering from the Universidad Rafael Urdaneta, Maracaibo, Venezuela.

Zach Turi

*B.S. in Petroleum Engineering,
Marietta College*

Zach Turi began his career working for Halliburton in the Permian Basin. While at Halliburton, he took on various roles in the Well Construction group, including operations, engineering, and business development.

In 2021, Zack joined DrillChem. He has taken on a technical leadership position to help generate new business while simultaneously

assisting in new product development.

Zack is the coauthor of several Society of Petroleum Engineers (SPE) and American Association of Drilling Engineers (AADE) publications.

He received his B.S. degree in Petroleum Engineering from Marietta College, Marietta, OH.

Brandon Hayes

*B.S. in Chemical Engineering,
University of Louisiana at
Lafayette*

Brandon Hayes is the CEO of DrillChem. Over his 22 year tenure with DrillChem, Brandon has held varying technical, sales, and management positions at the company before rising to his current position.

Brandon is responsible for the creation of numerous drilling fluids additives used globally. He has published several papers in the Society

of Petroleum Engineers (SPE) and American Association of Drilling Engineers (AADE) publications, along with the *Houston Business Journal*, focusing on products, application, and leadership.

Brandon received his B.S. degree in Chemical Engineering from the University of Louisiana at Lafayette, Lafayette, LA.

Reduced Polymer Loaded Fracturing Fluid for Extreme Temperature Proppant Fracturing

Prasad B. Karadkar, Ataur R. Malik, Mohammed I. Al-Abdrabnabi and Dr. Feng Liang

Abstract /

Guar gum and its derivatives-based fracturing fluids are most commonly used in hydraulic fracturing. For high temperature wells, guar-based fracturing fluids must be formulated with higher polymer loading and at high pH levels that leaves insoluble residue and tends to form scales with divalent ions.

In this article, a newly developed reduced polymer loaded fracturing fluids-based acrylamide polymer was deployed from lab developments to field implementation. A thermally stable acrylamide-based polymer with a reduced polymer loading of 30% to 40% less than guar-based fracturing fluid was considered to minimize formation damage concerns. The crosslinked fracturing fluid viscosity was optimized at 340 °F bottom-hole static temperature (BHST), and 315 °F, 290 °F, 265 °F, and 240 °F cool-down temperatures, respectively, using a high-pressure, high temperature (HPHT) rheometer. For successful field deployment, a novel reduced polymer fracturing fluid was evaluated in the following sequence: chemical management, quality control, optimization of fracturing fluid formulations with field water, field mixing procedure, on-site QA/QC, data frac analysis, and execution of the main treatment.

This article presents rheological studies of reduced polymer loaded fracturing fluids at BHST and cool-down temperatures of selected well candidates that demonstrate the superior thermal stability of this novel fracturing fluid. With a 35 lb/1,000 gal polymer loading, the fluid viscosity stayed above 300 cP at a 100 1/s shear rate for 60 minutes at 340 °F. The fracturing fluid formulations were optimized using both live and encapsulated breakers using a HPHT rheometer. Due to the fast hydration of the base polymer, the linear gel was mixed on-the-fly during the main fracturing treatment.

The main fracturing treatment was successfully executed with a 40 barrels per minute (bbl/min) pumping rate with increased proppant concentration up to 4.5 pounds per gallon (PPA) using a 40/70 high strength proppant (HSP). The fracturing fluid system, based on the novel acrylamide copolymer, offers advantages over guar-based fracturing fluid, such as low polymer loading, excellent high temperature stability, and less formation damage.

This article presents a systematic approach and lessons learned during novel fracturing fluid deployment.

Introduction

Low permeability or damaged reservoirs are frequently stimulated using hydraulic fracturing technology. Reservoir compatible fluids are pumped during hydraulic fracturing operations to initiate and propagate desired fracture geometry. In pre-pad and PAD stages, treated water, linear non-crosslinked gel, and crosslinked gel are pumped first to cool-down, provide ease on fracture initiation and propagation past the near wellbore and to the far field region. Later, fluid containing proppant is injected to extend and maintain the length and width of the propped fracture inside the formations. Once a fracturing treatment is completed, the fracture closes on the proppant, leaving a conductive channel connected to the wellbore for recovery of pumped fluids and enhanced hydrocarbon production. Conductive fracture networks with desired dimensionless conductivity often significantly enhances hydrocarbon production. Water-based fluids, such as slick water, linear fluids, crosslinked fluids, foamed fluids, and viscoelastic surfactant (VES) fluids, are the most frequently utilized hydraulic fracturing fluids¹⁻³.

Natural fractures that are randomly positioned across unconventional shales interact with hydraulic fractures⁶ and create a complex fracture network. A slick water fluid system is often utilized to build a complicated fracture network for brittle shale formations⁷, while crosslinked fluids are frequently employed to produce the typical bi-wing cracks in ductile rock. Guar or guar-based derivatives, such as carboxymethyl hydroxypropyl guar (CMHPG), carboxymethyl guar, or hydroxypropyl guar, are the most often utilized crosslinked fracturing fluids. A guar-based polymer's insoluble residue can result in excessive low retained proppant permeability, especially for high gel loading, which is required to maintain the fluid's stability at high temperature. Using high fluid pH to achieve high temperature fluid stability can also promote the development of unfavorable

divalent ion scales.

Numerous synthetic fluids with acrylamide bases have been created and promoted as affordable substitutes. In earlier research, metal crosslinkers such as chromium⁸, titanium or zirconium compounds⁹, and acrylamide-methacrylate copolymer systems crosslinking with Cr^{3+} were used to crosslink high molecular weight acrylamide-acrylate copolymers¹⁰. A high temperature fluid employing a terpolymer of acrylamide and vinyl phosphonate crosslinked with a zirconium-based crosslinker was described by Gupta and Carman (2011)¹¹. Liang et al. (2016)¹² and (2017)¹⁵ described a number of synthetic acrylamide copolymer-based high temperature fracturing fluids that were either crosslinked with nano-sized particulate crosslinkers or with zirconium crosslinkers that were boosted by nanomaterials.

Fracture fluids have recently been tested at temperatures exceeding 300 °F. Wang et al. (2019)¹⁴ tested synthetic polymers and organic zirconium crosslinked fracturing fluids at temperatures as high as 356 °F. Almubarak et al. (2018)¹⁵ studied the synergy between synthetic polyacrylamide-based polymers and CMHPG crosslinked with zirconium, and showed improvements in fluid stability at 300 °F. Ogunsanya and Li (2019)¹⁶ reported the use of thiosulfate oxygen scavengers to enhance the thermal stability of a CMHPG zirconium crosslinked fracturing fluid up to 350 °F. Al-Hulail (2018)¹⁷ published the use of an encapsulated breaker to minimize the thermal degradation of a CMHPG-zirconium crosslinked fracturing fluid. Surface modified nanoparticles are used as internal breakers in VES-based fracturing fluids for high temperature applications by Sangaru et al. (2017)¹⁸. Use of carbon nanotubes with zwitterionic VES leads to higher thermal stability of fracturing fluids¹⁹.

For high temperature wells, guar-based fracturing fluids need to be formulated with higher polymer loading, and at a high pH, that leaves insoluble residue, which enhances concerns of formation damage. During the research and development phase, polymer loading was reduced without compromising the proppant carrying capacity of the fracturing fluid. A thermally stable acrylamide-based polymer with a reduced polymer loading of 30% to 40% less than guar-based fracturing fluid was developed to minimize formation damage concerns. During development, the fluid system demonstrated robust stability at high temperatures while barely affecting core flow or proppant pack conductivity under laboratory testing conditions^{12,15}. Karadkar et al. (2020)²⁰ recently reported a systematic approach to field deployment of a newly developed reduced polymer loaded fracturing fluid.

A reduced polymer loaded fluid system for a well with an extreme bottom-hole static temperature (BHST) of 340 °F was tested. A successful field deployment was achieved by performing the following tasks: chemical management, quality control, optimization of fracturing fluid formulations with field water and reservoir cool-down conditions, improved field mixing procedures,

on-site QA/QC, data fracturing treatment with novel fluid and calibration of fracture design, and execution of the main fracture treatment.

Experimental Methods

Fluid Preparation

The reduced polymer loaded fracturing fluids were prepared using polymer suspension having 2.5 lb/gal of thermally stable acrylamide-based polymer, stabilized in mineral oil. At 511 l/s and 80 °F, the polymer suspension has a viscosity of 264 cP. To prepare 25 lb/1,000 gal (ppt) reduced polymer loaded fracturing fluids, 10 gal/1,000 gal (gpt) polymer suspension was used. A weak organic acid was used as a buffer to maintain the pH of the fracturing fluid system at 5. A metal crosslinker was used to crosslink the reduced polymer loaded fracturing fluid system, which can work up to 350 °F.

The breakers package included two breakers, one live and one encapsulated, depending on the fluid stability requirement. The viscosity of fracturing fluid prepared using synthetic polymer greatly depends on the water quality. The mixing water used for field implementation was sourced from one of the water wells.

Table 1 lists the geochemical analysis of the water used to prepare the fracturing fluid.

Linear Gel

The linear gel or non-crosslinked gel was prepared by hydrating the polymer in mixing water for 10 minutes.

Table 1 The geochemical analysis for water used to prepare the fracturing fluid.

Parameter	Unit	Mixing Water
Color	—	Clear
pH	—	7.9
Temperature	°F	73.1
Specific Gravity	—	1.006
Sulfate	mg/L	279
Chloride	mg/L	308.94
Bicarbonate	mg/L	215.79
Carbonate	mg/L	0
Calcium	mg/L	112
Magnesium	mg/L	45.198
Iron	mg/L	0.04
Conductivity	mS/cm	1.33
Turbidity	NTU	0.9
TDS	mg/L	533.2
Salinity	mg/L	0.62

Fig. 1 The viscosity of the linear gel at different polymer loadings.

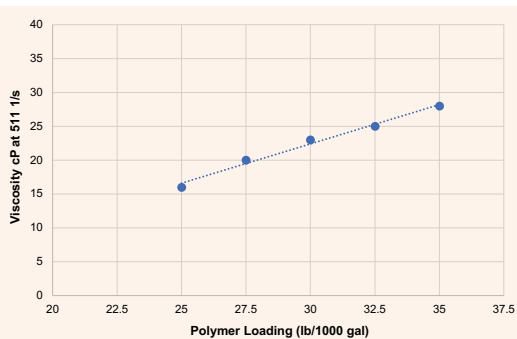
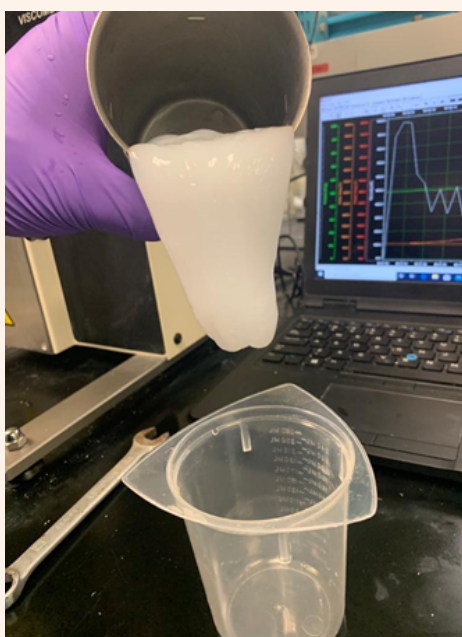


Fig. 2 The 35 ppt reduced polymer loaded crosslinked gel.



To enhance hydration, the pH of the linear gel was maintained at 5. The apparent viscosity and pH were measured using a FANN 35 viscometer at a 511 s^{-1} shear rate to help ensure complete hydration of the polymer.

Figure 1 shows the viscosity of the linear gel at different polymer loadings.

Crosslinked Gel

To prepare the crosslinked gel, a required amount of flow back enhancers, a clay-control agent, breakers, gel stabilizers, and crosslinkers were added to the linear gel. The pH of the fluid was adjusted to 5 using a buffer before the addition of the crosslinker. The rheology performance tests were carried out on the high-pressure, high temperature (HPHT) Chandler 5550 rheometer in accordance with the shear history

simulation specified in BS ISO 13503-1:2003 (2003)²¹.

Figure 2 shows a lip of crosslinked reduced polymer loaded fracturing fluid observed after 3 minutes and 30 seconds.

Fluid Rheology

Rheological tests were conducted to evaluate the proppant carrying capacity of fracturing fluid under bottom-hole conditions. The rheological properties of fracturing fluids influence fluid leakoff, which governs fracture width and extension. The fluid stability was judged by its viscosity measurements using a HPHT viscometer, applying a 100 1/s shear rate with 75 1/s, 50 1/s, and 25 1/s shear cycles. The fluid stability criteria was defined as the time required to reach 300 cP of viscosity at 100 1/s. The reduced polymer loaded fracturing fluid was optimized for one of the well candidates having a 340 °F BHST, which was considered for pad stage. The cool-down temperatures, 315 °F, 290 °F, 265 °F, and 240 °F were considered for the proppant laden stage fluid optimization.

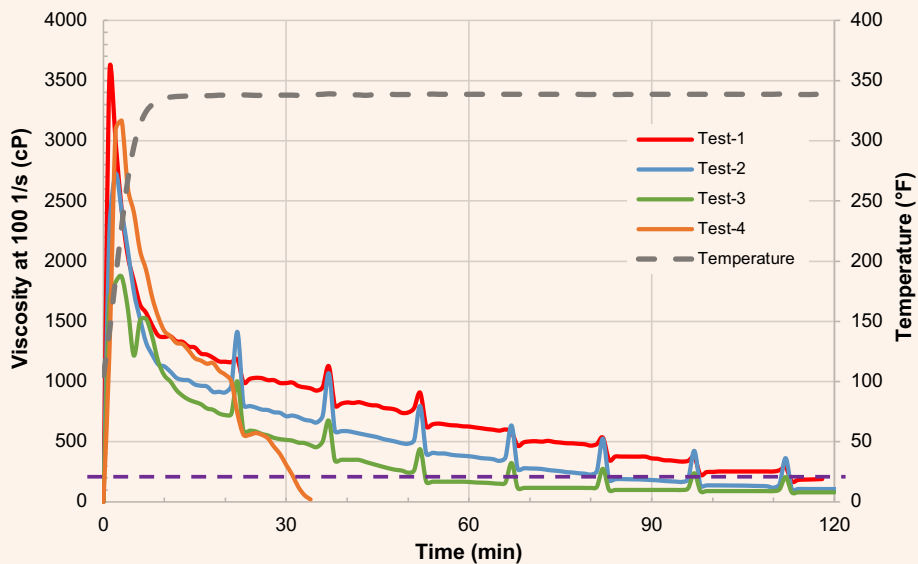
Table 2 shows the fluid formulations used to optimize reduced polymer loaded fracturing fluids at 340 °F, and Fig. 3 shows the fluid stability with the respective test number. A 35 ppt polymer loading with a 28 cP at 511 1/s shear rate linear gel viscosity was used for the 340 °F test temperature. Test-1, also known as the control test or the test without breakers, yielded 97 minutes of fluid stability. With the addition of 1 ppt of the encapsulated breaker, the reduced polymer loaded fracturing fluid stability was decreased to 47 minutes, Test-3. The fluid stability was further enhanced by increasing the high temperature stabilizer and gel stabilizer to 68 minutes, Test-2. The fluid viscosity was aggressively reduced to 30 minutes after using a 0.2-gpt live breaker, Test-4.

As the job progresses, the formation gets cooler and it is also required to optimize the fracturing fluid system with more breakers or reduce the polymer loading to further minimize formation damage and expedite the recovery of pumped fluids. Table 3 shows the fluid formulation, and Fig. 4 shows the rheology tests conducted at 315 °F and 290 °F. The reduced polymer loaded fluid polymer loading was reduced to 30 ppt from 35 ppt for the mid-temperature range. At 315 °F, 100 minutes and 60 minutes of fluid stability were achieved by reducing the high temperature stabilizer to 3 gpt and keeping both the live and encapsulated breakers constant. For 290 °F, after completely eliminating the high temperature stabilizer, 130 minutes of fluid stability was achieved. It was further decreased to 30 minutes by increasing the live breaker to 1.5 gpt.

Table 4 shows the fluid formulation, and Fig. 5 shows the rheology tests conducted at 265 °F and 240 °F. The reduced polymer loaded fluid was reduced to 27.5 ppt from 30 ppt for the low temperature range. For the low temperature tests, the gel stabilizer was completely eliminated, and the live breaker was increased to 2 gpt. The optimized fluid formulation was utilized to design the blender schedule for the selected candidate well.

Table 2 The 35 ppt reduced polymer loaded fracturing fluid formulation at 340 °F.

Additive	Unit	Test-1	Test-2	Test-3	Test-4
Biocide	ppt	0.5	0.5	0.5	0.5
Polymer	gpt	14	14	14	14
Surfactant	gpt	2.0	2.0	2.0	2.0
Clay Control	gpt	2.0	2.0	2.0	2.0
High Temperature Stabilizer	gpt	5.0	7.0	5.0	5.0
Gel Stabilizer	gpt	4.0	7.0	4.0	4.0
Buffer (pH 5)	gpt	3.2	3.2	3.2	3.2
Crosslinker	gpt	1.0	1.0	1.0	1.0
Live Breaker	gpt	0.0	0.0	0.0	0.2
Encap. Breaker	ppt	0.0	1.0	1.0	1.0

Fig. 3 The 35 ppt reduced polymer loaded fracturing fluid stability at 340 °F.

Field Execution

The candidate well was drilled as a horizontal well, targeting the tight HPHT sandstone reservoir. The well was completed with 4½” 15.1 lb/ft and 13.5 lb/ft carbon steel tubing, 4½” 15.1 lb/ft cemented liner, and a 7 × 4½” liner hanger. The BHST of this well was considered extreme ultra-high and at near the limit of most conventional fracturing fluids and e-line and coiled tubing bottom-hole assemblies. A total of six stages were initially planned to be proppant fractured using the plug and perf technique, however, the first two stages were skipped due to the low injectivity. Stage-3 was perforated with a total of 15 ft in two clusters

(1 × 5 ft and 1 × 10 ft clusters with 6 shot/ft density and 60° phasing). A proppant fracture treatment was performed using reduced polymer loaded fracturing fluids through the two perforation clusters in stage-3.

The formation fracture was initiated and an injection test, Fig. 6, was performed with 150 bbl of treated water that exhibited maximum surface and bottom-hole treatment pressures of 13,399 psi, and 19,300 psi, respectively, at a maximum pumping rate of 15.4 bpm. The closure pressure (P_c) and the reservoir transmissibility were determined to be 10,250 psi, the fracture gradient (FG) = 0.72 psi/ft, and 260 md.ft/cP, respectively, from the pressure decline analysis, Fig. 7.

Table 3 The 30 ppt reduced polymer loaded fracturing fluid formulation at 315 °F and 290 °F.

Additive	Unit	315 °F		290 °F	
		Test-1	Test-2	Test-3	Test-4
Biocide	gpt	0.5	0.5	0.5	0.5
Polymer	gpt	12	12	12	12
Surfactant	gpt	2.0	2.0	2.0	2.0
Clay Control	gpt	2.0	2.0	2.0	2.0
High Temperature Stabilizer	gpt	5.0	3.0	0.0	0.0
Gel Stabilizer	gpt	4.0	3.0	3.0	3.0
Buffer (pH 5)	gpt	3.2	3.2	3.2	3.2
Crosslinker	gpt	1.0	1.0	1.0	1.0
Live Breaker	gpt	1.0	1.0	1.0	1.5
Encap. Breaker	gpt	2.0	2.0	2.0	2.0

Fig. 4 The 30 ppt reduced polymer loaded fracturing fluid stability at (a) 315 °F, and (b) 290 °F.

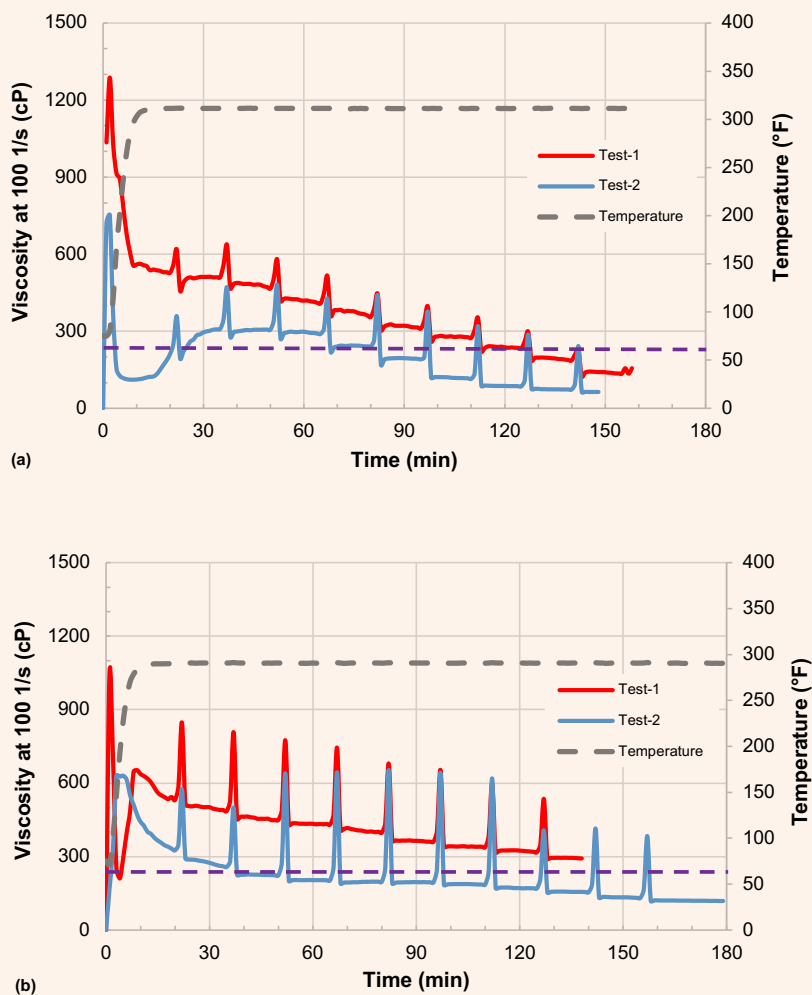


Table 4 The 27.5 ppt reduced polymer loaded fracturing fluid formulation at 265 °F and 240 °F.

Additive	Unit	265 °F		240 °F	
		Test-1	Test-2	Test-3	Test-4
Biocide	gpt	0.5	0.5	0.5	0.5
Polymer	gpt	11	11	11	11
Surfactant	gpt	2.0	2.0	2.0	2.0
Clay Control	gpt	2.0	2.0	2.0	2.0
High Temperature Stabilizer	gpt	0.0	0.0	0.0	0.0
Gel Stabilizer	gpt	1.0	0.0	0.0	0.0
Buffer (pH 5)	gpt	3.2	3.2	3.2	3.2
Crosslinker	gpt	1.0	1.0	1.0	1.0
Live Breaker	gpt	1.0	1.0	1.5	2.0
Encap. Breaker	gpt	2.0	2.0	2.0	2.0

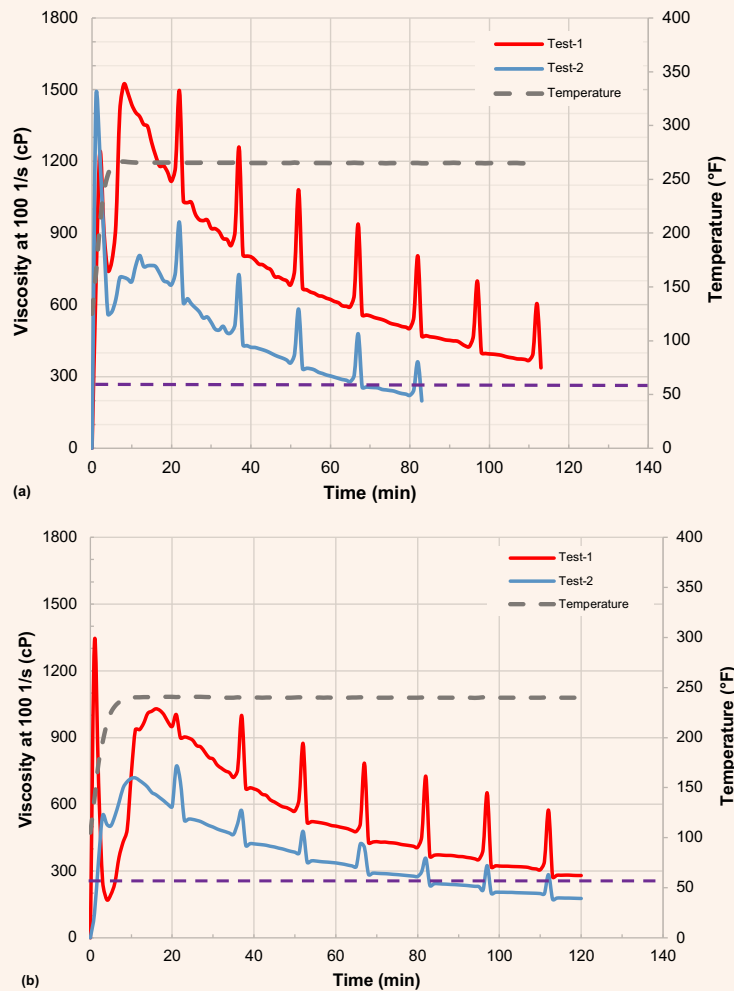
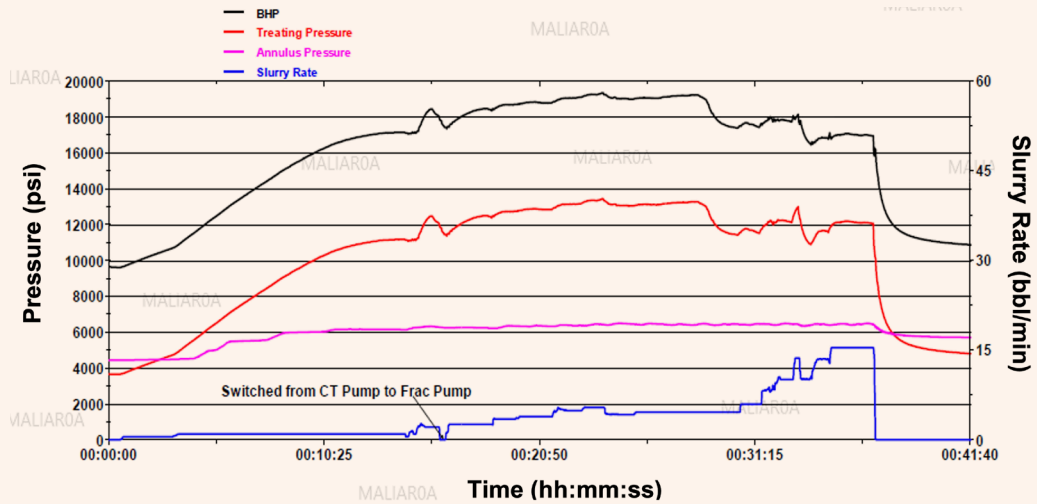
Fig. 5 The 27.5 ppt reduced polymer loaded fracturing fluid stability at (a) 265 °F, and (b) 240 °F.

Fig. 6 The results of the injection test.



Next, the step rate and step down tests were performed, Fig. 8, by pumping 147 bbl of treated water at a maximum pumping rate of 26 bpm. The fracture extension rate and pressures were determined to be 14,000 psi and 3.3 bpm, respectively, Fig. 9. The near wellbore pressure loss was calculated to be 1,800 psi at a pumping rate of 26 bpm.

A calibration injection test, Fig. 10, was done by injecting 340 bbl of reduced polymer loaded fracturing fluid at a maximum injection rate of 40 bpm. The maximum surface and bottom-hole pressures reached during the calibration injection test were 13,420 psi,

and 17,600 psi, respectively. The fracture closure and reduced polymer loaded fluid efficiency were determined to be 11,000 psi ($FG = 0.75$ psi/ft) and 30%, respectively, from pressure decline analysis using the G function method, Fig. 11.

The calibration treatment pressure was matched, Fig. 12, using a P_c of 11,000 psi that exhibited a fracture height growth of 113 ft.

Based on data obtained from the minifrac analysis, the fracture design was calibrated with 37% clean PAD, and 212,000 lb of 40/70 high strength proppant (HSP) stepping up the proppant concentration from

Fig. 7 The pressure decline analysis.

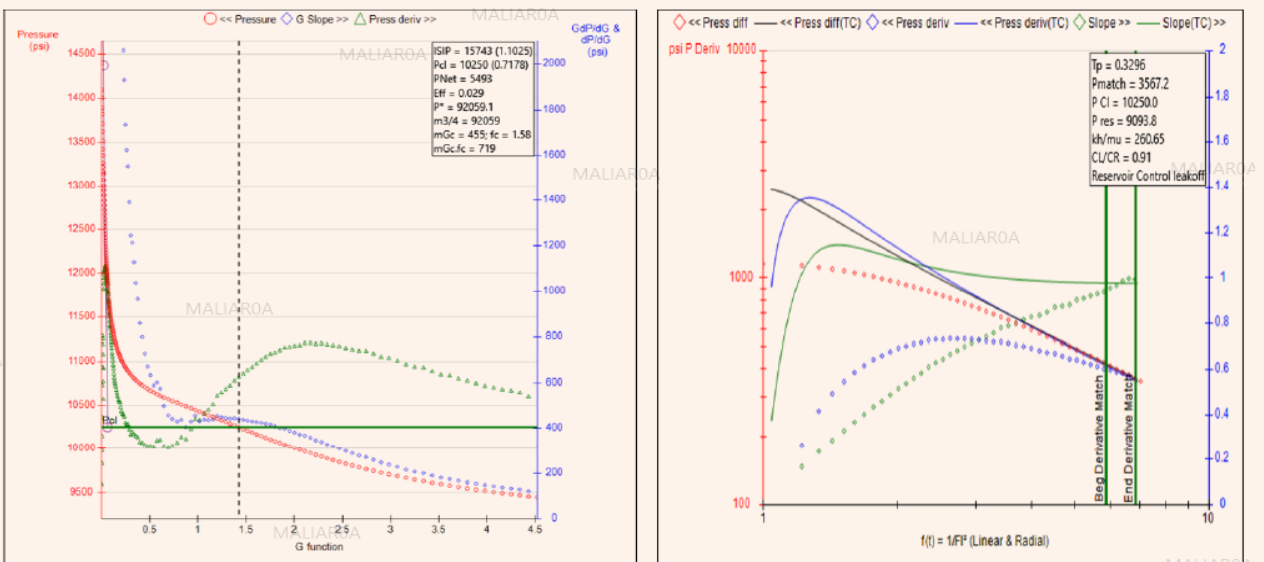


Fig. 8 The step rate and step down tests.

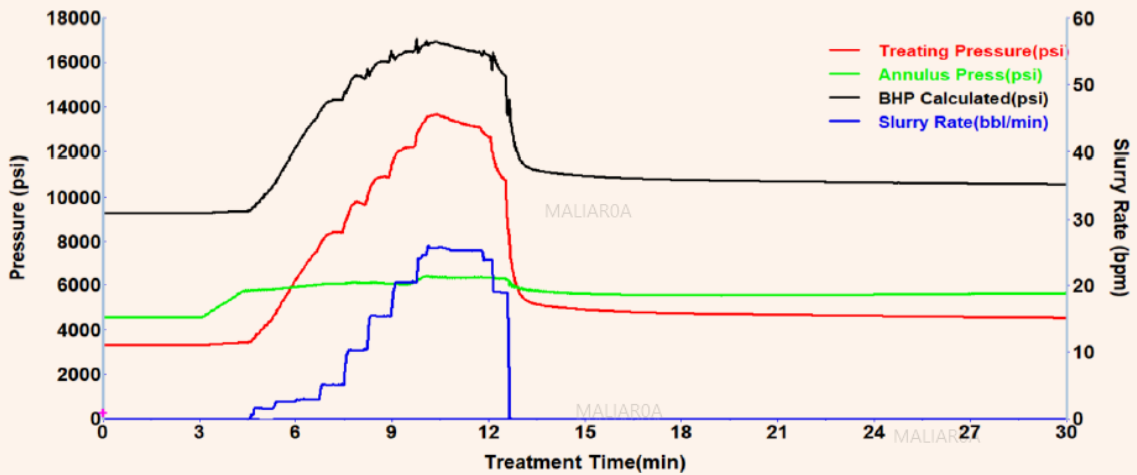
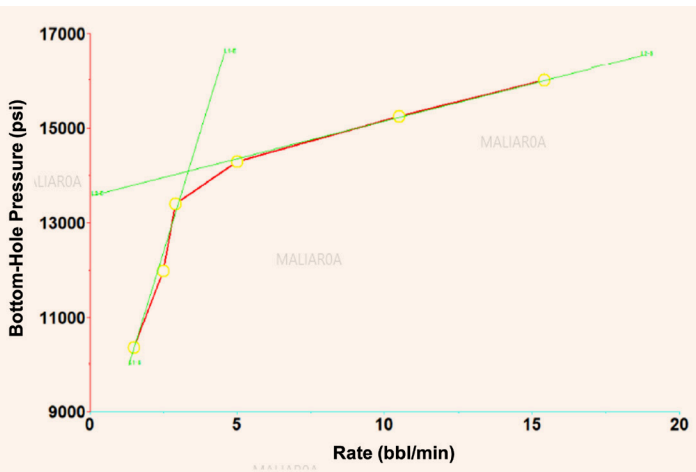


Fig. 9 The step rate and step down test analysis.



0.5 pounds per gallon (PPA) to 4.5 PPA at a pumping rate of 40 bpm.

Table 5 lists the simulated fracture geometry parameters and generated net pressure for clusters 1 and 2.

Quality Control On-Site

Table 6 lists the crosslinked reduced polymer loaded fluid quality check during the main fracturing job. Both linear gel and crosslinked gel samples were collected from the blender and high-pressure manifold, respectively. The fluid quality check was done by measuring the pH, linear gel viscosity using Fann 35, and lip/crosslink time at all stages throughout the main treatment.

Main Proppant Fracture Treatment

The main fracture treatment using reduced polymer loaded fracturing fluid was successfully pumped, Fig.

13. The fracturing treatment consisted of pumping a total of 218,000 lb of 40/70 HSP proppant in 2,624 bbl of reduced polymer loaded fluid (36 ppt gel loading) at a maximum pumping rate of 40.5 bpm. The proppant concentration was stepped up from 0.5 PPA to 4.5 PPA as per design. The treatment was flushed with 302.7 bbl of linear gel. All fluid additives pumped during the treatment were in accordance with the recipe based on lab tests at the surface and bottom-hole conditions. The maximum surface and bottom-hole pressures reached during the treatment were 12,908 psi and 16,994 psi, respectively. The surface instantaneous shut-in pressure was recorded at 5,775 psi, which then declined to 4,966 psi in 15 minutes.

The main fracture treatment pressure was matched, Fig. 14, using the P3D Model, and the actual fracture geometry parameters (fracture half-length, height, and width) are listed in the Table 7. The designed fracture geometry, previously shown in Table 5, and the actual fracture geometry obtained, Table 7, are very close, indicating reliable performance of the reduced polymer loaded fracturing fluid.

Conclusions

In comparison to guar-based fracturing fluid, the newly developed acrylamide copolymer-based nondamaging fracturing fluid system has several benefits, including low polymer loading and outstanding high temperature stability. The following conclusions can be reached based on efforts to transfer this technology from the laboratory to the field:

- During the pre-job laboratory testing, the reduced polymer loaded fracturing fluid was optimized at a BHST of 340 °F, and simulated reservoir cool-down temperatures of 315 °F, 290 °F, 265 °F, and 240 °F, as per BS ISO 13503-1:2003²¹, the shear history simulation.

Fig. 10 The calibration injection test with reduced polymer loaded fracturing fluid.

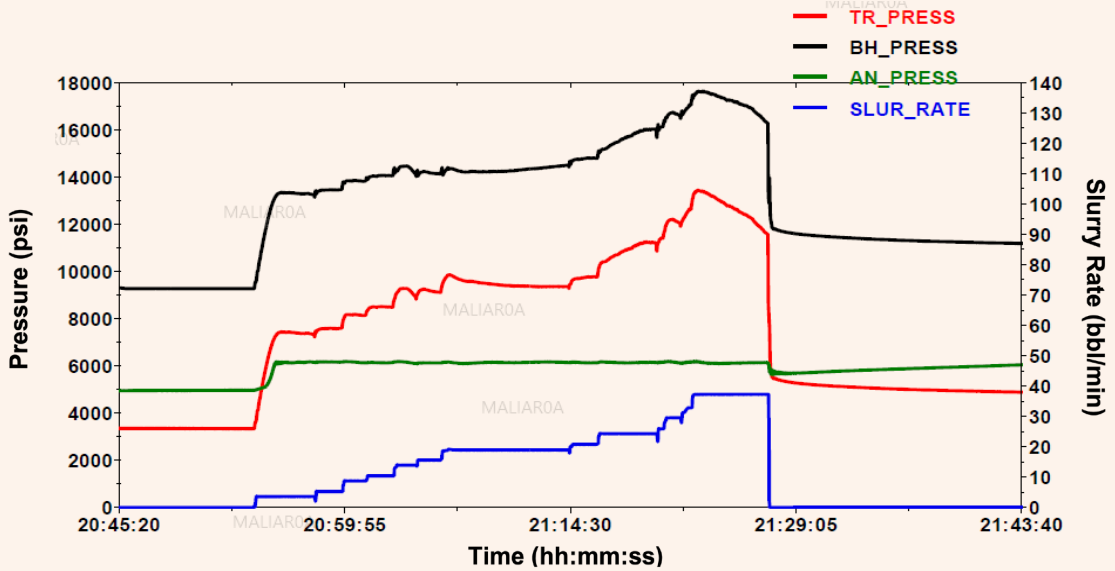
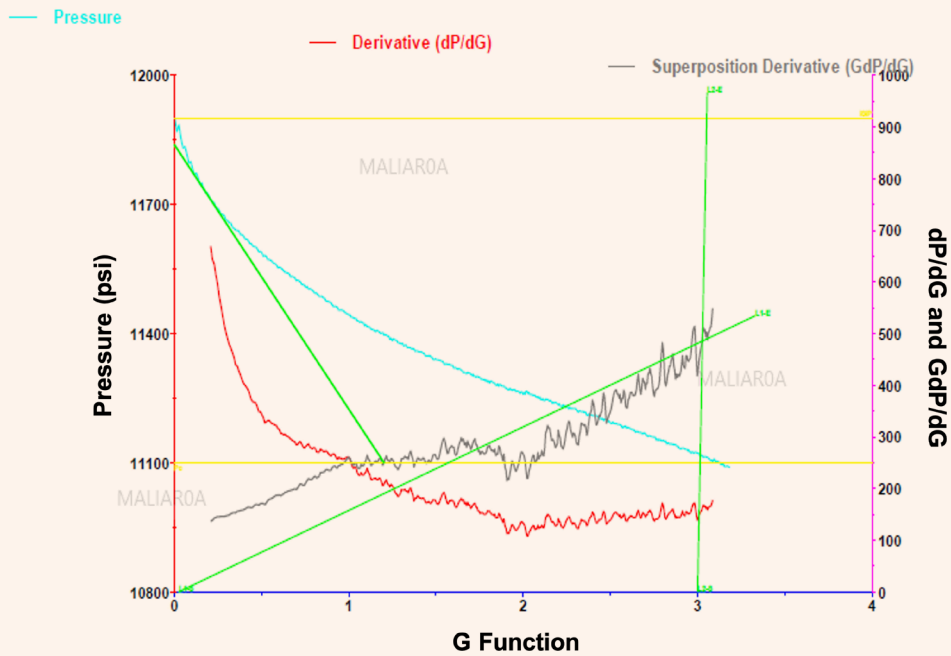


Fig. 11 The calibration (with a reduced polymer loaded fluid) decline plot.



- The reduced polymer loaded fluid was formulated utilizing only 35 ppt of polymer loading for extreme temperatures, 340 °F, and 27.5 ppt for cool-down conditions. The reduced polymer loaded fracturing fluid was used to successfully place the main fracturing treatment.
- During the main treatment, a total of 218,000 lb of 40/70 HSP proppant in 2,624 bbl of reduced

polymer loaded fracturing fluid, 36 ppt gel, was loaded at a maximum pumping rate of 40.5 bpm was pumped.

- Enhanced retained proppant permeability was achieved through reduced gel loading, and a larger volume of proppant pumped over a longer pumping period due to improved reduced polymer loaded stability of the PAD stage.

Fig. 12 The calibration (with a reduced polymer loaded fluid) treatment pressure match.

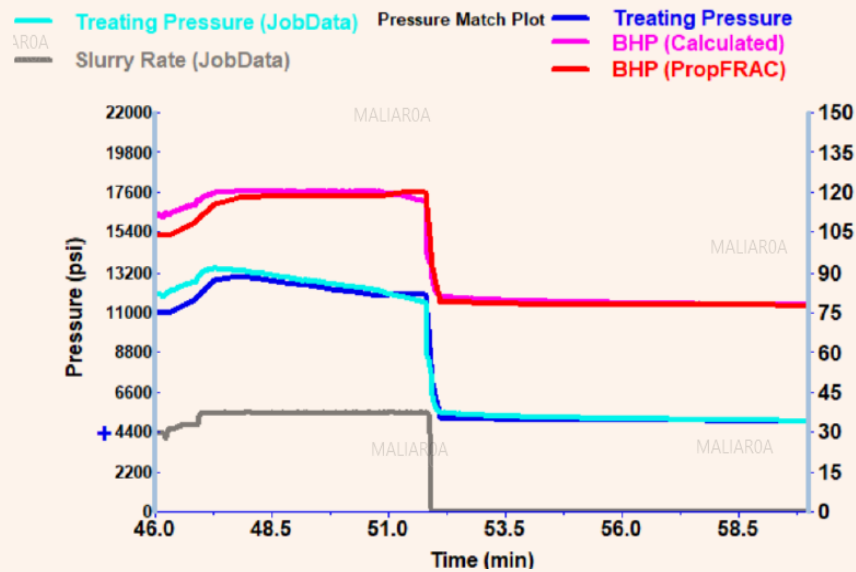


Table 5 The simulated fracture geometry parameters and generated net pressure for clusters 1 and 2.

Cluster	1	2
Propped Fracture Half-Length	146.1 ft	335.4 ft
EOJ Hyd Height at Well	105.2 ft	131.8 ft
Average Propped Width	0.10"	0.12"
Net Pressure	2,698 psi	2,707 psi

- The reduced polymer loaded fracturing fluid can be further optimized to a BHST as high as 400 °F.
- Due to the lower pH, the reduced polymer loaded fracturing fluid can be optimized to generate a foam system using CO₂.

Acknowledgments

This article was presented at the Gas and Oil Technology Showcase and Conference, Dubai, UAE, March 13-15, 2023.

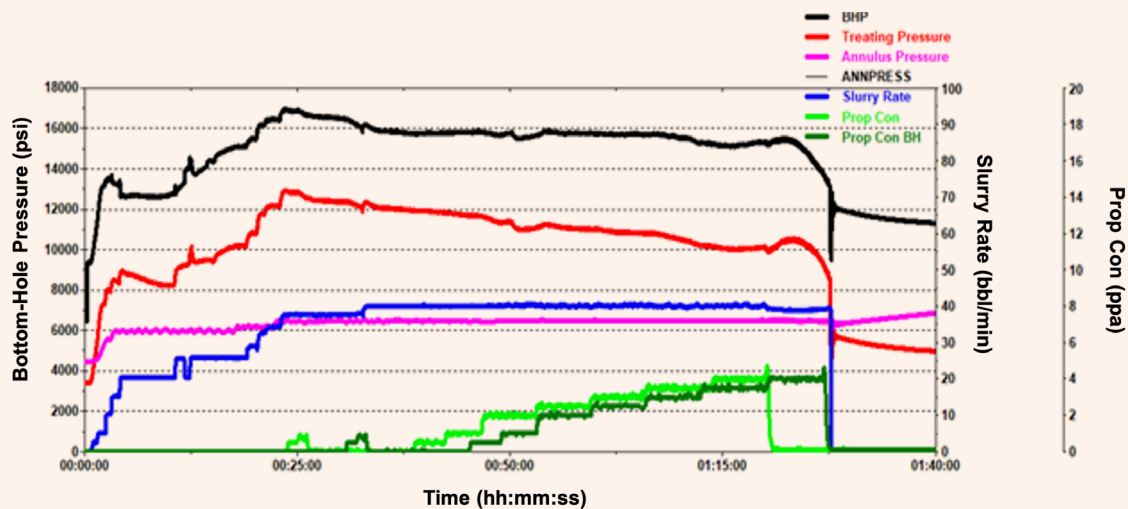
References

1. Fink, J.K.: *Oil Field Chemicals*, Gulf Professional Publishing, 2005, 506 p.
2. Rahman, M.M.: "Productivity Prediction for Fractured Wells in Tight Sand Gas Reservoirs Accounting for Non-Darcy Effects," SPE paper 115611, presented at the SPE Russian Oil and Gas Technical Conference and Exhibition, Moscow, Russia, October 28-20, 2008.
3. Al-Muntasheri, G.A.: "A Critical Review of Hydraulic Fracturing Fluids over the Last Decade," SPE paper 169552, presented at the SPE Western North American and Rocky Mountain Joint Meeting, Denver, Colorado, April 17-18, 2014.
4. Li, L., Al-Muntasheri, G.A. and Liang, F.: "A Review of Crosslinked Fracturing Fluids Prepared with Produced Water," *Petroleum*, Vol. 2, Issue 4, December 2016, pp. 313-325.
5. Wang, X., Sun, H., Zhou, J., Guerin, M., et al.: "A Non-Damaging Polymer Fluid System for Conventional and Unconventional Formations," SPE paper 174280, presented at the European Formation Damage Conference and Exhibition, Budapest, Hungary, June 5-5, 2015.
6. Rahman, M.M. and Rahman, S.S.: "Fully Coupled Finite Element-Based Numerical Model for Investigation of Interaction between an Induced and a Preexisting Fracture in Naturally Fractured Poroelastic Reservoirs: Fracture Diversion, Arrest, and Breakout," *International Journal of Geomechanics*, Vol. 15, Issue 4, July 2013, pp. 390-401.
7. Chong, K.K., Grieser, W.V., Passman, A., Tamayo, C.H., et al.: "A Completions Guide Book to Shale-Play Development: A Review of Successful Approaches toward Shale-Play Stimulation in the Last Two Decades," SPE paper 155874, presented at the Canadian Unconventional Resources and International Petroleum Conference, Calgary, Alberta, Canada, October 19-21, 2010.
8. Rhudy, J.S. and Knight, B.L.: "Fracturing Fluid," U.S. Patent No. 3,958,594, February 1976.
9. Williams, D.A., Newlove, J.C., Horton, R.L. and Chumley, R.E.: "Method of Treating Subterranean Formations Using a Non-Damaging Fracturing Fluid," U.S. Patent No. 5,007,481, March 1994.
10. Golinkin, H.S.: "Process for Fracturing Well Formations Using Aqueous Gels," U.S. Patent No. 4,157,182, January 1979.
11. Gupta, D.V. and Carman, P.: "Fracturing Fluid for

Table 6 The reduced polymer loaded fracture fluid quality check during the main treatment.

Stage Number	Stage Name	Linear Gel		Crosslinked Gel	
		pH	Viscosity, cP at 511 1/s	pH	Viscosity, cP at 511 1/s
1	Pre-Pad	7.1	28	—	—
2	PAD-1	—	—	6.33	2.5 min
3	0.5 PPA Slug	—	—	6.62	2.5 min
4	1.0 PPA Slug	—	—	6.7	2.5 min
5	PAD-2	—	—	6.24	2.2 min
6	0.5 PPA 40/70 proppant	7.09	24	6.42	2.5 min
7	1.0 PPA 40/70 proppant	—	—	6.2	3 min
8	2 PPA 40/70 proppant	—	—	5.8	3 min
9	2.5 PPA 40/70 proppant	7.81	23	6.82	3 min
10	3.0 PPA 40/70 proppant	7.07	20	6.21	2.5 min
11	3.5 PPA 40/70 proppant	7.08	20	6.65	2.35 min
12	4.0 PPA 40/70 proppant	7.73	20	6.1	2.2 min
13	Flush	—	—	—	—

Fig. 13 The main treatment chart.



Extreme Temperature Conditions is just as Easy as the Rest,” SPE paper 140176, presented at the SPE Hydraulic Fracturing Technology Conference, The Woodlands, Texas, January 24-26, 2011.

12. Liang, F., Al-Muntasheri, G.A. and Li, L.: “Maximizing Performance of Residue-Free Fracturing Fluids Using Nanomaterials at High Temperatures,” SPE paper 180402, presented at the SPE Western Regional Meeting, Anchorage, Alaska, May 25-26, 2016.

13. Liang, F., Al-Muntasheri, G.A., Ow, H. and Cox, J.: “Reduced Polymer Loading, High Temperature Fracturing Fluids by Use of Nanocrosslinkers,” *SPE Journal*, Vol. 22, Issue 2, April 2017, pp. 622-651.

14. Wang, J., Yao, E., Qiu, Y., Zhou, F., et al.: “Research and Evaluation of a Novel Low Friction, High Density and High Temperature Resistance Fracturing Fluids System,” ARMA paper 2019-0265 presented at the 53rd U.S. Rock Mechanics/Geomechanics Symposium,

Fig. 14 The treatment pressure match using the P3D Model.

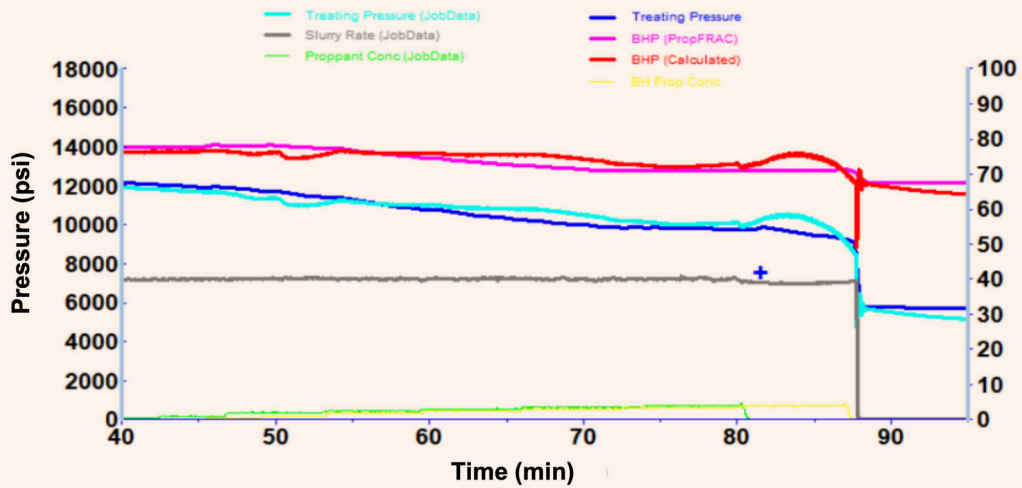


Table 7 The pressure match summary using the actual fracture geometry parameters.

Cluster	1	2
Propped Fracture Half-Length	155.2 ft	349.2 ft
EOJ Hyd Height at Well	109.8 ft	136.2 ft
Average Propped Width	0.11"	0.12"
Net Pressure	1,305 psi	1,583 psi

New York City, New York, June 25-26, 2019.

15. Almubarak, T., Ng, J.H., Sokhanvarian, K., Khaldi, M., et al.: "Development of a Mixed Polymer Hydraulic Fracturing Fluid for High Temperature Applications," URTEC paper 2896529, presented at the SPE/AAPG/SEG Unconventional Resources Technology Conference, Houston, Texas, July 25-25, 2018.
16. Ogunsanya, T. and Li, L.: "Safe Boundaries of High Temperature Fracturing Fluids," SPE paper 190029, presented at the SPE Western Regional Meeting, Garden Grove, California, April 22-26, 2018.
17. Al-Hulail, I., Al-Khabbaz, H., Al-Janabi, Y., Rahal, R., et al.: "Fracturing Fluid Encapsulated Breaker: High Temperature up to 350 °F," SPE paper 190379, presented at the SPE EOR Conference at Oil and Gas West Asia, Muscat, Oman, March 26-28, 2018.
18. Sangaru, S.S., Yadav, P., Huang, T., Agrawal, G., et al.: "Surface Modified Nanoparticles as Internal Breakers for Viscoelastic Surfactant-Based Fracturing Fluids for High Temperature Operations," SPE paper 188050, presented at the SPE Kingdom of Saudi Arabia Annual Technical Symposium and Exhibition, Dammam, Kingdom of Saudi Arabia, April 24-27, 2017.
19. Afra, S., Samouei, H., Mahmoudkhani, R. and Nasr-El-Din, H.A.: "A Novel Nanotube/VES-Based High Temperature High-Pressure Fracturing Fluid," SPE paper 199251, presented at the SPE International Conference and Exhibition on Formation Damage Control, Lafayette, Louisiana, February 19-21, 2020.
20. Karadkar, P., Alabdrabalnabi, M., Liang, F. and Buenrostro, A.: "A Systematic Approach to Deploy a Novel Nondamaging Fracturing Fluid to Field," OTC paper 30267, presented at the Offshore Technology Conference Asia, Kuala Lumpur, Malaysia, November 2-6, 2020.
21. BS ISO Standard 15505-1:2005: "Petroleum and Natural Gas Industries — Completion Fluids and Materials — Part 1: Measurement of Viscous Properties of Completion Fluids," September 2005, 20 p.

About the Authors

Prasad B. Karadkar

*M.S. in Chemical Engineering,
Nagpur University*

Prasad B. Karadkar is a Petroleum Engineer with the Production Technology Team of Saudi Aramco's Exploration and Petroleum Engineering Center – Advanced Research Center (EXPEC ARC). Prior to joining Saudi Aramco in April 2016, he worked as a Senior Technical Professional for Halliburton for 9 years. Prasad's areas of expertise include developing new fluid systems in the area of hydraulic fracturing,

acidizing, diversion, and water shutoff.

He has authored and coauthored 16 papers, published one patent, and has several patent applications in process.

In 2003, Prasad received his B.S. degree in Chemical Engineering from Shivaji University, Kolhapur, India, and in 2007, he received his M.S. degree in Chemical Engineering from Nagpur University, Nagpur, India.

Ataur R. Malik

*M.E. in Chemical Engineering,
City College of the City University
of NY*

Ataur R. Malik is a Petroleum Engineer Consultant who joined the North Ghawar Gas Production Engineering Division of Saudi Aramco's Southern Area Production Engineering Department in 2008. Prior to joining Saudi Aramco, he worked with Schlumberger as a Well Stimulation Specialist in Canada and offshore Malaysia. Ataur has comprehensive well services and production enhancement experience in onshore and offshore operations. He has been deeply involved in the design, execution, and evaluation of hydraulic fracturing treatments in carbonate, sandstone, and coal seam reservoirs.

In 1995, Ataur received his B.S. degree in Chemical Engineering from Washington State University, Pullman, WA, and in 1998, he received his M.E. degree in Chemical Engineering from City College of the City University of New York, New York, NY.

He is registered as a Professional Engineer with the Association of Professional Engineers, Geologists, and Geophysicists of Alberta (APEGA), Canada, and is a member of the Society of Petroleum Engineers (SPE). Ataur has published numerous SPE papers related to well intervention, stimulation, and production enhancement.

Mohammed I. Al-Abdrabalnabi

*B.S. in Chemical Engineering,
King Fahd University of Petroleum
and Minerals*

Mohammed I. Al-Abdrabalnabi is a Petroleum Engineer working with the Production Technology Division of Saudi Aramco's Exploration and Petroleum Engineering Center – Advanced Research Center (EXPEC ARC). The team targets well productivity enhancements such as laser oriented fracturing, optimized

fracture conductivity, and water shut-off by chemical means.

In 2015, he received his B.S. degree with honors in Chemical Engineering from King Fahd University of Petroleum and Minerals (KFUPM), Dhahran, Saudi Arabia.

Dr. Feng Liang

*Ph.D. in Organic Chemistry,
Rice University*

Dr. Feng Liang is currently the Production Technology Leader at the Aramco Americas (formally Aramco Services Company), Aramco Research Center-Houston. She has now been with the company for over nine years.

Prior to joining the Aramco Research Center, Feng was a Principal Scientist at Halliburton for nearly eight years. Her research interests are the new materials and product development in fracturing fluid, advanced fluid additives, waterless fracturing technologies, biodegradable diversion materials, sand control products, cement additives, nanomaterial reinforced elastomers and sustainability areas such as CCUS and hydrogen production technologies.

Feng is a contributor to many patents and technical papers. She holds over 80 issued U.S. patents and 30 additional published patent

applications. Feng is the author and coauthor of more than 90 technical papers, with a few in very high impact factor journals such as the *Journal of the American Chemical Society* and *Nano Letters*. She has also coauthored two book chapters as well. Feng's publications have received over 4,800 citations.

She is a member of the Society of Petroleum Engineers (SPE) and the American Chemical Society (ACS). Feng received the 2017 SPE Production and Operations Award for the Gulf Coast North American Region. She also received the 2017 Effective Publication Award from Saudi Aramco's Exploration and Petroleum Engineering Center – Advanced Research Center (EXPEC ARC).

Feng received her Ph.D. degree in Organic Chemistry from Rice University, Houston, TX.

Global First 18.625" and 13.375" Level-2 Casing-while-Drilling Successful Deployment through Open Hole and Cased Hole Sidetracked Wellbores to Isolate Severe Unstable Zones

Salahaldeen S. Almasmoom, Ahmed S. Refai, Faris A. Al-Qahtani and David B. Stonestreet

Abstract /

During nonproductive time (NPT) such as stuck pipe incidents, reducing the operational time and associated cost of the trouble mitigation should always be the goal. Therefore, our engineering team searched for new and innovative ways to reduce the NPT when stuck pipe incidents happen, and successfully utilized an existing technology in a new way not yet performed on a global basis.

In very few incidents, drilling or tripping through unstable zones (especially when drilling through sticky shales and loose sandstone zones charged with downhole faults/fractures) with complete loss of circulation, severe tight spots, stalling tendencies, hard backreaming, etc., might be experienced. In the worst-case scenario, the pipe might get stuck and cannot be freed. The engineering team investigated several options to allow drilling and casing off the trouble zones in such incidents, while reducing the NPT at the same time. Sidetracking through open hole and/or cased hole whipstock, then utilizing Level-2 casing-while-drilling (CwD) technology to drill and case off the instable zones was the best cost-effective option.

Successful deployment of Level-2 16" × 13% CwD technology through an 18% cased hole sidetrack whipstock and Level-2 22" × 18% CwD technology through an open hole sidetrack led to drilling and casing off severe unstable sections in two separate wells in different areas of interest. The Level-2 13% CwD utilization to drill and case off trouble zones through a cased hole sidetrack was the global first. The Level-2 18% CwD utilization to drill and case off trouble zones through open hole sidetrack was the country first.

Both led to significantly reducing the NPT that resulted from the stuck pipe incidents in a cost-effective manner. Extensive engineering simulations, technical limits, and risk assessments were set to ensure flawless execution. During the job execution, the drilling performances were constantly monitored. The engineering simulations are updated using the actual parameters to ensure accurate measurements of the accumulated fatigue while being rotated to preserve the casing, due to exposure to high dogleg severity (DLS) in the sidetracked wellbore. Furthermore, the hydraulics are optimized in real-time to ensure hole cleaning without further increase in the equivalent circulating density (ECD).

Even with no prior global experience of the utilization of this technology through such an operation, the pursuit of the technical limit was to reduce the NPT as much as possible. This article will highlight the planning steps, challenges, detailed engineering simulation, risk mitigations and engineered solutions, and the successful results of the deployment of Level-2 CwD runs through sidetracked wellbores.

Introduction

Casing-while-drilling (CwD) is a relatively new commercial well construction process in which standard casing is used as a drillstring to deliver both rotary and hydraulic power to a drill bit and/or bottom-hole assembly (BHA) connected to the casing. Attempts to use CwD were reported in 1920¹. Since commercial CwD technology was introduced for testing trials in 1999², it has gradually matured to address various drilling problems and challenges to the extent it is now used in many applications to drill from one casing shoe to the next casing point in vertical, tangent, and directional sections.

Maturity of the technology has led to multiple casing drilling technology configurations being available for implementation, Fig. 1. The two types of the CwD systems are the non-retrievable system, and the retrievable BHA system.

The non-retrievable system uses a rotating tool to turn the casing at the surface and a drillable bit made up

to the casing on the bottom to drill the formation. The casing in this system is considered as the drillstring. Accessories are installed along the casing string to limit vibration and centralize the string for cementing after reaching the section target depth. This system can be implemented in any size of casing. Drilling is typically performed in a single run and does not allow the use of directional or logging tools.

The retrievable BHA system employs the same casing rotating tool and accessories as the non-retrievable system, but replaces the drillable bit with a retrievable BHA. While the casing remains as the drillstring, the retrievable system allows for the inclusion of conventional drilling BHA components, such as a mud motor, rotary steerable system, and/or measurements-while-drilling. The retrievable system allows for the retrieval of the BHA through the drift of the casing at any point in the drilling process using standard drillpipe and specialized retrieval tools.

The deployment of CwD allows for the casing to be constantly on bottom, reducing the potential for incidents causing nonproductive time (NPT) due to wellbore instability. CwD stabilizes the formation while drilling. Each foot of borehole is drilled and cased off simultaneously, eliminating the need for a separate casing run.

Benefits of CwD Technology Implementation

CwD technology provides an excellent solution where total losses and/or borehole instability is registered as a critical drilling challenge. The solutions that CwD introduces toward addressing these challenges are briefly described as:

1. Challenge: NPT caused by loss of circulation and poor wellbore instability.

Solutions:

- a. Often reduces losses through the plastering effect, Fig. 2³.
- b. The ability to drill blind with no or partial returns.
- c. Better control on the mud cap and related chemicals.

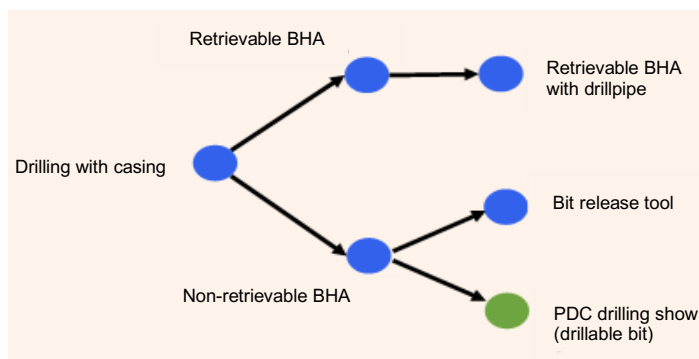
2. Challenge: Poor wellbore stability in highly depleted formations and/or interbedded sections.

Solutions:

- a. The plastering effect strengthens the borehole wall (smearing cuttings on the wellbore wall) while rotating the casing⁴. The smearing action strengthens the wellbore while it seals pores in the formation to reduce fluid loss, Fig. 2.
- b. The assurance of casing setting at the desired depth.
- c. Casing string elimination if the casing string is used for wellbore problems.

3. Challenge: Complex casing designs and time savings (faster process).

Fig. 1 A flow chart of the CwD techniques³.



Solution:

- a. The ability to slim well designs through CwD implementation. With the ability to case off combined trouble sections while drilling, casing strings can be eliminated by gaining the ability to set the parent casing deeper than originally planned, or by combining different trouble zones together in one section.

4. Challenge: Optimizing well duration in some areas of interest, and reducing associated cost accordingly.

Solution:

- a. Hole cleaning improvement: In general, CwD introduces significantly higher annular velocities, a critical factor in hole cleaning, than conventional drilling with the same flow rates, Fig. 2.

CwD System Selection

The CwD systems have widely expanded since its introduction as a new commercial technology in 1999. The system is divided into two different types with implementation in multiple locations around the world, Fig. 3. The Level-2 system requires a special drill shoe; combination of drillable alloy body, fixed cutter bit profile, and polycrystalline diamond compact (PDC) cutters. This drill shoe can be safely cleaned out to allow access to drilling lower formations. Having these features allow it to be drilled out with a standard PDC bit without the need of a dedicated clean out trip, improving drilling performance and effective hole cleaning.

After extensive cost comparison between the two systems to be selected for two different projects, utilizing the Level-2 CwD system was selected instead of the Level-3 CwD. The sidetracks are initiated using motor BHAs, and then drilling a comfortable section above the trouble zones. The CwD system is then run to drill and case off the trouble zones.

Two wells in separate areas of interest faced severe wellbore instability while drilling through sticky shales and loose sandstone zones, charged with downhole natural fractures. In both cases, both the loose sandstone

Fig. 2 The plastering effect and wellbore geometry while drilling with casing³.

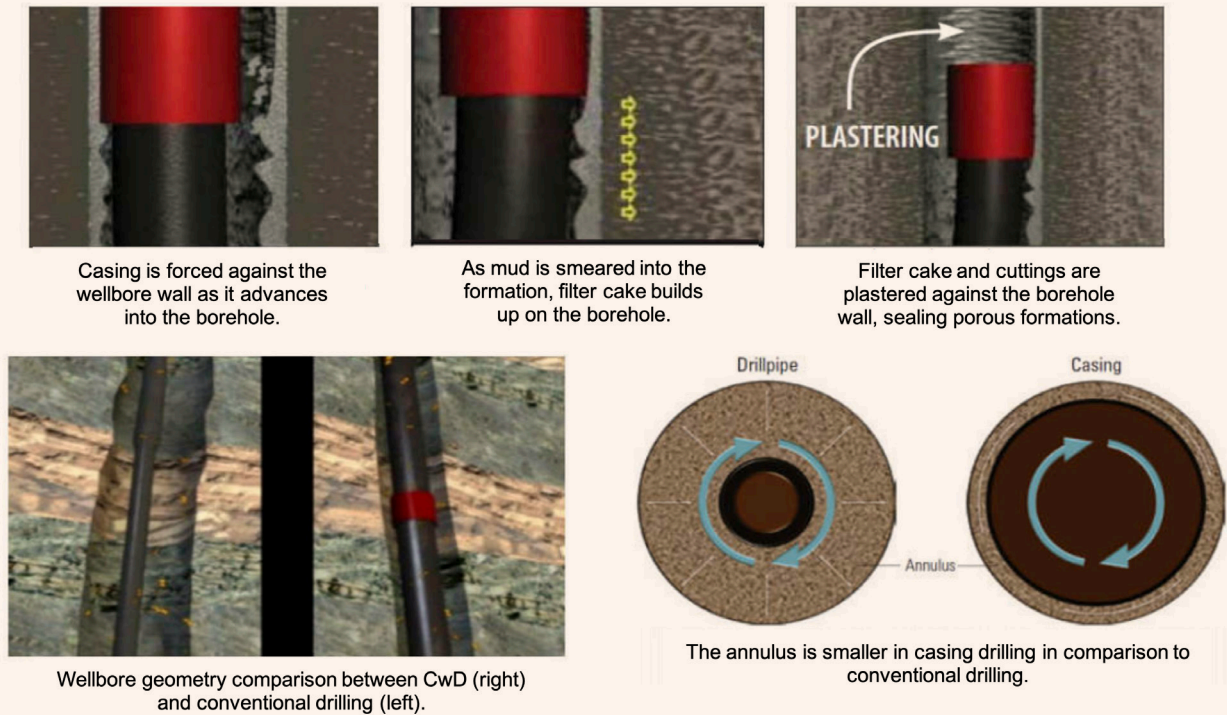


Fig. 3 The commonly used CwD systems. Level-2 was selected for the two wells to drill and case off the trouble zones through sidetracked wellbores³.



and the sticky shale zones became aggravated further due to drilling with complete loss of circulation, leading to wellbore collapse and the drilling string getting stuck at the BHA. The stuck pipe incidents in both wells happened off-bottom while backreaming out of the open wellbore. The wellbore section sizes were 16" and 22".

A cased hole sidetrack through an 18 $\frac{3}{4}$ " casing whipstock was performed successfully in the first well. A directional motor BHA was used to initiate the sidetrack and drill to above the lost circulation zone in the original wellbore. The Level-2 16" \times 15 $\frac{3}{8}$ " CwD system was implemented to drill through both the lost circulation and unstable zones, and case them off successfully. An open hole sidetrack through a cement plug was performed successfully on the second well. A directional motor BHA was used to initiate the sidetrack and drill down to above the lost circulation zone in the original wellbore. The Level-2 22" \times 18 $\frac{3}{8}$ " CwD system was implemented to drill through trouble zones and case them off successfully.

Challenges of CwD through Sidetracked Wellbores

During sidetracking, stepping away from the original wellbore requires a high dogleg

severity (DLS). Stepping away is necessary to avoid falling back to the original wellbore. Cased hole sidetracks might generate higher DLS when stepping away from the original wellbore when compared to open hole sidetracks. Overall, the DLS at the starting depth of the sidetrack might be within 3.0° to $10.0^\circ/100$ ft. Drilling/reaming with casing through this DLS range is challenging, requiring extra considerations when compared to the normal Level-2 CwD system.

Fatigue

Some of the casing joints will be exposed the most to the high DLS area in the well profile. Normally, the casing joints across the high DLS area at the time of initiating the casing rotation will be the highest casing joints with the risk to being fatigued. This is due to being exposed the most to the additional strain from the resultant rotation and/or drilling loads⁵.

Casing joint connections have a fatigue failure curve. The rotary/drilling loads have to be estimated and compared with the fatigue failure curve to determine the operational limits available before failing. Based on the well profile, the maximum estimated bending stress must be calculated first to calculate the resultant fatigue life of the casing joints most exposed to the bending loads. Based on the estimated accumulated fatigue life of the joints, the maximum total accumulated revolutions can be estimated.

Furthermore, since there is no control on the well profile while drilling with casing with the Level-2 CwD system, the drop in inclination due to drilling with casing has to be taken into consideration. An assumed gradual drop of $1^\circ/100$ ft can be used. Then, the effect of the inclination drop is taken into the bending stress estimation.

Rotating at the same location for a prolonged period should be completely avoided. With the high DLS around the sidetracked area, high accumulated fatigue due to the excessive generated side forces can be a

reason for premature failure of the casing string. It is critical in the case of cased hole sidetracks as the casing string is being affected by both the side forces generated, and the sharp cut in the body of the cemented casing string. The instantaneous rate of penetration (ROP) performance becomes critical when it dramatically drops. Therefore, continuous real-time analysis is required to evaluate the situation, and may stop drilling if the drilling performance does not improve.

Torque and Drag

The highest estimated surface torque is calculated and compared with the optimal makeup torque of the casing connections. If total losses are expected, extra safety factors might need to be applied to account for the cuttings that cannot be evacuated to the surface or into the fractures. Surface torque may build up.

The expected buckling in the casing string while applying weight on bit (WOB) on the surface needs to be estimated. The maximum WOB is determined and taken into consideration in regards to the expected total revolutions of the job. Any limitation of the WOB might affect the drilling performance.

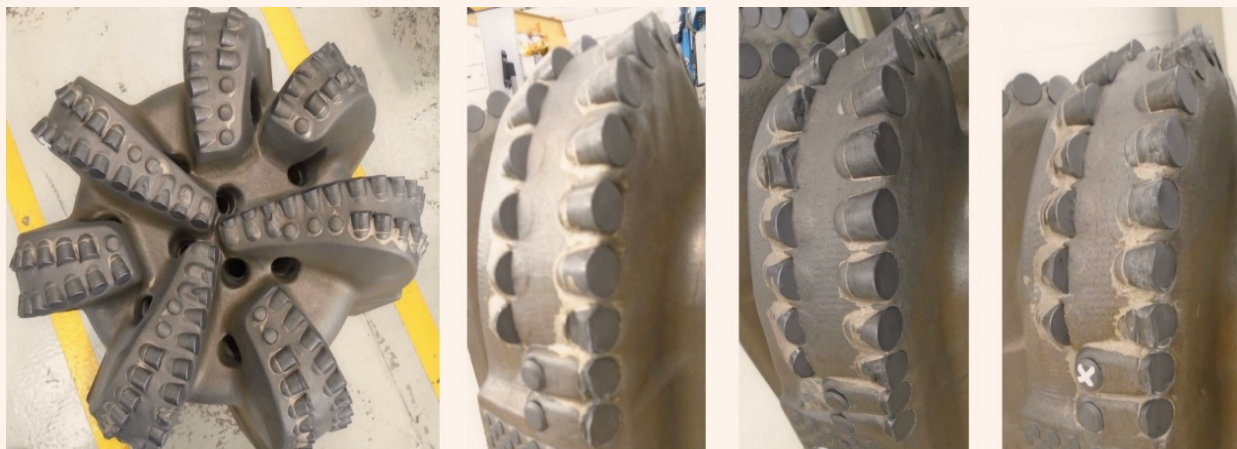
Job Planning

Drill Shoe Bit Selection

In the past, drill shoe design inherited a basic PDC bit profile since the application targeted drilling softer formations. Therefore, the older bits' designs usually are not optimized enough to be considered.

For the 16" bit design, two different profiles of PDC bits were used to find the optimized baseline profile. The tested designs are: 6-blades with 16-mm cutter length, 7-blades with 13-mm cutter length, and 7-blades with 16-mm cutter length designs. After gathering the 16" PDC bit's historical data in different areas of interest, the 7-blades with the 16-mm cutter profile design showed the best results in terms of drilling performance (ROP) and bit wear, Fig. 4. It is chosen

Fig. 4 The typical wear condition of newly run 16" PDC bit 7-blades with 16-mm PDC cutters when drilling through similar formations. The wear condition is excellent to be reused again to drill through the same application several times⁶.



as a baseline to build the drill shoe design, Fig. 5.

Another enhancement is related to the hydraulics. Lower flow rates are required to compensate for the high annular velocity due to the small clearance between the casing and borehole wall, Fig. 6. Applying the same flow rates of the conventional drillstrings will enforce higher equivalent circulating densities

(ECD) in the wellbore. Therefore, with the normally lower flow rates while drilling with casing compared with the flow rates when drilling with the conventional drill string (± 600 to 700 vs. $\pm 1,000$ gallons/min), the overall hydraulic horsepower per square inch of the drill shoe will be lower.

This increases the risk of bit-balling, especially when drilling in the sticky formations (shales and loose sand). Those potentially sticky formations are commonly found in the surface sections in both areas of interest in question.

To combat this risk, an anti-balling coating is applied on the outer body of the bit. This feature is proven on the normal PDC bit runs in the 16" size and other sizes, especially when drilling through sticky shale deeper zones. The anti-balling coating is a metallic coating, Fig. 7, that is applied to the surface of the bit body. It greatly reduces the risk of cuttings sticking to the bit (bit-balling), and increases the chances of cleaning a balled up bit.

Multi-Torque Rings

Based on the torque and drag analysis, the torque at the drill shoe for the CwD is normally higher than the torque at bit for the conventional drilling ($\pm 5,000$ to $9,000$ vs. $\pm 3,500$ ft-lb). Adding this to the expected accumulated torque across the casing string to the surface, the torque close to the surface will most likely exceed the makeup of the typical American Petroleum Institute (API) connections.

Both CwD jobs through sidetracked wellbores presented have and an API standard buttress connection⁷. The API buttress connection for the 13 $\frac{3}{8}$ " 68 lb/ft casing has an optimum makeup torque of $\pm 13,000$ ft-lb. The buttress connection for the 18 $\frac{3}{8}$ " 115 lb/ft casing has an optimum makeup torque of $\pm 18,000$ ft-lb.

Torque rings, Fig. 8, are installed on the API-type

Fig. 5 The baseline 7-blades with a 16-mm cutter length PDC conventional drill bit design is on the left⁶, and the final design of the 16" drill shoe bit is on the right.

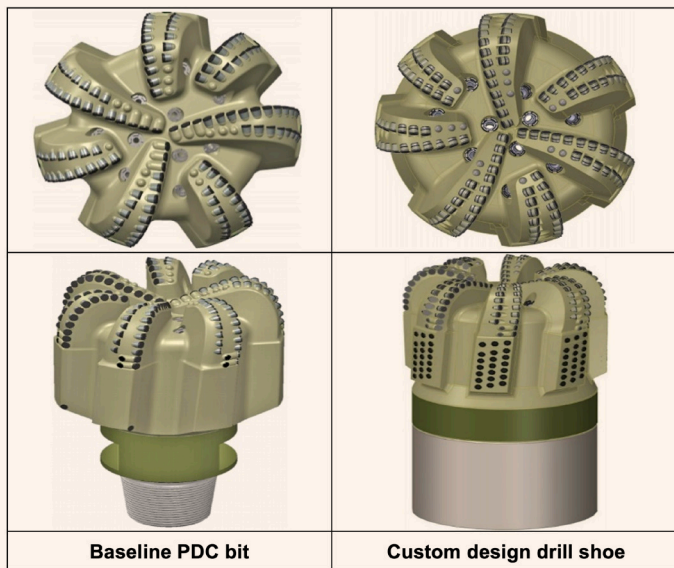


Fig. 6 The borehole wall clearance difference between casing drilling vs. conventional drillpipes/drill collars drilling⁶.

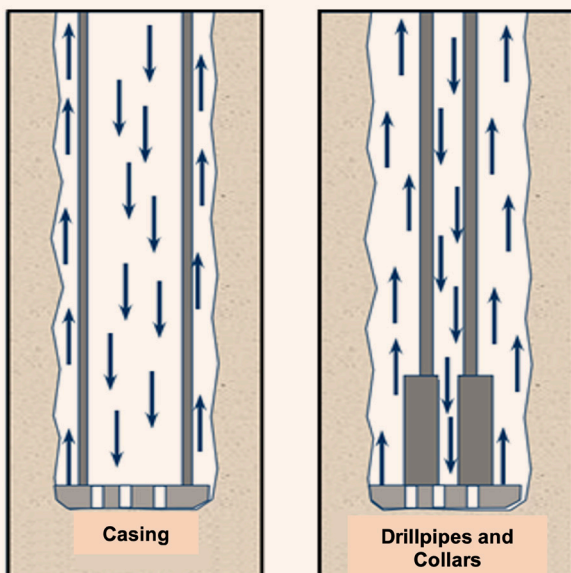


Fig. 7 The metallic anti-balling coating applied on the blades of the drill shoe, behind the cutters⁶.



Fig. 8 The different lengths of the multi-torque rings with different color codes, allowing for the small differences in the casing joint's connection lengths. The chart shows the capability to increase the makeup torque strength of the API casing connections.

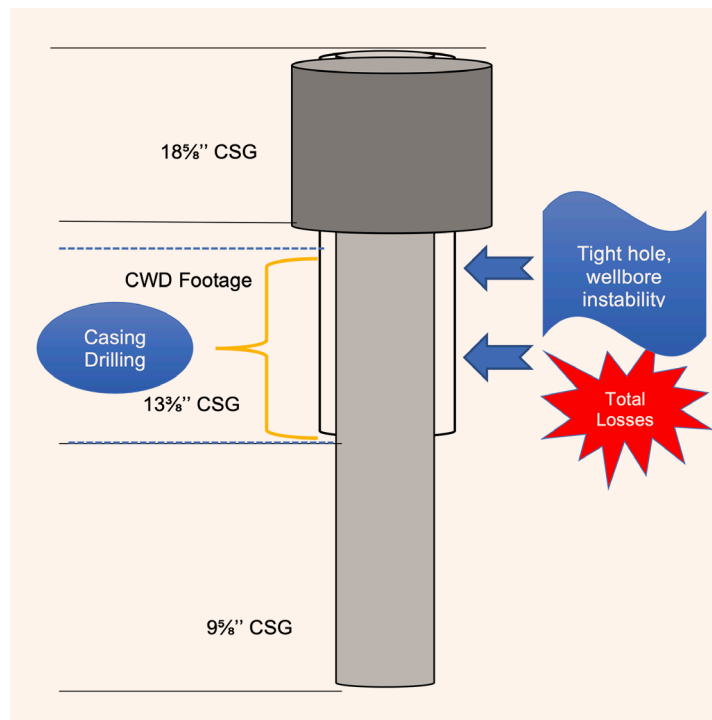


casing connections to increase the ability of the casing connections to handle higher torque values⁷. The connections are then converted to metal-to-metal seal-type connections, allowing the application of up to 50,000 ft-lb makeup torque on the connections. They come in slightly different lengths indicated by different color codes. The different torque rings will cover the differences in the connection lengths, Fig. 9. The slight differences in the length of the connections are normal during manufacturing of the casing joints.

Level-2 16" × 13³/₈" CwD through Cased Hole Sidetracked in 18⁵/₈" Casing

Subject Well-X was planned as a vertical development well. Offset well analysis has shown particular wellbore instability across a 16" section related to drilling through sticky shales and loose sandstone zones, charged with downhole faults/fractures to a lost circulation zone. Lost circulation is commonly experienced, which increases the complexity of controlling the wellbore's collapse; it is almost always drilled and cased off without issues. In the case of Well-X, it was managed to drill a 16" section to the casing point with total loss of circulation, and proper programmed specifications mixed on the fly drilling fluids and a 75 lb/ft³ mud cap. While pulling the string out, severe tight spots and a stalling tendency were experienced after the BHA got across the sticky shale and loose sand zone. The deeper sticky

Fig. 9 The planned Level-2 16" × 13³/₈" CwD drilling interval across a cased hole sidetrack.



shale zone is about five stands below the previous 18½” casing shoe. The drillstring required hard backreaming and slow pipe movement until the drillstring became stuck off-bottom near the previous casing shoe. After several unsuccessful attempts to free the pipe, the well was sidetracked through a 18½” cased hole whipstock, utilizing the Level-2 16” × 13⅝” CwD technology to drill and case off the instable zones, which was the best and most cost-effective option.

Challenges

The main challenges of utilizing the Level-2 16” × 13⅝” CwD technology across the 18½” whipstock were:

- The actual drilling performance with the CwD system with no previous history of the 7-blade drill shoe design.
- Reaching high fatigue when running the CwD system through the high DLS across the cased hole window (planned 6.0°/100 ft, actual 9.92°/100 ft).
- The inclination drop while drilling with the casing. The risk was drifting back to the abandoned wellbore.

Planning

Before running with casing across the cased hole window, the sidetrack motor BHA that initiated the sidetrack wellbore continued drilling to 30 ft above the lost circulation zone in the original wellbore. The wellbore inclination where the motor BHA stopped drilling was 7°. The intention is to compensate for the anticipated inclination drop when drilling through the planned zone with the 13⅝” 68 lb/ft casing.

To confirm that applying casing drilling is technically feasible, torque and drag, stress, and fatigue engineering simulations are performed. All simulations confirm that the results are within the technical acceptable range. With the cased hole whipstock in place, the well had

become more challenging with regards to downhole torque, stresses, and high fatigue on the casing string.

Torque and Drag Analysis: The torque and drag analysis was performed based on the maximum high-lighted parameters:

- WOB: 35,000 lb.
- Surface revolution per minute (rpm): 60 rpm.
- Flow rate: 700 gal/min.
- Open hole friction factor at 0.5 and cased hole friction factor of 0.3.

Based on the actual well profile of 9.92°/100-ft DLS at the cased hole window, and starting the CwD operation with 7° of inclination, the expected torque and drag results are illustrated in Fig. 10.

- There are no risks of buckling the casing with the planned maximum WOB.
- The expected total accumulated torque at the surface is ±15,000 ft-lb.
- The expected torque at the drill shoe is ±9,000 ft-lb.

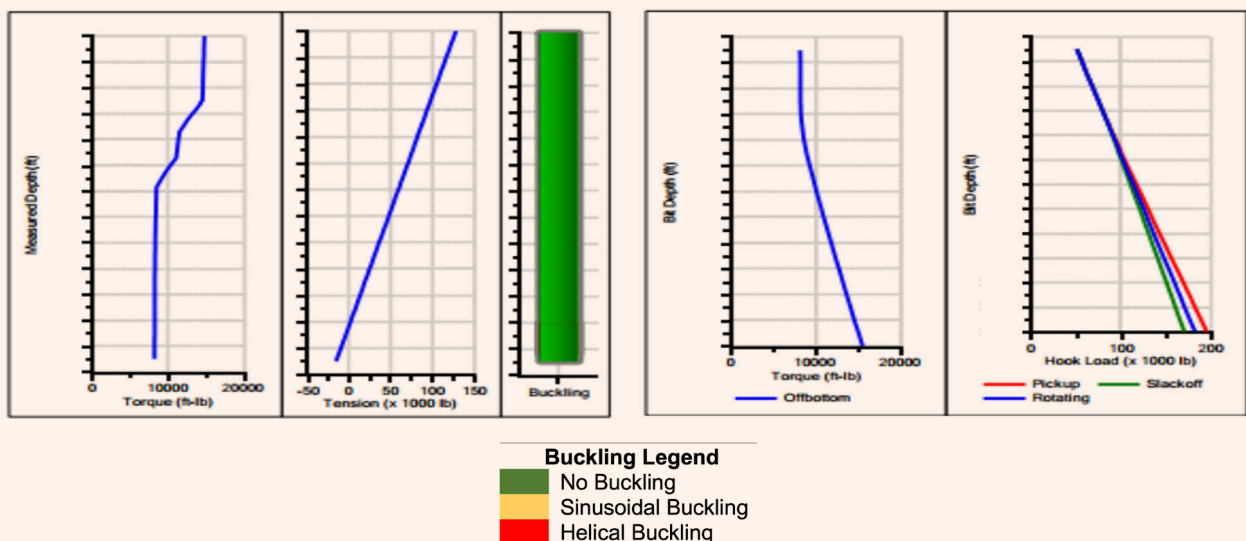
Hydraulic Sensitivity: The main estimation when running the hydraulics is the expected pumping pressure at the surface. It is compared with the maximum surface collapse pressure rating for the casing string. The maximum flow rate to be used is established (the maximum flow rate the drill shoe can handle can be used if the results of the simulation are acceptable).

Based on the simulation, the expected surface pumping pressure while using a 700 gpm flow rate is 525 psi, and is 630 psi with 800 gpm. Both estimated pumping pressures are less than the collapse pressure of the 13⅝” 68 lb/ft casing.

Casing Stress Analysis and Accumulated Fatigue

Life: The expected side forces on the casing string while rotating is estimated based on the well profile, which

Fig. 10 The torque and drag analysis for the 13⅝” casing of subject Well-X.



is done for each casing joint. From that, the maximum bending stress on the casing string is estimated. The accumulated bending stress will be used to estimate the maximum revolutions allowed while conducting the CwD operation.

Based on the casing stress analysis in Fig. 11, the expected maximum bending stress on the casing string is estimated to be 14,104 psi. Furthermore, the joints that are exposed to the maximum amount of side forces are (the peaks):

- Casing joint located across the sidetrack area when rotation is initiated.
- Casing joint across the sidetrack when the casing reaches the section total depth (TD).

The casing string is exposed to multiple uncertainties while drilling that might cause twist offs. Casing joints have been known to twist off while drilling, even when the actual accumulated fatigue life used does not reach 8%. As a result, the acceptable level of the used fatigue life while planning was set at 5%. In Fig. 12, the simulation presents the casing joint, which accumulates the most fatigue life used. It is the joint that is exposed to the highest risk of failure. The result illustrated in the right chart of Fig. 12 is actually of the casing joint across the sidetrack area when rotation is initiated. This casing joint will have the maximum exposure of the side force loads.

Based on the maximum bending stress, the estimated maximum total revolutions for the job is set at 250,800 revolutions, resulting in an estimated fatigue life use of 4.3%. The fatigue analysis with the actual survey, parameters to be applied, and the ROP expected had shown an alarming result of 4.3% of the casing joint. Therefore, close monitoring of the actual casing fatigue

life with respect to performance was done to ensure the total revolutions will not exceed the 5% mark.

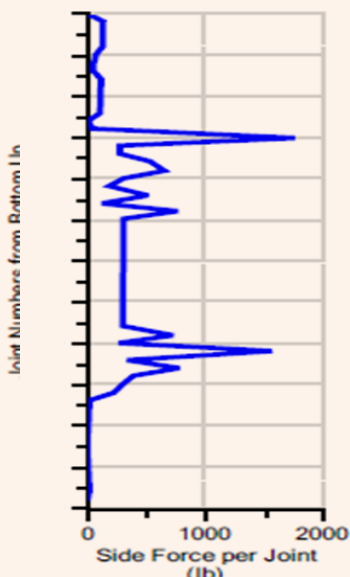
Execution and Results

A full magnetic particle inspection for the casing connection pin, connection box, and 2 ft from both ends of the connections were conducted for all casing joints, which are planned to be used. The fatigue accumulated the most toward both ends of the casing joints.

The Level-2 casing drilling BHA, Fig. 13, was picked up at 30 ft above the lost circulation zone experienced in the abandoned wellbore. An appropriate float collar was selected to ensure it can withstand the high flow rates required for drilling and hole cleaning, without compromising valve integrity during the cementing operations. Two float collars were used as a precaution to have two float valves in the casing string. The casing connections were fitted with the multi-torque rings to provide the torque capabilities required during drilling and reaming, with efficient seal ability. The drill shoe was tack welded in place as a torque ring cannot be fitted in its connection. The 28,000 ft-lb of makeup torque was applied as indicated in Fig. 13, based on the engineering torque and drag simulation.

Reaming started with casing with controlled parameters through the window, then casing drilling began operations with full returns. Table 1 lists the parameters used to ream and drill with casing. Despite having a total loss of circulation in the abandoned wellbore, which is about 50 ft away from the sidetracked wellbore, no losses were observed while drilling with casing due to the blistering effect, previously highlighted in Fig. 2. During the CwD operation, no vibration or bit whirl was observed. Furthermore, the torque and drag trends were in the acceptable range as per the engineering simulation. Moreover, no borehole instability issues

Fig. 11 The maximum bending stress and side forces for the 13 3/4" casing of subject Well-X.



Stress Analysis	
Maximum Bending Stress	14.104 Kpsi
Maximum % Yield	40.6%
Maximum Equivalent Reversing Stress	30.578 Kpsi
Stress calculations include the effect of coupling efficiency factor (in tension) for both bending and tension.	

Fig. 12 The planned accumulated fatigue analysis based on the planned well profile of subject Well-X.

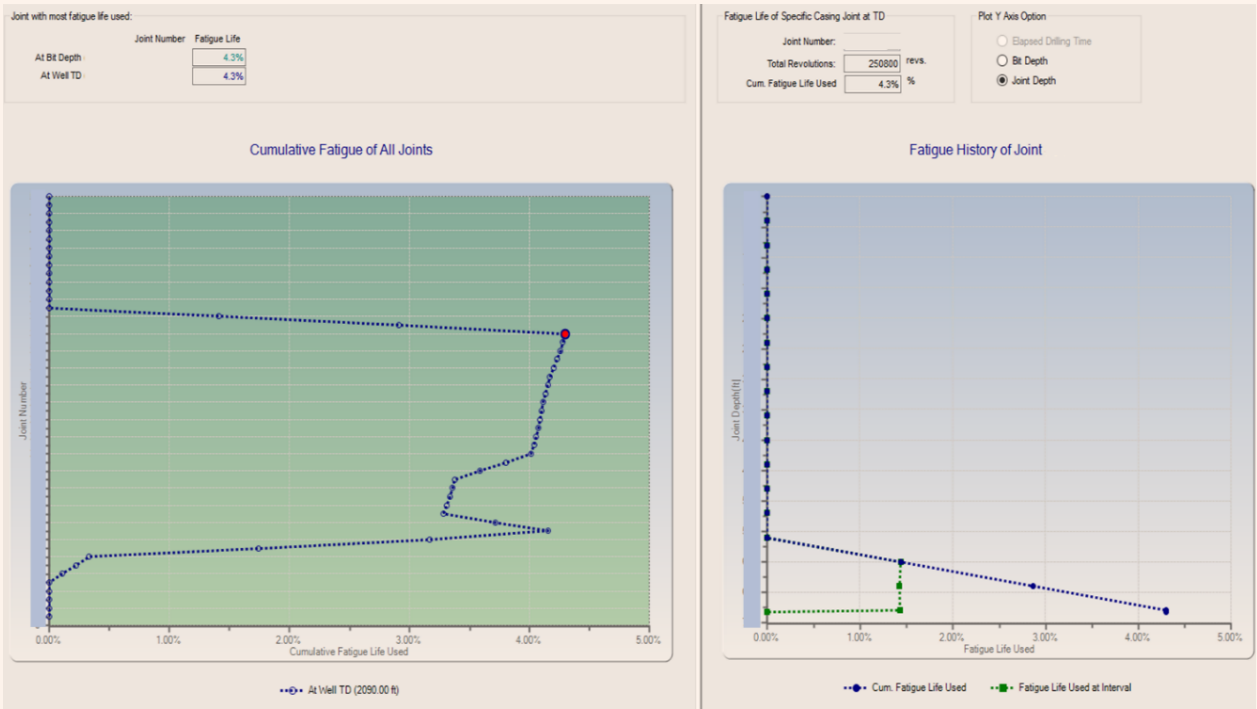


Fig. 13 The Level-2 16" x 13 3/8" CwD BHA.

PU Order	COMPONENTS	OD in	ID in	M/U Torque with MLT-TQ (Ft.lbs)			Weight ppf	Connection (Top/Bottom)		16"X13-3/8" Casing Drilling BHA Assembly
				Min	Opt.	Max.		Type	Gender	
G	CASING (All the rest to the Surface)	13 3/8	12.42		28,000		68.00	BTC	Box	
F	CASING JOINT	13 3/8	12.42		28,000		68.00	BTC	Box	
E	Float Collar	13 3/8	12.42		28,000		68.00	BTC	Pin	
D	CASING JOINT	13 3/8	12.42		28,000		68.00	BTC	Box	
C	Float Collar	13 3/8	12.42		28,000		68.00	BTC	Pin	
B	CASING Joint	13 3/8	12.42		28,000		68.00	BTC	Box	
A	16-in 7-bladed 16-mm cutters Drill-shoe	13 3/8	12.42		16,000			BTC	Box	

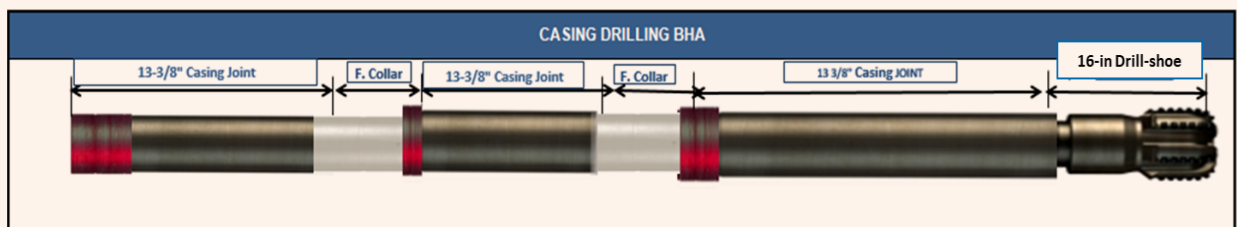


Table 1 The road map parameters for reaming and drilling with casing.

Operation	RPM	GPM	WOB K-LB
Ream Down	10 – 20	660	0 – 10
Casing Drilling	50 – 60	700	10 – 30

were observed. Drilling continued through the different section formations while applying the optimized drilling parameters as per the road map in Table 1 to section TD.

During the job execution, the drilling performances were constantly monitored. The engineering simulations were updated using the actual parameters to ensure accurate measurements of the accumulated fatigue while being rotated to preserve the casing due to exposure to high DLS (actual 9.92 vs. planned 6°/100 ft) in the sidetracked wellbore. Furthermore, the hydraulics are optimized real-time to ensure proper wellbore cleaning without further increase in the ECD.

Accumulated fatigue simulation was constantly

updated during the job execution to ensure that the total revolutions will not exceed the maximum pre-set value. The total revolutions actually were 120,643, Fig. 14. Subsequently, based on the actual well profile, which is tougher than the planned one, the actual accumulated fatigue consumed for the most critical joint was 6.3% compared to the planned 4.3%. It did exceed the acceptable technical limit set at 5.0%, but the casing withstood the fatigue resulting in a success. Figure 14 illustrates how important evaluating the actual real-time results are. The engineering simulations are updated and monitored accordingly.

Even with no prior global experience of the utilization of this technology through such an operation, the CwD operation went as planned, with no registered incidents. The average ROP was 33 ft/hour. The actual parameters and drilling performance are summarized in Fig. 15. The maximum surface torque was around 22,000 ft-lb, and the maximum pressure observed was around 1,100 psi. Both were higher than the estimated values, but still within the acceptable technical limits of the casing. The bit was drilled out with a previously used conventional PDC bit.

A used 12” conventional PDC bit was used to drill out the cemented in place 16” drill shoe. It was also used to dress the drill shoe with and without rotation,

Fig. 14 The planned accumulated fatigue analysis based on the actual well profile of subject Well-X.

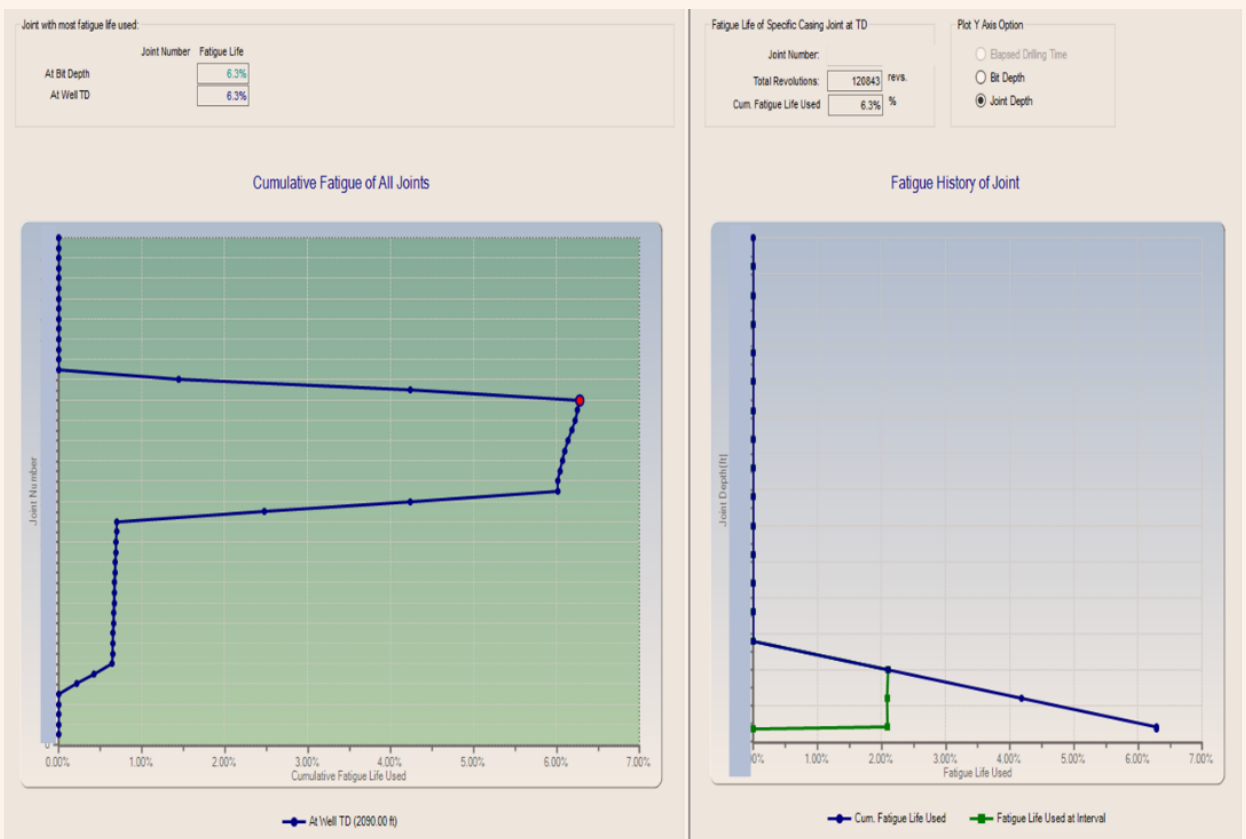
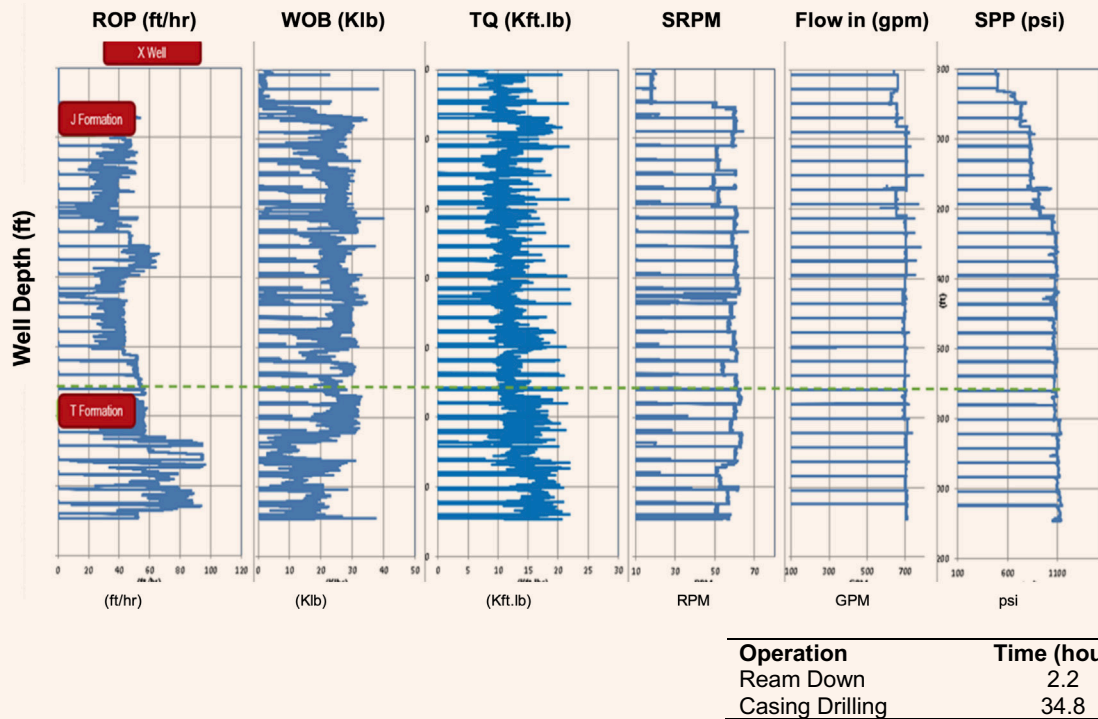


Fig. 15 The actual CwD performance of the first global utilization of the CwD Level-2 16" x 13 1/2" system through a 18 3/4" cased hole whipstock in subject Well-X.



and then drill a 10 ft hole. Figure 16 shows pictures of the used PDC bit before and after drilling out the drill shoe. The bit came out in a good shape through carefully applying the pre-set drilling out parameters. The WOB used did not exceed 15,000 lb, and the surface rotation used did not exceed 40 rpm.

Major Achievements and Highlights

1. No safety related incidents.
2. The first global utilization of the CwD Level-2 system to drill with casing through 18 3/4" cased hole

whipstock with the vendor supplying the CwD services.

3. The utilization of torque rings proved to enhance torque capabilities (actual around 22,000 ft-lb vs. optimum 15,000 ft-lb for the API buttress connections).
4. The hydraulics were optimized to ensure proper wellbore cleaning without increasing the ECD to induce losses.
5. The plastering effect efficiency was proven by drilling with casing to the planned depth with full

Fig. 16 A comparison between the used 12" conventional bit condition before and after drilling out the 16" cemented in place drill shoe. Also, a picture of the actual debris of the drill shoe collected on the surface.



returns, although the main wellbore was under total loss of circulation.

Well Surveys After the CwD Operation

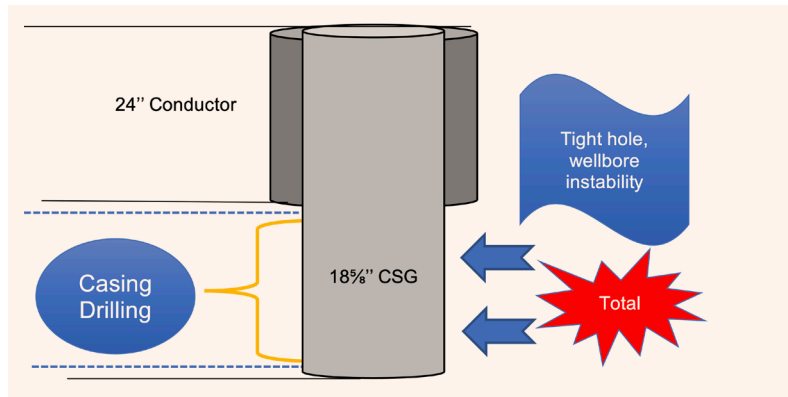
After the execution of the 16" x 13 3/8" CwD operation, a wellbore survey was taken to check the level of inclination drop. The results showed a total of 1.74° drop in inclination from 7.0° to 5.2°, after drilling a significant length with the casing, Table 2.

Level-2 22" x 18 5/8" CwD through Open Hole Sidetrack in 22" Wellbore

Subject Well-Y, Fig. 17, was planned as a horizontal development well. Offset well analysis has shown a non-major wellbore instability when drilling through the first 22" section of the well. The near surface formations consist of carbonates, loose sand, and shale. Moreover, the carbonate section is the main challenging zone while drilling with a complete loss of circulation; it is almost always drilled and cased off without issues.

In the case of Well-Y, it was managed to drill a 22" section below the total lost circulation zone. The plan was to trip out of the hole to change the BHA to remove the roller reamers to allow for smoother drilling to the section TD, as successfully done in the

Fig. 17 The planned Level-2 22" x 18 5/8" CwD drilling interval across an open hole sidetrack.



previously offset wells when such an incident happens. After encountering the total lost circulation zone, it was drilled further with the proper programmed mixed on the fly drilling fluids and a 80 lb/ft³ mud cap. While pulling the string out, severe tight spots and a stalling tendency were experienced after the BHA got across the loose sand zone.

The loose sand zone is shallower than the lost circulation zone. The drillstring required hard back reaming and slow pipe movement until the drillstring became stuck off the bottom near the surface. After several unsuccessful attempts to free the pipe, the well was sidetracked through a cement plug utilizing the Level-2 22" x 18 5/8" CwD technology to drill and case off both the loose sand and total lost circulation zone, which was the best and most cost-effective option. Extensive engineering simulations, technical limits, and risks assessment are set to ensure flawless execution.

Challenges

The main challenges of utilizing the Level-2 22" x 18 5/8" CwD technology were:

- The actual drilling performance with the CwD system with no previous history with the 8-blades with 16-mm cutter drill shoe.
- The well reached high fatigue when rotating the casing through the actual 3.38°/100-ft DLS vs. the planned 3.00°/100 ft across the sidetracked open hole wellbore.
- The inclination drop while drilling with casing, as it might drift back and contact the abandoned already drilled open wellbore.

Execution and Results

A full magnetic particle inspection was conducted for the casing connection pin, the connection box, and 2 ft from both ends for all casing joints planned to be used. The fatigue accumulates the most toward both ends of the casing joints.

After spotting a cement plug above the loss zone and across the loose sand zone, a motor BHA was used to initiate the sidetrack out of the original wellbore

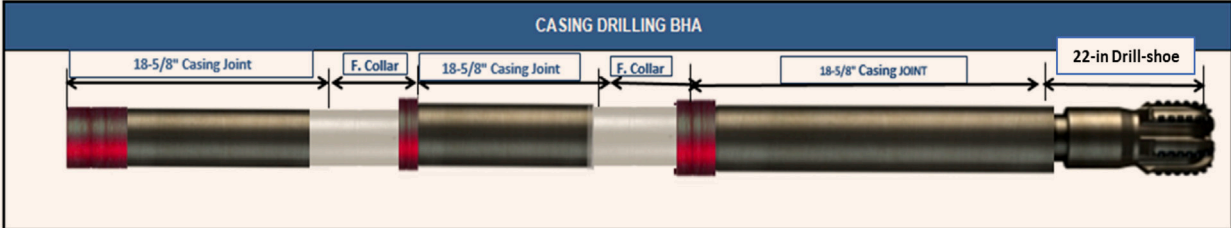
Table 2 The actual well surveys after completing the CwD operation.

Inclination (°)	DLS (°/100 ft)	
0.07	0	
4.72	9.92	
6.13	1.49	
6.79	0.78	
7.00	0.25	← Starting CwD Depth
6.87	0.14	
6.71	0.18	
6.52	0.20	
6.38	0.14	
6.10	0.32	
6.25	0.16	
6.19	0.06	
5.85	0.37	
5.61	0.26	
5.37	0.26	
5.32	0.10	
5.25	0.24	
5.26	0.04	← Section Total Depth

Fig. 18 The Level-2 22" × 18 $\frac{5}{8}$ " CwD BHA.

CASING DRILLING SHOE TRACK									
PU Order	COMPONENTS	OD in	ID in	M/U Torque with MLT-TQ (FT.lbs)			Weight ppf	Connection (Top/Bottom)	
				Min	Opt.	Max.		Type	Gender
G	CASING (All the rest to the Surface)	18 5/8	17.43	30,000			115.00	BTC	Box
F	CASING JOINT	18 5/8	17.43	30,000			115.00	BTC	Pin
E	Float Collar	18 5/8	17.43	30,000			115.00	BTC	Box
D	CASING JOINT	18 5/8	17.43	30,000			115.00	BTC	Pin
C	Float Collar	18 5/8	17.43	30,000			115.00	BTC	Box
B	CASING Joint	18 5/8	17.43	30,000			115.00	BTC	Pin
A	22-in 8-bladed 16-mm cutters Drill-shoe	22.00	17.43	18,000				BTC	Box

22"X18-5/8" Casing Drilling BHA Assembly



and drill the 22" section to 50 ft above the loss zone (maximum DLS was 3.38%/100 ft, 3° inclination). Then the Level-2 22" × 18 $\frac{5}{8}$ " CwD system (BHA in Fig. 18) was picked up, and reamed with a 18 $\frac{5}{8}$ " casing, and then drilling of the section began.

Figure 19 shows the used 22" × 18 $\frac{5}{8}$ " drill bit. After encountering the lost circulation zone, the drilling stopped and the casing was picked up to work the high accumulated torque as the loose sand started to fall in the annulus. Then, drilling was resumed to the section's TD. During drilling with casing and after getting thrown in the lost circulation zone, wellbore instability was experienced while making connections. It was closely monitored and dealt with right away by applying the optimized drilling parameters as per the road map in Table 5.

An appropriate float collar was selected to ensure it can withstand the high flow rates required for drilling and hole cleaning without compromising valve integrity during the cementing operations. Two float collars were used as a precaution so as to have two float valves in the casing string.

Accumulated fatigue simulation was performed during the job execution to ensure that the total maximum revolutions were not exceeded. Figure 20 shows that the accumulated fatigue life consumed was 3.1% at

a total of 35,640 revolutions. The accumulated fatigue consumed is almost the same as the planning phase (3.5% for the planning stage). Therefore, it is still within the acceptable technical limit of 5%. The accumulated fatigue limit was planned to be kept as

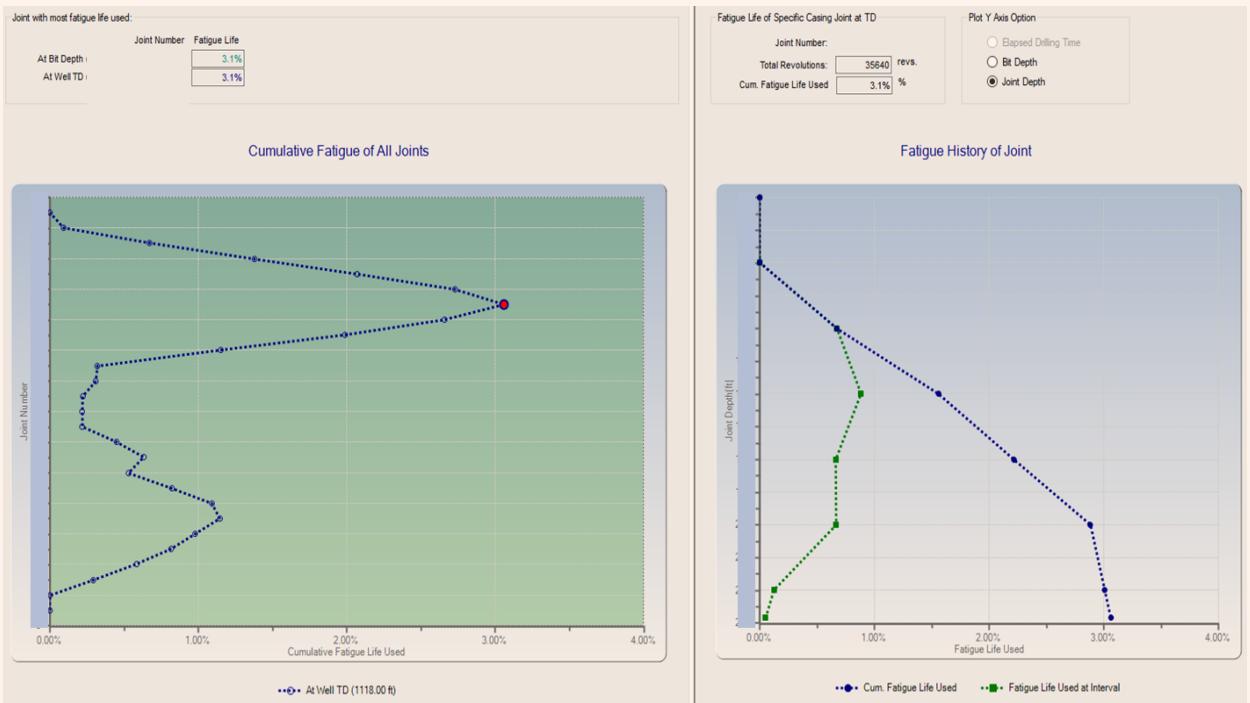
Fig. 19 The used 22" 8-blade bit with 16-mm cutter length with no backup raw drill shoe.



Table 3 The road map for the planned drilling parameters.

RPM	Recommended Makeup Torque = 30,000 for Casing Connection W/MLT			Comments
	WOB (Klb)	GPM	Max Torque (ft-lb)	
40 – 50	25 – 35	700 – 800	14,000	Monitor vibration, WOB maximum could be applied to 44 Klb. Monitoring hydraulic lift trend to ensure hole cleaning.

Fig. 20 The actual accumulated fatigue analysis for the 18 3/4" casing string with the actual well surveys.



low as possible as rotating the big casing under high DLS could lead to connection fatigue when compared with the 13 3/4" casing.

The actual parameters and drilling performance are summarized in Fig. 21. The maximum surface torque was set at 24,000 ft-lb. The actual surface torque was reaching the limit causing the applied drilling parameters to be controlled in the majority of the section.

Well Surveys After the CwD Operation

Based on Table 4, the inclination after the completed operations behaved different when compared to Table 2 for the smaller size casing. The different sidetrack system (open hole vs. cased hole), and the bigger casing size could be factors for the difference. The inclination dropped at first by almost 2.08°, then started to build

by approximately 1.11°.

Achievements and Highlights

1. No safety related incidents.
2. The first country Level-2 22" × 18 3/4" CwD system through an open hole sidetrack with the vendor supplying the CwD services.
3. The utilization of multi-torque rings to enhance torque capabilities (actual maximum torque experienced at the surface was approximately 24,000 ft-lb vs. a makeup torque of 18,000 ft-lb) for the API buttress connection without the torque rings.
4. Secured the total lost circulation zone.

Fig. 21 The actual CwD performance of the utilization of the CwD Level-2 22" × 18%" system through an open hole sidetrack in subject Well-Y.

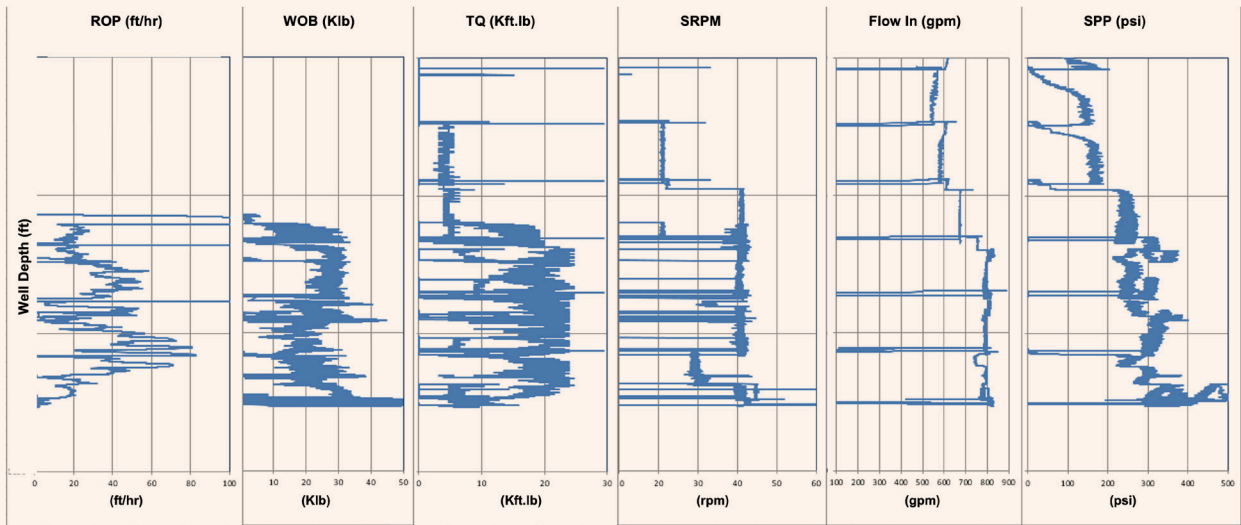


Table 4 The actual well surveys after completing the CwD operation.

Inclination (°)	DLS (°/100 ft)
2.88	2.22
0.96	2.61
0.80	1.32
1.11	0.63
1.26	0.65
1.91	0.66

Conclusions and Future Considerations

The CwD technology has many benefits, including reducing the associated cost, especially during the NPT period. The initial startup and planning required a thorough engineering analysis performed by the multidisciplinary engineering team, as these operations were globally unique. After the successful global utilization of the technology, further plans will be developed to build through such incidents to utilize the technology for further optimization efforts. This is an ongoing engineering process. Further performance improvement and optimization can be achieved.

Applying optimized parameters and connection practices can lead to more optimization by eliminating the need for a dedicated drill out trip to clean both drill shoes. Also, further development of the 22" drill shoe will be required to enhance the design and improve the performance. Increasing the number of cutters and the length of the blades are two design features to study.

Acknowledgments

This article was presented at the Middle East Oil and Gas Show and Geosciences Conference and Exhibition, Manama, Kingdom of Bahrain, February 19-21, 2023.

References

- Patel, D., Thakar, V., Pandian, S., Shah, M., et al.: "A Review on Casing while Drilling Technology for Oil and Gas Production with Well Control Model and Economical Analysis," *Petroleum*, Vol. 5, Issue 1, March 2019, pp. 1-12.
- Warren, T., Houtchens, B. and Madell, G.: "Casing Drilling Technology Moves to More Challenging Applications," paper AADE 01-NC-HO-52, presented at the AADE National Drilling Conference, Houston, Texas, March 27-29, 2001.
- Aljawder, A.E., Aljanahi, A.M., Almannai, H.E., Matar, O.A., et al.: "Casing while Drilling Successfully Implemented for the First Time in High Risk Area of the Bahrain Field," SPE paper 208068, presented at the Abu Dhabi International Petroleum Exhibition and Conference, Abu Dhabi, UAE, November 15-18, 2021.
- Karimi, M., Moellendick, T.E. and Holt, C.: "Plastering Effect of Casing Drilling; A Qualitative Analysis of Pipe Size Contribution," SPE paper 147102, presented at the SPE Annual Technical Conference and Exhibition, Denver, Colorado, October 30-November 2, 2011.
- Eriwwo, O., Roed, H., Javaid, M.O., Ngau, C.U., et al.: "Integrating Casing Drilling and Conductor Sharing Technology to Optimize Brownfield Redevelopment Plans," SPE paper 156054, presented at the SPE Annual Technical Conference and Exhibition, San Antonio, Texas, October 8-10, 2012.
- Sehsah, O., El Kawass, A., Siddik, S.M., Refai, A., et al.: "Casing while Drilling Transformation into Standard Operation in Middle East," IPTC paper 19730, presented at the International Petroleum Technology Conference, Dhahran, Kingdom of Saudi Arabia, January 15-15, 2020.

7. Al Fakih, A., Cengiz, H.O., Aldape, A.G., Halma, J., et al.: "First Use Worldwide of a Conventional Stage Tool Integrated with an Inflatable Packer Element for Casing while Drilling," SPE, paper 192209, presented at the SPE Kingdom of Saudi Arabia Annual Technical Symposium and Exhibition, Dammam, Kingdom of Saudi Arabia, April 25-26, 2018.

About the Authors

Salahaldeen S. Almasmoom

*M.S. in Petroleum Engineering,
University of Southern California*

Salahaldeen S. Almasmoom is a Senior Drilling Engineer with more than 12 years of professional working experience with Saudi Aramco. He is currently working in Saudi Aramco's Unconventional Resource Drilling Department, where over the last four years, Salahaldeen has been designing, planning, and executing unconventional vertical/horizontal wells. The scope of the wells span as exploration, appraisal, development, water disposal, and workover wells. Throughout his career, he has worked as a Drilling Engineer in various areas, including exploration and deep gas high-pressure, high temperature wells.

In addition to Salahaldeen's role as a Drilling

Engineer, he has been involved with several specialized teams focusing on improving drilling practices, introducing new technologies, and forecasting required materials/services. He has contributed to the introduction of new technologies for the first time on a country/global level.

He is a member of the Society of Petroleum Engineers (SPE) and has contributed as an author and coauthor on several industry papers.

Salahaldeen received his B.S. degree in Petroleum Engineering from the University of Louisiana, Lafayette, LA, and his M.S. degree in Petroleum Engineering from the University of Southern California, Los Angeles, CA.

Ahmed S. Refai

*B.S. in Mechanical Engineering,
University of Ain-Shams*

Ahmed S. Refai has been working in the Casing Drilling Technical Domain within SLB Saudi for the past four years.

Throughout his 20 years in the oil and gas industry, Ahmed has worked for different oil and gas operating companies with operations in the Middle East (onshore and offshore), including Qatar, Oman, Kuwait, the UAE, and Saudi Arabia. His focus was introducing and

developing casing-while-drilling as a new technology, collaborating with oil and gas companies to implement the casing-while-drilling technology in fields where unconventional methods are not successful.

In 2001, Ahmed received his B.S. degree in Mechanical Engineering from the University of Ain-Shams, Cairo, Egypt.

Faris A. Al-Qahtani

*B.S. in Petroleum Engineering,
King Fahd University of Petroleum
and Minerals*

Faris A. Al-Qahtani joined Saudi Aramco in 2012 as a Drilling Engineer. He began his career working in the Drilling and Workover Services Department for 3 years dealing with drilling services contacts. Faris was then assigned to an out-of-Kingdom Unconventional Resources program in Houston, Texas. In 2016, he joined the Unconventional Resource Drilling Department, working in both the Engineering and Operations divisions.

Faris has been designing, planning,

executing, and field supervising unconventional vertical and horizontal wells throughout the Kingdom.

He is a member of the Society of Petroleum Engineers (SPE) and has contributed as an author and coauthor on several industry papers.

In 2012, Faris received his B.S. degree in Petroleum Engineering from King Fahd University of Petroleum and Minerals (KFUPM), Dhahran, Saudi Arabia.

David B. Stonestreet

*B.S. in Petroleum Engineering,
University of Tulsa*

David B. Stonestreet has been working as a Drilling Engineering Supervisor within Saudi Aramco's Unconventional Resource Drilling Department for the past eight years.

Throughout his 35 years in the oil and gas industry, David has worked for different oil and gas operating companies with operations in

Texas (onshore and offshore), New Mexico, Oman, Algeria, and Saudi Arabia, primarily supervising and managing drilling, completion, and workover operations.

In 1986, David received his B.S. degree in Petroleum Engineering from the University of Tulsa, Tulsa, OK.

New Horizon for Downhole Scale Management toward Sustained Well Production

Hussain A. Almajid, Ibrahim K. Al-Thwaiqib and Carlos E. Amancio Ribeiro

Abstract /

Iron sulfide (FeS) scales are considered one of the most commonly encountered formation scale in the oil and gas industry, which can adversely impact well deliverability and integrity. Traditional chemical treatments using inorganic acids, such as hydrochloric (HCl) acid, are not favorable due to its corrosive nature and rapid generation of hydrogen sulfide (H₂S) gas. The success rate for such an operation is further challenged by the molar ratio of iron to sulfur and the existing polymorph of FeS, such as pyrite, pyrrhotite, troilite, marcasite, and mackinawite.

This article strives to share the laboratory development and field application results for a revolutionary chemistry that was developed as an integrated solution to dissolve FeS scales and inhibit further scale nucleation. Extensive laboratory testing was conducted under anaerobic conditions to create an evolved chelating agent with high FeS dissolution, minimal corrosion rate, and no H₂S generation. The experimental setup included in situ mixing of Fe(+2) and S(-2) to create FeS scale that were placed in glass vial reactors and exposed to specific temperature and pressure. Furthermore, a thorough evaluation of sulfide scale properties and behavior under varying reservoir pressure and temperature is incorporated into a computational model to understand and accurately control the scale deposition process.

Several clean out jobs have been successfully performed in the field using this treatment. Lab results showed a minimal presence for the ferrous ion and total sulfide once filtered from the aqueous phase. Furthermore, the results for FeS dissolution at different pH levels will be shared to determine the optimum pH values for the chelating agents. The collected data showed that this dissolver was able to outperform tetrakis (hydroxymethyl) phosphonium salt-based dissolvers without the adverse effects of HCl acid.

Post-job results will be discussed, including job design, field execution, lessons learned, and solid compositional analysis. Furthermore, an inhibition program has been implemented based on the acquired results from this model, and frequent inspections conducted showed no scale deposition over extended production periods.

The novelty of this approach is its ability to efficiently remove FeS scales and inhibit nucleation at early stages without relying on inorganic acids. Lab results will be discussed in detail to examine the role of chelating agents in FeS dissolution at different pH levels under anaerobic conditions. Field deployment data will be shared to definitively prove the effectiveness of this treatment in removing and preventing further FeS precipitation. This study will help to provide some information on an issue that has long concerned the oil and gas industry, and up to this date, no effective prevention mechanism has been discovered.

Introduction

Iron sulfide (FeS) and calcium sulfate (CaSO₄) scales are a recurrent problem in the oil and gas production, and its precipitation on the well completion tools or inside the surface flow lines restricts the flow of the produced fluids and might affect the integrity of the pipelines or the surface and subsurface tools. Moreover, the presence of fine particles of FeS in the produced crude oil can cause many operational problems in gas-oil separation plants.

The formation of this type of scale is mainly attributed to the presence of two main components, which are iron and sulfur¹. The iron component can be acquired as a corrosion byproduct from the well completion or as an existing rock mineral that is dissolved in the produced water, and later on interacts with the other element, which is sulfur. The second component is sulfur, which is normally found as a byproduct from downhole microbial interaction or hydrogen sulfide (H₂S) generation and release.

Sulfur can also exist due to the thermal degradation of H₂S, thereby forming FeS scale². As a result, the formation of this type of scale can result in several adverse effects, including but not limited to the decline

in injection rate due to formation damage, reduced production rate, loss of wellbore accessibility, and premature electric submersible pump (ESP) failures, as well as damage to existing downhole completions.

The purpose of this article is to share the acquired experience in tackling the presence of FeS scale and restore both wellbore accessibility and productivity after treatment operations.

FeS Precipitation Process

Typically, FeS scale is formed by the reaction between H_2S and iron. It can be present in several forms: Pyrrhotite (Fe_7S_8), troilite (FeS), pyrite (FeS_2), greigite (Fe_3S_4), and mackinawite (Fe_9S_8). FeS is present in crude oil, gas, and injector wells that are contaminated with sulfate reducing bacteria. An additional source of FeS is the iron that is produced either from the formation brine or by the corrosion of the tubing³.

Hydrochloric (HCl) acid has been used for descaling, as FeS scale deposits contain low sulfur content because it would have a higher degree⁴. Its major disadvantages include low pyrite solubility and H_2S gas release, which makes the process more expensive, as there is a high cost associated with the handling of H_2S gas.

Even though the solubility of FeS scale has proven to increase with the decrease of pH⁵, several substances are being used to remove FeS scale, rather than HCl acid and organic acids, such as: acrolein, tetrakis (hydroxymethyl) phosphonium salts, and chelating agents³.

Traditional Treatment Method

Gamal et al. (2019)⁵ suggested in their study that glutamic acid and diacetic acid (GLDA) could be introduced as a candidate for pyrite scale removal. In addition, the blended GLDA/diethylenetriaminepentaacetic acid formulation could also be recommended because it has a neutral pH — less corrosive to well equipment — and nearly relatively high dissolution performance. The biodegradability of GLDA exceeds 80% in 30 days⁶. GLDA has been reported for several field applications; in particular, it has been used as an iron control agent in stimulation operations, as a stand-alone stimulation fluid, and as a scale removal chemical⁷.

Meanwhile, $CaSO_4$ scale has been identified as one of the most common scales contributing to several serious operating problems in oil and gas wells and water injectors. $CaSO_4$ precipitation in downhole equipment, such as ESPs, can have a negative impact on well performance by lowering well injectivity and productivity. Typically, this scale can be encountered as three distinct forms: gypsum ($CaSO_4 \cdot 2H_2O$), bassanite ($CaSO_4 \cdot \frac{1}{2}H_2O$), and anhydrite ($CaSO_4$)⁸.

Therefore, the objective from this article is to build upon the existing literature, and the difficulties to remove such a complex aggregate (hydrocarbons impregnated mixed scales with sand). This study strives to present an alternative to convert/dissolve anhydrite-pyrite mixed scales covered by oil.

Laboratory Testing and Analysis

To evaluate the effectiveness of the new proposed

Fig. 1 Field scale samples: H-22, FeS impregnated with oil; H-33, $CaSO_4$ impregnated with oil; and H-208 mixed scales impregnated with oil.

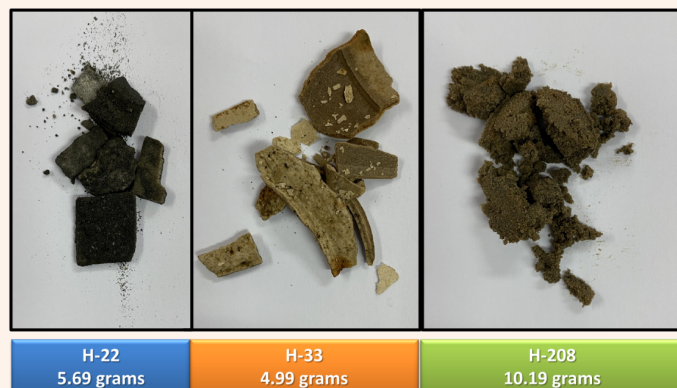
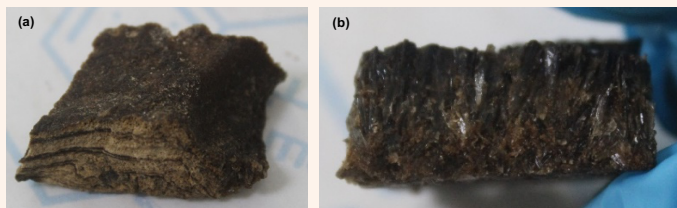


Fig. 2 A field sample of hard scale (a) and soft scale (b), collected from the surface flow line network.



chemical solution, which utilized enhanced chelating agents to breakdown the FeS and $CaSO_4$ scale structure, several downhole scale samples were collected from the field and sent to the lab for laboratory analysis and testing, Fig. 1.

In addition, the laboratory analysis scope includes the testing procedure for both downhole and surface scale samples to evaluate the treatment effectiveness and performance under anaerobic and surface conditions, therefore, the field samples were collected from the surface flow line network, Fig. 2.

Chemical Dissolution Process

The chemical solution process to overcome scale accumulation was designed in multiple stages to ensure effective dissolution under both anaerobic and surface conditions. Based on existing literature and accumulated field experience, it was determined that pre-conditioning the wellbore region to receive the treatment fluids was vital to ensure effective dissolution and successful operations⁹. Therefore, a pre-flush fluid was utilized to separate the oil and water phases to condition the wellbore and formation surface rocks to receive treatment fluids.

This pre-flush system is a strong paraffin and asphaltene solvent formulated locally, and it consists of

four proprietary products that can be mixed in diesel (carrier fluid) during pumping operations. The main objective for this pre-flush fluid is to help overcome several downhole challenges, including dissolving paraffin, asphaltene and oily sludges, oil-soluble surfactant to make surface water-wet and break emulsions as well as H_2S scavengers in case of any generated H_2S gases.

Proprietary formulation of this pre-flush fluid is recommended to change the surface wettability of the scale and ensure it is accessible for the scale removal treatment stages. This surfactant treatment will be circulating after the hydrocarbon solvent stage, and eventually, once the fluid is changed, based on the treatment's design.

Thereafter, the scale removal process can be initiated in two stages. The first stage was designed to utilize the enhanced chelating agent's chemical solution, which is a strong water-soluble proprietary scale converter, used to remove the scales. By changing the chemistry of the persistently insoluble FeS derivatives (pyrrhotite, troilite, pyrite, greigite, and mackinawite), $CaSO_4$, and barium sulfate hard scales, and convert them into a soluble material, they can be easily washed by acid systems.

Meanwhile the second stage relies on a strong proprietary aminopolycarboxylate-based chelating agent scale dissolver. The chemical works through controlling metal ions in water-based systems and alter the chemistry of the hard scales to significantly enhance their solubility and facilitate their removal. In addition, it can be used as a secondary dissolver for the iron oxide hard scales.

Table 1 summarizes the added chemical solutions that were tested in 100 milliliter boron-silicate bottles, and 30 mL test tubes were used to contain the treatment solutions. Each sample was then gently manipulated to ensure the integrity of the scales. In between each treatment stage, the scale samples were filtered with Whatman filter paper.

Results and Discussion

The three field scale samples, previously shown in Fig.

Table 1 A summary of the added chemical solutions that were tested.

#	Component	Description
1	Pre-flush	Paraffin/surfactant mixture
2	First stage scale dissolver	Enhanced chelating agent
3	Second stage scale dissolve	Enhanced chelating agent
4	Post-flush	Distilled water + scavenger
5	7.5% HCl acid	Calcium carbonate scale dissolver

1, are impregnated with hydrocarbons, and it implies that the solvent system followed by the surfactant stage must precede the conversion (anhydrite and gypsum)/descaling treatments. Figure 3 lists the treatment design and its timeframes.

Figure 4 shows the dissolution design treatment for these downhole field scale samples, which are taken from Well H-22.

Figure 5 shows the scale sample from Well H-22 after the application of treatment fluids, which caused the removal and separation of the impregnated.

The scale sample from Well H-22 was completely removed in HCl acid 15%_(wt) after completing all treatment stages. This process helped to reassure the effectiveness of this treatment without heavily relying on HCl acid as the traditional treatment design. Similarly, this treatment recipe was utilized in the dissolution design for the field scale samples collection from Well H-33, Fig. 6.

The hydrocarbon removal can be observed in Fig. 7 as a consequence of adding the pre-flush solution system, followed by the second stages of the FeS scale dissolver, which is utilizing a proprietary design in handling this type of hard scales.

Figure 8 shows the conversion of anhydrite and gypsum into acid-soluble scales.

The scale sample from Well H-33 presented an 86%_(wt) removal of the hydrocarbon cover. Scale was converted to calcium carbonate by a scale switch system and removed by an HCl acid system.

Figure 9 shows the dissolution design treatment for the field scale from Well H-208.

Post-Laboratory Analysis

Extensive laboratory analysis was conducted to help determine the optimum design that could provide the highest results in terms of scale dissolution and achieve the best scale weight reduction index for the field sample of mixed FeS and $CaSO_4$ scales impregnated with hydrocarbons. A preliminary hydrocarbon solvent

Fig. 3 The treatment flowchart for generic hydrocarbon impregnated mixed scales.

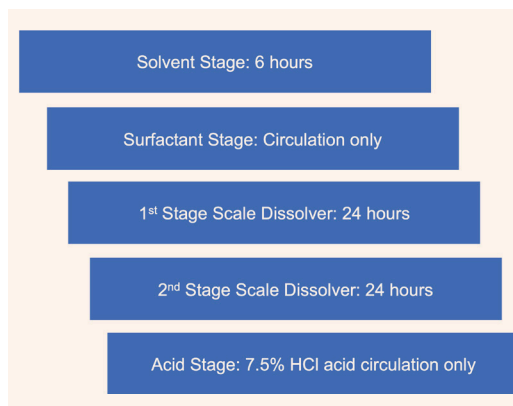
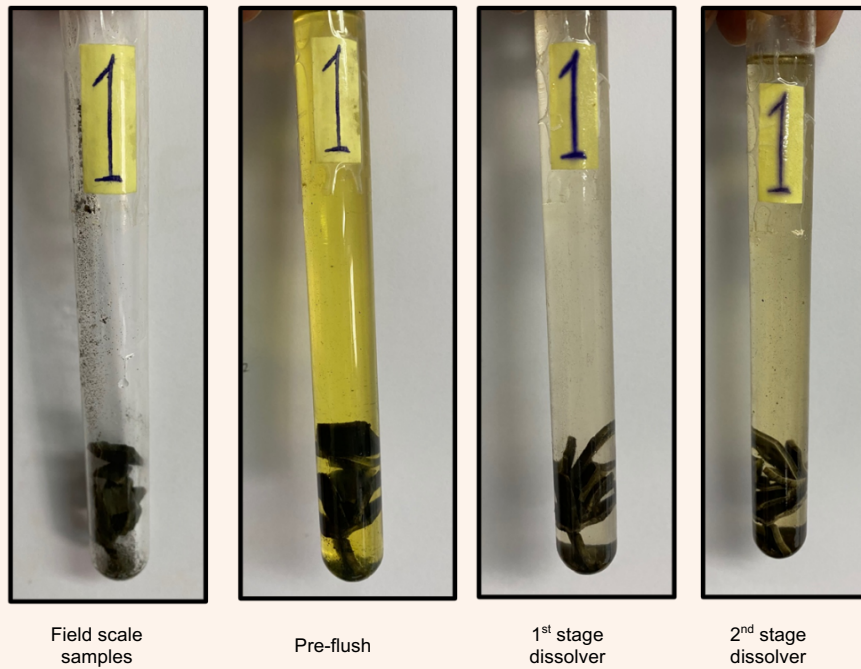


Fig. 4 The proposed treatment for field scale; taken from Well H-22.



treatment was necessary to remove the impregnated oil, thereby releasing the trapped volume of hydrocarbon fluids generating a water-wet surface rock and creating the ultimate medium for the subsequent chemical interaction, Fig. 10.

Furthermore, it was necessary that a surfactant treatment be implemented to change the wettability on the scale surface and create a water-wet surface rock that will aid in the chemical interaction; the same surfactant treatment is utilized to clean out the samples in between each treatment stage.

All the remaining scale solids were kept inside the desiccator for 24 hours, and the weight was measured in a four digits for balance (accuracy ± 0.2 mg).

Field Job Execution

Adequate laboratory testing was conducted to evaluate the treatment effectiveness prior to moving to the execution of the field job. The proprietary design utilized enhanced chelating agents that were able to effectively dissolve the downhole scale samples, which have been collected from the field. The job design was carried

Fig. 5 The scale sample from Well H-22 after removing the impregnated hydrocarbons.

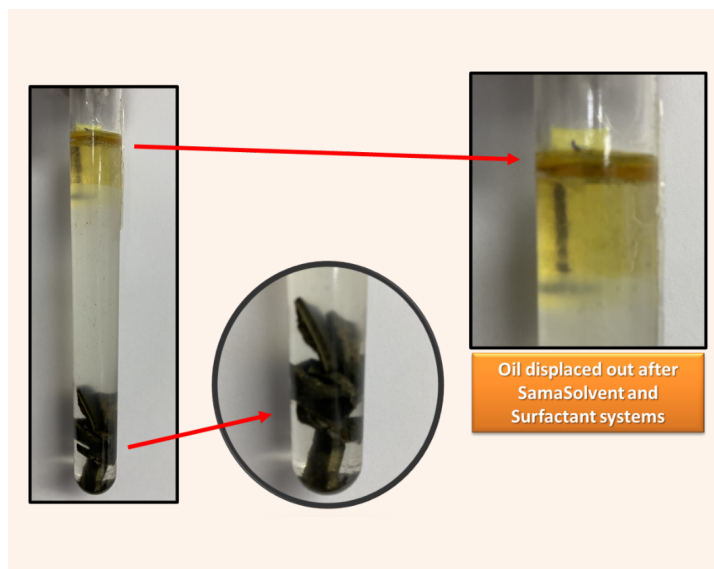


Fig. 6 The proposed treatment for field scale; taken from Well H-33.

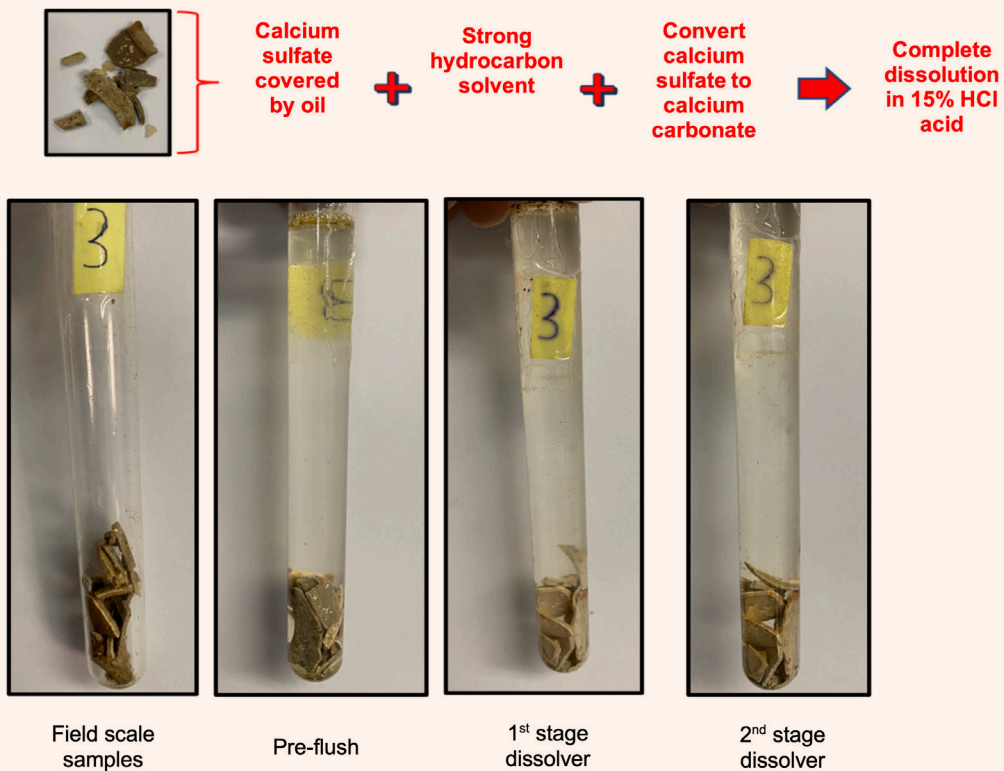
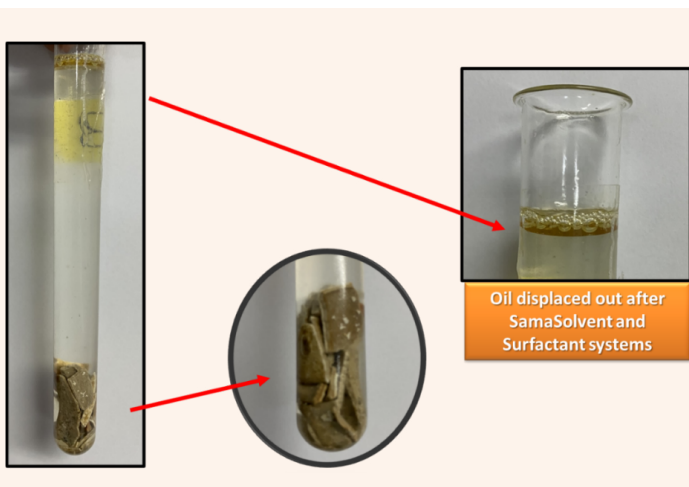


Fig. 7 The scale sample from Well H-33 after removing the impregnated hydrocarbons.



out in a similar fashion that was implemented in the laboratory analysis to achieve the target success rate in terms of scale dissolution.

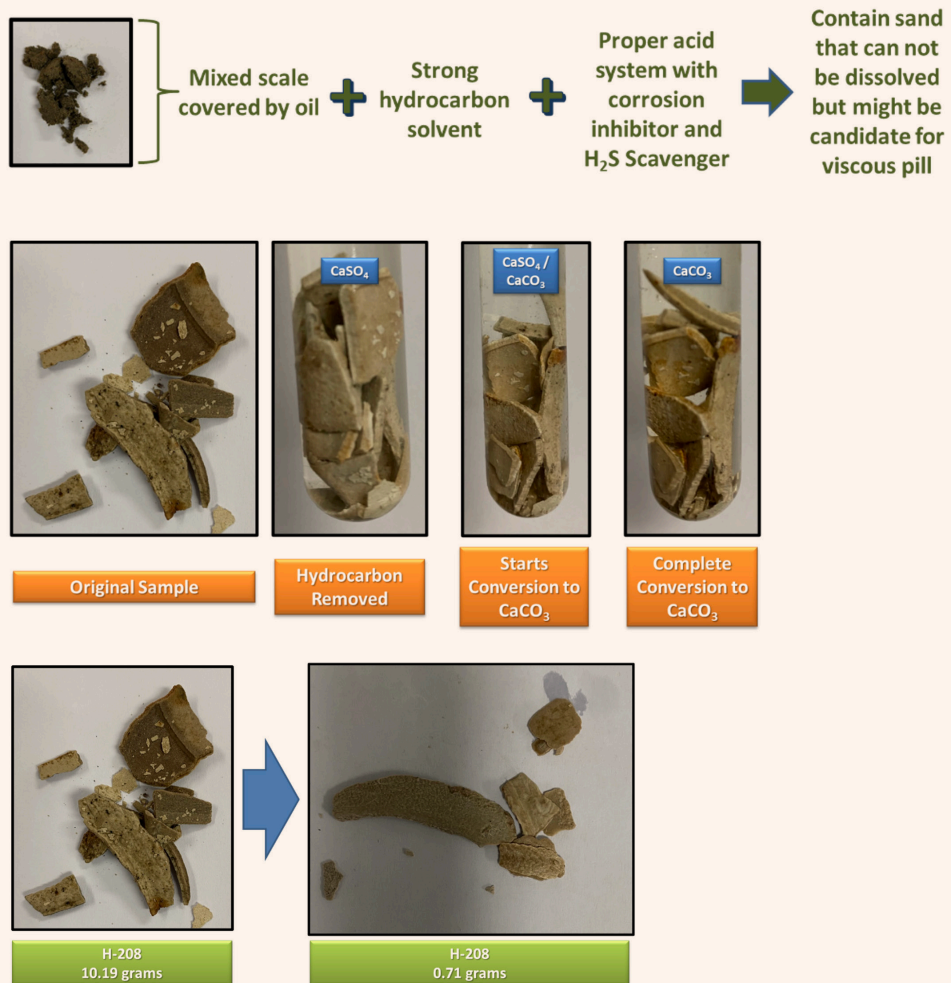
Consequently, a coil tubing unit with a rotary jetting nozzle was utilized to convey the treatment fluids to the required target depth to ensure optimum fluid

placement and minimize operational costs by reducing the total amount of required chemical volume fluids. In addition, a flow back testing system was utilized to monitor the returns from the well, perform X-ray diffraction analysis for the collected samples, measure well flow rates, and assess the overall success rate from these scale removal jobs.

The job was commenced by pumping a stage of the hydrocarbon solvent treatment system to release any impregnated oil phase fluids. This process was aided by a strong surfactant treatment recipe to help create a water-wet surface rock and create the optimum medium conditions for the subsequent chemical interactions. Thereafter, the scale dissolver system was pumped into two stages with a total of 48 hours of soaking after pumping each stage, to ensure that the chemical interaction will be able to take its full effect.

This allowed the scale dissolver to breakdown the molecular structure bond between the iron and sulfide scale components so it can be flowed back to the surface in the later stages. Finally, a post-flush treatment fluid was pumped to circulate all the dissolved and broken scale particles back to the surface where flow rates were being measured and solid samples were collected frequently for future laboratory analysis. A contingency stage of 7.5% HCl acid was included since the collected downhole scale samples indicated the presence of calcium carbonate scale.

Fig. 8 The conversion of anhydrite and gypsum into acid-soluble scales.



Conclusions

This article discusses the application of FeS scale removal technology in a cost-effective approach that does not rely on aggressive and highly corrosive solutions, such as HCl acid. The engineering challenges, best practices and lessons learned from this technology are summarized. Post-job analysis indicates that this scale switch technology is a viable and effective means to remove scale fill accumulations from wellbores with large completion and low bottom-hole pressure.

The following points summarize the lessons learned and are cultivated from the implemented field applications.

1. The incorporation of a proprietary solvent system as the first step in the treatment design helped to create the optimum downhole conditions for the subsequent treatment stages.
2. The newly developed solvent system helped to enhanced the oil and water separation process, which was able to separate the impregnated oil phase from the scale samples and created a water-wet surface rock, which is the ideal condition for the upcoming treatment fluids.
3. The proposed scale switch technology provides an innovative approach to breakdown the molecular bond inside the FeS structure so that it may be flowed back to the surface in later stages, thereby avoiding highly corrosive and aggressive solutions, such as HCl acid.
4. The utilization of a rotary jetting nozzle helped to optimize the placement of treatment fluids inside the wellbore, and ensure high exposure for the accumulated downhole scale deposits and achieve high removal at a lower cost.
5. Utilization of water mixed with an oil dispersant and a friction reducer helped to extend the reach depth of the coil tubing in extended horizontal section wells.
6. Using updated software with real-time field data,

Fig. 9 The initial scale sample from Well H-208 and clean sand after the hydrocarbon and scale treatment.

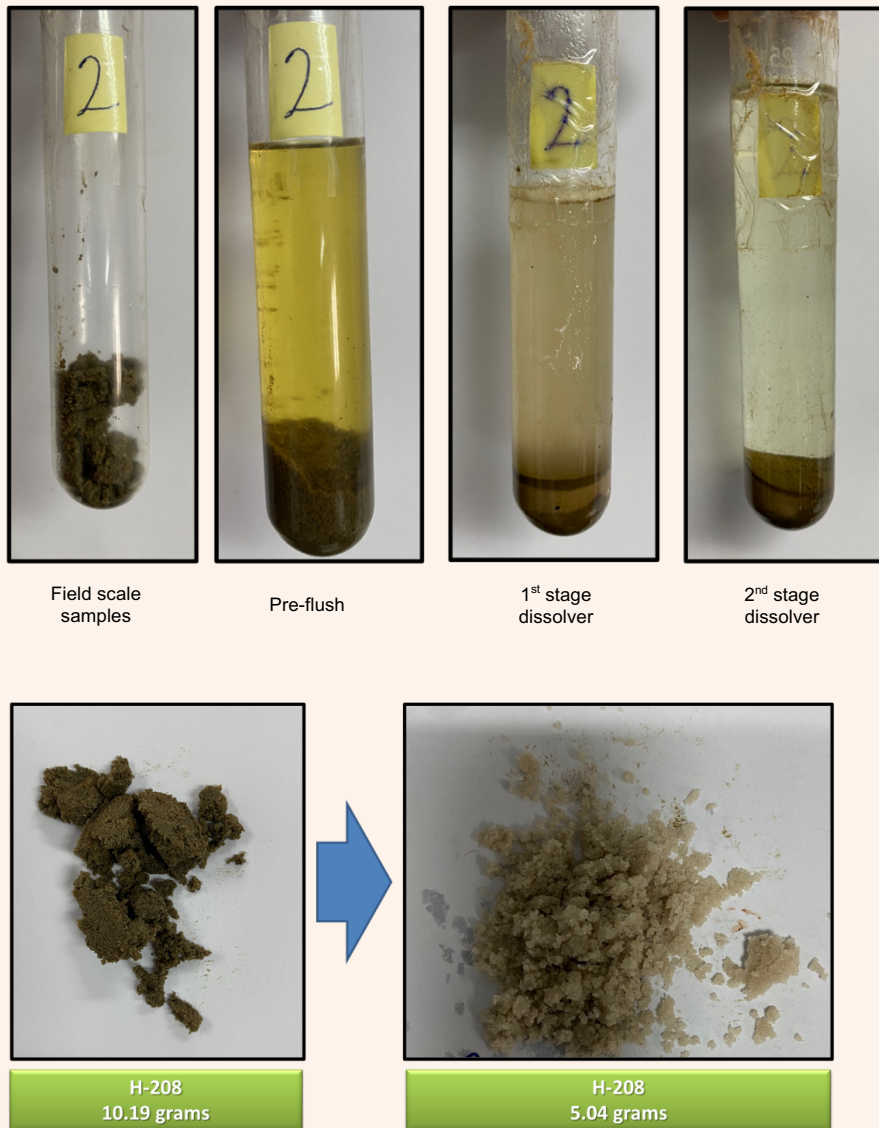
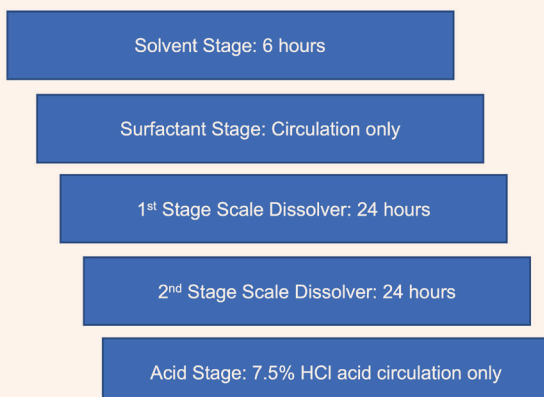


Fig. 10 A flowchart showing the design treatment stage.



and considering the parameters involved in the scale removal process, can help field engineers to design, optimize, and execute such operations in an efficient and cost-effective manner.

Acknowledgments

This article was presented at the Middle East Oil, Gas and Geosciences Show, Manama, Kingdom of Bahrain, February 19-21, 2023.

References

1. Ahmed, M.E., Hussein, I.A., Onawole, A.T., Mahmoud, M., et al.: "Pyrite-Scale Removal Using Glutamic Diacetic Acid: A Theoretical and Experimental Investigation," *SPE Production & Operations*, Vol. 36, Issue 3, August 2021, pp. 751-759.
2. Dougherty, J.A., Tauseef, S., Brownlee, J.K. and Hausler,

- R.H.: "Solving Iron Sulfide Problems in an Offshore Gas Gathering System," paper presented at the CORROSION 2000, Orlando, Florida, March 26-31, 2000.
5. Nasr-El-Din, H.A. and Al-Humaidan, A.Y.: "Iron Sulfide Scale: Formation, Removal, and Prevention," SPE paper 68315, presented at the International Symposium on Oil Field Scale, Aberdeen, Scotland, U.K., January 30-31, 2001.
 4. Ford, W.G.F., Walker, M.L., Halterman, M.P., Parker, D.L., et al.: "Removing a Typical Iron Sulfide Scale: The Scientific Approach," SPE paper 24327, presented at the SPE Rocky Mountain Regional Meeting, Casper, Wyoming, May 18-21, 1992.
 5. Gamal, H., Abdelgawad, K.Z. and Elkhatatny, S.: "New Environmentally Friendly Acid System for Iron Sulfide Scale Removal," *Sustainability*, Vol. 11, Issue 25, November 2019, pp. 6727-6759.
 6. Mahmoud, M.A., Kamal, M., Bageri, B.S. and Hussien, I.A.: "Removal of Pyrite and Different Types of Iron Sulfide Scales in Oil and Gas Wells without H₂S Generation," IPTC paper 18279, presented at the International Petroleum Technology Conference, Doha, Qatar, December 6-9, 2015.
 7. Mahmoud, M.A., Hussein, I.A., Sultan, A., Saad, M.A., et al.: "Development of Efficient Formulation for the Removal of Iron Sulfide Scale in Sour Production Wells," *The Canadian Journal of Chemical Engineering*, Vol. 96, Issue 12, December 2018, pp. 2526-2533.
 8. Ramanathan, R. and Nasr-El-Din, H.A.: "Chelating Agents for Iron Sulfide Scale Removal at 500 °F (149 °C)," paper prepared for presentation at the CORROSION 2020, Houston, Texas, event canceled.
 9. Wang, Q., Ajwad, H., Shafai, T. and Lynn, J.D.: "Iron Sulfide Scale Dissolvers: How Effective are They?" SPE paper 168063, presented at the SPE Saudi Arabia Section Technical Symposium and Exhibition, al-Khobar, Kingdom of Saudi Arabia, May 19-22, 2015.

About the Authors

Hussain A. Almajid

*B.S. in Petroleum Engineering,
Louisiana State University*

Hussain A. Almajid is a Production Engineer working in Saudi Aramco's Southern Area Production Engineering Department. His work experience includes work in several oil fields, including in North Ghawar and in the Southern Area. During this time, Hussain developed his experience as a skilled Production Engineer dealing with intelligent field equipment, electric submersible pumps, and smart well comple-

tions.

He has written and presented several Society of Petroleum Engineers (SPE) papers and presentations. Hussain is a certified SPE engineer.

In 2010, he received his B.S. degree in Petroleum Engineering from Louisiana State University, Baton Rouge, LA.

Ibrahim K. Al-Thwaiqib

*B.S. in Petroleum Engineering,
King Fahd University of Petroleum
and Minerals*

Ibrahim K. Al-Thwaiqib is a Production Engineer working in Saudi Aramco's Southern Area Production Engineering Department. He has 17 years of experience in the oil and gas industry. Ibrahim has worked as a Production Engineer, Intelligent Field Engineer, Operation Foreman, and Production Engineering Supervisor in

different oil fields, such as South Ghawar, North Ghawar, Shaybah, and Central Arabia.

He received his B.S. degree in Petroleum Engineering from King Fahd University of Petroleum and Minerals (KFUPM), Dhahran, Saudi Arabia.

Carlos E. Amancio Ribeiro

*M.S. in Chemical Engineering,
University of Federal do Rio de
Janeiro*

Carlos E. Amancio Ribeiro is a R&D and Lab Manager at the Sama Chemical Products Factory with 12+ years of experience assisting the upstream industry. He specializes in formation stimulation, including descaling chemical

solutions, thermochemical stimulation, and filter cake removal treatments.

In 2014, Carlos received his M.S. degree in Chemical Engineering from the University of Federal do Rio de Janeiro, Rio de Janeiro, Brazil.

Automatic Placement of Sidetrack Wells during Simulation Run Time

Babatope O. Kayode, Dr. Karl D. Stephen and Dr. Babatunde O. Moriwawon

Abstract /

To maximize recovery while minimizing investment costs, it is often necessary to perform a sidetrack of existing wells instead of drilling new wells. Drilling a sidetrack rather than a new one can significantly reduce drilling costs because the main well has already been drilled. In this study, we discuss the application of automation to determine optimum sidetrack locations and directions using numerical simulation.

The automation algorithm considered in this study creates central surveillance vertical wells that penetrate from the top to the bottom of a reservoir model, and coincide with the topmost perforation of each simulated historic well. It then creates four cardinal surveillance vertical wells, each at the north, south, east, and west of the central surveillance wells at x-grid blocks distance. When the water cut of a historic simulation well reaches a user-defined target, the algorithm receives the water saturation (s_w) vs. depth log for the historic simulated well and its associated surveillance wells from the simulator. The algorithm then uses the user-defined specifications to identify reservoir sweet spots defined as porosity $\times\log_{10}(\text{permeability})\times\text{thickness}\times(1-s_w)$, which is then used to determine the optimal depth and direction of the sidetrack well. The sidetrack well is created automatically in the simulation run time and replaces the historic well.

Automating sweet spot identification and creation of perforation resulted in a 95% reduction in the time required by engineers to implement optimum sidetrack wells in the numerical simulation. In addition, because the sidetrack wells are targeted at sweet spots, this methodology allows field development that explicitly incorporates water production management objectives. The simulator automatically shuts in high water producers and replaces them with sidetracks intelligently targeted at sweet spots to maintain field production while limiting water production.

It is common practice to use pulsed-neutron logs (PNLs) to detect unswept reservoir zone(s) to be targeted with sidetrack wells. PNLs help to detect the zone but cannot determine the direction. The present work complements PNLs in determining the optimal direction to drill a sidetrack. The algorithm also provides an economic evaluation of all the sidetrack wells created during a simulation run to provide information to decide which are the best candidates to maximize return on investment.

To our knowledge, this work is the first to consider the application of run time sidetrack well placement in numerical reservoir simulation.

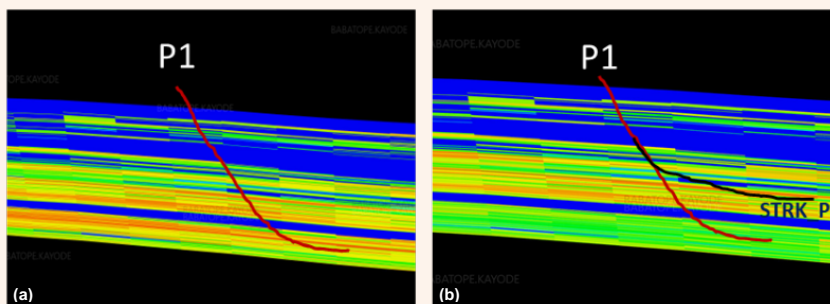
Introduction

After a history matching exercise, the resulting model is used for performance forecasting using historic wells (a no further action forecast scenario) and other scenarios involving sidetrack and wells. During forecast runs, an engineer uses a completed simulation run to identify the locations of unswept or bypassed oil. New wells are then included in subsequent simulation runs to target these locations. These new wells can be infill wells drilled at new locations or sidetrack wells¹ drilled from existing wells.

The usual industry approach used to determine and define a sidetrack well location requires the application of multiple software frameworks and processes. First, a base case prediction simulation is made with, e.g., Eclipse. Then, the timestep results are loaded into a 3D viewer, such as Floviz or Petrel. A cross-section of the grid was created along the target historic well. Next, a diagnostic map such as net-oil-thickness/porosity/oil saturation (HuPhiSo) is created at the date of the intended sidetrack well.

Variants of the diagnostic map are the mobile net-oil-thickness map (HuPhi ($s_o - s_{or}$)) and the sweet spot map (HuKPhiSo). The diagnostic map used in the present study shows the sweet spots. The identified sweet spot along a historic well is targeted by a sidetrack well. As illustrated in Fig. 1, after some years of production, Well-P1 was produced with a 90% water cut. The cross-section of the calculated sweet spot when the water cut reached 90% was made using Petrel (or any other 3D visualization application), and it was observed that the lower section of the well was watered out and a sidetrack well could be used to target the upper zone.

Fig. 1 The sweet spot cross-section at a location of Well-P1: (a) The start of the simulation, and (b) The timestep when Well-P1 produced at a water cut of 90%, showing the proposed location of the sidetrack well, Well STRK_P1. This cross-section is from a hypothetical model.



One could argue that a water shut-off in the lower zone and reperforation in the upper zone is possible. This is correct, but in this case, the well reservoir contact of the resulting perforation interval could be too short to provide the required productivity. By drilling a horizontal sidetrack, the horizontal well could be drilled to provide the required well reservoir contact, Fig. 1b.

Therefore, planning a sidetrack well in a simulation usually requires finding the date at which a historic well reaches the trigger condition, e.g., water cut > 0.9, and a post-processor, such as Petrel, creates a cross-section visualization in various directions. The engineer would then have to decide on the zone and direction for a sidetrack well, design the well, export the perforation file for the sidetrack in the simulator's format, and include the exported file as input data for a new simulation run. Next, the well event file must be edited to shut-in the historic well and open its sidetrack at the proper timestep.

These processes may take several months to complete in large reservoirs containing hundreds of wells². Incorporating all these processes into a numerical simulator is beneficial for such reservoirs. Instead of manually designing wells to harness the bypassed oil, the numerical simulator performs this task automatically during the simulation run.

An earlier approach to automating the placement optimization of sidetracks², used a pre-processing software external to the simulator to randomly explore several locations and directions for each well. Once a particular location is selected based on instantaneous productivity using Joshi's formulation^{3,4}, the selected sidetrack is then implemented in the reservoir simulator. Although Magizov's automatic approach² allows faster exploration of several sidetrack specifications than the traditional manual and laborious process, it does involve several simulation scenarios. As reported in their work², several hundred simulation runs were required to determine the optimum sidetrack specifications.

Magizov's approach² can be regarded as semi-manual, because it still requires expert evaluation of potential sidetrack locations based on indices that are calculated by pre-processing software. The new approach helps

to automate the steps associated with the traditional approach such that several sensitivity analyses can be performed on the specifications of the sidetrack. It remains unclear from Magizov's work² whether the pre-processing software used the original geological grid properties to evaluate sidetrack locations, or whether it used the grid properties at the timestep when the historic well was due for sidetrack intervention.

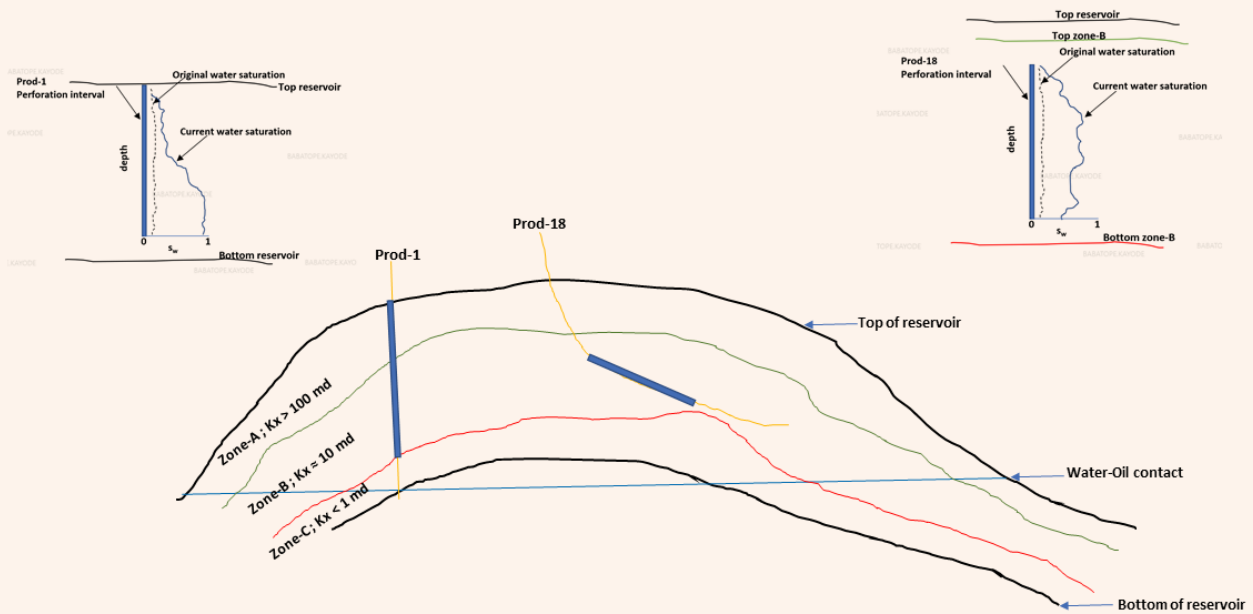
The methodology presented in the current work is designed to enable the simulator to make decisions regarding the optimum location for sidetrack placement automatically during run time. This new approach is therefore faster and requires less computational resources compared to Magizov's approach. The sidetrack evaluation is performed using grid properties at the simulation timestep when the historic well is due for sidetracking.

Autonomously determining the location and direction of a sidetrack with a numerical reservoir simulator involves a few key challenges.

First, the simulator must observe what is happening from the top to the bottom of the reservoir around each historic simulation well. Although historic wells in a reservoir may penetrate from the top to the bottom of the reservoir, such wells may not be perforated across their entire reservoir contact. In reservoir simulations, a well is known only by its well grid connections. Although numerical simulators calculate the properties for all grids at each timestep, well log plots show only the properties of the well grid connections. The grid properties at other sections of the well that have no connection to the grid cannot be effectively monitored by simulation. These unmonitored sections could potentially contain the unswept oil being sought.

In Fig. 2, the historic well, Well Prod-18, penetrates the top and middle reservoir zones, but is only perforated in the middle zone. The inset plot in Fig. 2 (right) shows Well Prod-18's water saturation log at different simulation timesteps. It may be observed that the well log result only covers the middle reservoir zone, where the well has connections to the grid. The well could not monitor the water saturation around itself in the upper and lower reservoir zones. Similar behavior

Fig. 2 An illustration of a challenge with commercial simulators regarding monitoring grid properties in the vicinity of the simulation wells.



may be observed for Well-P1.

Second, the simulator must determine the direction in which sidetrack well performance would be optimal. Identifying unswept oil in the vicinity of historic simulation wells with the simulator does not suffice; it is also important to know if this unswept oil seen at the historic well is laterally continuous. The lateral continuity of the sweet spot forms the basis for selecting the optimal sidetrack well direction.

Third, some wells may have sidetrack opportunities in multiple zones. The simulator must be able to screen and determine the optimum zone to locate the sidetrack well.

Traditional simulator technology allows for the replacement of watered out wells with new wells. Still, these new wells must be predefined in the simulation run and are activated when needed. An example is to use the Eclipse QDRILL keyword to activate the well(s) from a prior queue of wells defined in the simulation. The limitation of this approach is that one cannot always know in advance the possible presence of the unswept oil; therefore, the locations of the predefined wells may not be optimum at the time of activation.

It is also noted that commercial simulators, e.g., Eclipse, permit the management of water production through workover options, such as CON (shut-in worst offending connection) and CON+ (shut-in worst offending connection and all connections below it). This simulated water management approach provides numerically reasonable results, but the processes cannot be implemented in field operations.

This study uses a hypothetical model to describe the proposed methodology.

Methodology

The user inputs the keyword AFDL into the simulator, which triggers the performance of the automatic sidetrack. The user also specifies the well performance criteria at which sidetracking should be triggered, e.g., a well with a water cut more significant than 90%.

Once a simulation run is launched, and the simulator encounters the AFDL keyword, five observation wells are automatically created for every historic simulation well at the run initialization stage. The locations of the observation wells associated with each historic well are stored by the simulator, which would then be used to monitor the reservoir properties in the vicinity of each historic simulation well. The configuration and characteristics of these observational wells are briefly discussed next.

One central observation well is defined as a vertical well perforated from the top to the bottom of the reservoir and intersecting the top perforation of the historic simulation well, for the slanted well, Well Prod-18, Fig. 3.

Four cardinal observation wells are defined as vertical wells located in the four cardinal directions, north, south, east, and west of the central observation well, at a distance x , defined as the number of grid blocks equivalent to the expected length of a horizontal sidetrack well and input by the user. For example, if horizontal sidetrack wells are expected to be 500 m long, the simulation grid block sizes are 100 m \times 100 m. Then, each cardinal observation well would be located five grid blocks away from the central observation well, Fig. 4.

A total of $5n$ vertical observation well locations are stored in the memory at initialization, where n is the

Fig. 3 An illustration of the definition of the central observation (scanning) well of historic simulation well, Well Prod-18.

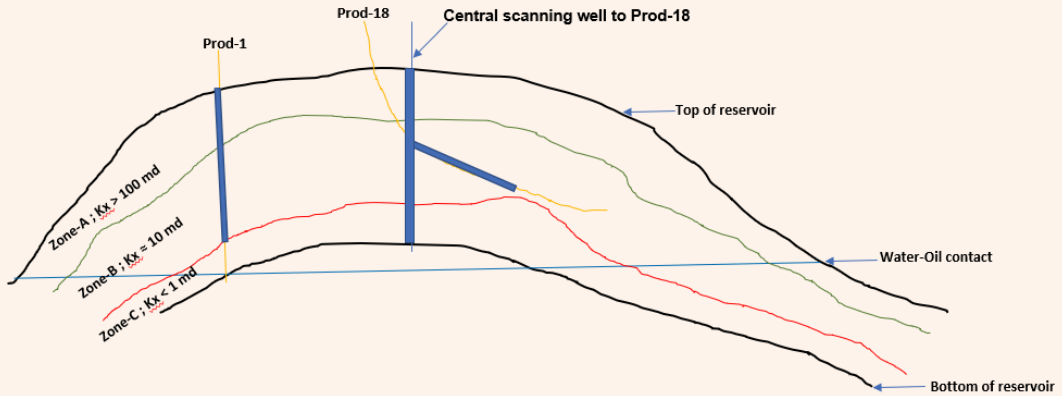
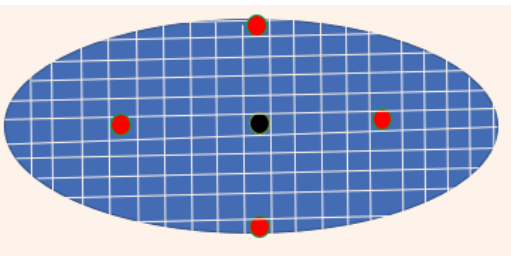


Fig. 4 A top view illustration of the central and cardinal observation wells whose locations are created in memory for each historic simulation well.



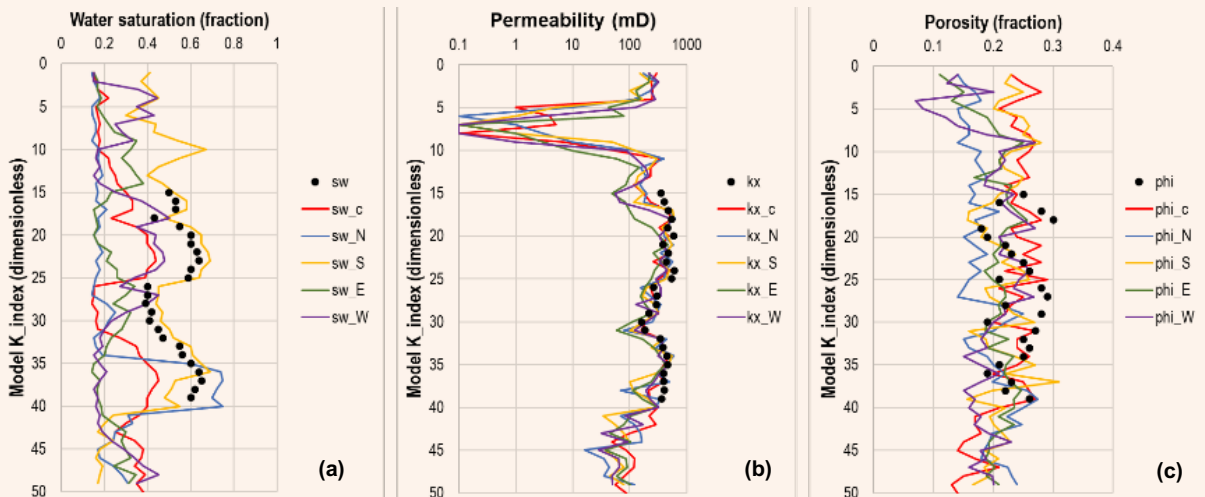
number of historic simulation wells. In the current discussion, the term historic simulation wells refer to all the producing simulation wells.

At each simulation timestep, the simulator checks for any historic simulation well that meets the sidetrack trigger criteria — in this case, well water cut > 0.9. For any well that meets the sidetrack criteria at a given timestep, the simulator extracts the water saturation logs of the historic well and its five associated observation wells.

In Fig. 5a, a plot of water saturation vs. the k_index of the simulation model for the five observation wells associated with a historic simulation well at the timestep when its water cut reaches 90% is illustrated. The water saturation log along the well grid connections of the historic well is shown as black dots. The saturations of the central, Fig. 5c, and cardinal directions (north, south, east, west) are shown as line plots. In addition, the permeability and porosity logs of the five observation wells were extracted, Figs. 5b and 5c, respectively.

As observed in Figs. 5a, 5b, and 5c, the well grid

Fig. 5 The water saturation (a), permeability (b), and the porosity of the historic simulation well and its associated observation wells (c), extracted at the simulation run time for calculation of the sweet spot to be used for placement of the sidetrack well.



connections of the historic simulation well traverse only the model k_index 15 – 39; therefore, the associated observation wells could allow an assessment of the properties of the model above and below the perforation interval of the historic well.

The simulator calculates the sweet spot log given by Eqn. 1 for the five scanning wells:

$$sweet_{spot} = dz * \phi * \log_{10}(k) * (1 - s_w). \quad 1$$

Table 1 lists the full complement of the required user specifications.

The value of the sweet spot is set to zero at any grid block where water saturation is greater than input sw_cutoff or less than input kx_cutoff , resulting in the sweet spot zones having different thicknesses separated by zones of zero values of sweet spot. Figure 6a shows the sweet spot log of the central observation well for $sw_cutoff = 0.25$ and $kx_cutoff = 1$ mD, showing six zones separated by zero values.

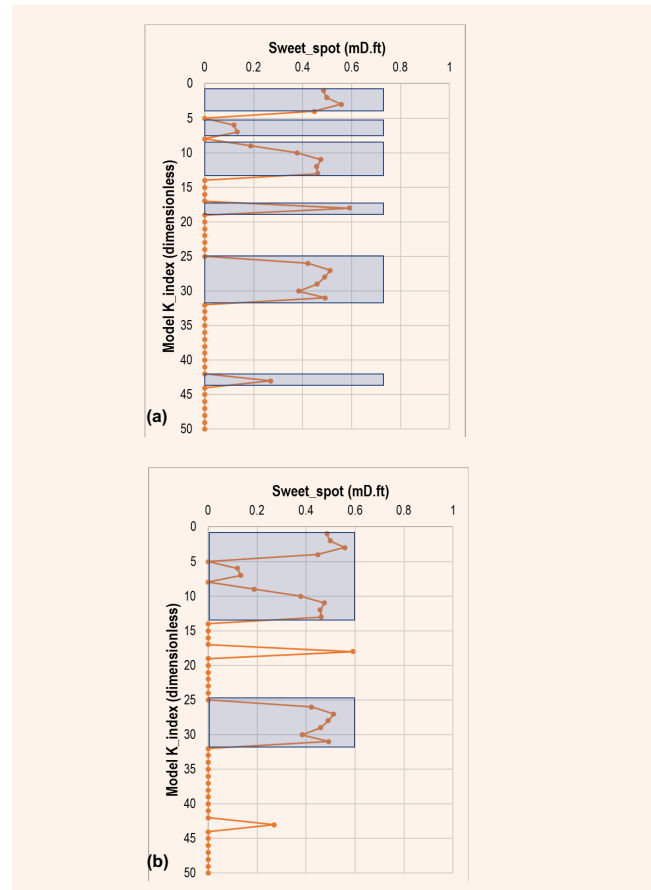
If the zone thickness is less than the user input, $Min_Perf_thickness$, the sweet spot zone is discarded. If the number of $k_indices$ between two successive sweet spot zones is less than the user input, $zone_merge_threshold$, these two zones are merged into a single zone. Figure 6b shows the result of fine-tuning Fig. 6a using $zone_merge_threshold = 3$ and $Min_Perf_thickness = 5$. The six sweet spot zones identified in Fig. 6a are merged into two sweet spot zones in Fig. 6b.

The sweet spot zone of the *central observation* well with the largest sweet spot coefficient is selected for locating the sidetrack well. The sweet spot coefficient is defined as the area under the sweet spot log, measured in md.ft.

In the illustration shown in Fig. 6b, the upper sweet spot zone has a coefficient of 4.2 md.ft while the lower zone has 2.8 md.ft. The sidetrack is placed in the upper zone.

The central observation well is closer to the historic simulation well than the cardinal observation wells. It is used to observe the immediate vicinity of the historic

Fig. 6 The shaded rectangles representing: (a) All the identified sweet spot zones based on input sw_cutoff and kx_cutoff , and (b) The refined sweet spot zones using input $zone_merge_threshold$ and $Min_Perf_thickness$.



well, which has no well grid connection. Therefore, using the central observation well to determine the sidetrack target allows the simulator's decision to be

Table 1 The user input specifications for the AI-driven sidetrack well placement and their description.

Kx_cutoff	Minimum permeability of target interval
Sw_cutoff	Maximum water saturation of target interval
Min_Perf_thickness	Minimum thickness of target interval
zone_merge_threshold	Minimum thickness between adjacent target intervals
Scanning wells spacing	Number of cells between central and cardinal observation wells
Wcut_trigger	Value of water cut at which sidetrack workflow should be activated
kmax	Number of k-layers in the model
Well_length	Number of simulation cells equivalent to the expected length of well laterals
Max_re-entry	Maximum number of sidetracks that can be allowed per well

checked against a time-lapse pulsed-neutron log (PNL) before the actual drilling of the proposed sidetrack.

Using the same interval as the largest sweet spot coefficient on the central observation well, the sweet spot coefficient on each of the cardinal observation wells are calculated, and the direction that gives the largest value is selected as the direction of the sidetrack well. We assumed here that the reservoir is continuous between the central and cardinal observation wells; therefore, the larger the magnitude of the sweet spot coefficient at a cardinal observation well, the larger the total reservoir capacity (kh) between that direction and the central observation well would be. The larger the kh within which a sidetrack well is located, the better its instantaneous and long-term production performance. Herein is the sidetrack optimization philosophy used in this study:

- Locate the sidetrack at the central observation well, within a zone that maximizes the sweet spot coefficient.
- Maximize kA (md.ft²) by orientating the sidetrack in a direction of the cardinal observation well having the largest sweet spot coefficient across the selected sidetrack zone.

Figure 7 shows the sweet spot zones along the cardinal observation wells. The zone of interest is the k_index interval from 1 to 13 because it is chosen from the central observation well. In the illustration, the largest cumulative sweet spot coefficient occurs along the south observation well (3.9 md.ft). Therefore, the sidetrack well is oriented toward the south.

Using the ij coordinates of the central observation well and having determined the top k_index , bottom k_index , and the orientation (I or J) of the sidetrack well, a well grid connection can be automatically defined for the sidetrack well. In an example application, the sidetrack is defined as a horizontal well parallel to the structure, passing through a fixed value of k_index . To

maximize the reservoir’s sweep efficiency, especially in the case of aquifer influx or water injection, a horizontal lateral could be placed at the upper section of the identified sweet spot zone.

In the current illustration, let the ij location of the central observation well be (60,35), top $k_index = 1$, bottom $k_index = 13$, well orientation = South (J-), and the horizontal lateral be placed two cells below the top of the sweet spot zone. Then, for an example commercial simulator, the well grid connection (ij,k) for a 500 m lateral length is automatically defined as:

```
Wellname = STRK_PI
60 35 3 /
60 34 3 /
60 33 3 /
60 32 3 /
60 31 3 /
60 30 3 /
```

Note that because the horizontal sidetrack is oriented south, the J_index decreases along the well path.

Figure 8a shows the trajectory of a historic well at the start of simulation. After some elapsed time, water arrived at and flushed the vicinity of the well. At an elapsed time, Fig. 8b, the historic well’s water cut reaches the user specified $wcut_trigger$, the simulator implemented the methodology discussed and automatically located a sidetrack well up-dip and eastwards of the historic well.

The automatic placement of the sidetrack by the simulator in this case is consistent with what an expert practitioner could have arrived at, albeit taking much less time to do the task.

A full-field simulation run with an automatic sidetrack enabled could be used as a reservoir management tool for planning the acquisition of a time-lapse PNL to validate the zone and orientation of the simulator

Fig. 7 The sweet spot zones identified along the cardinal observation wells, showing the cumulative sweet spot coefficient of the zone of interest.

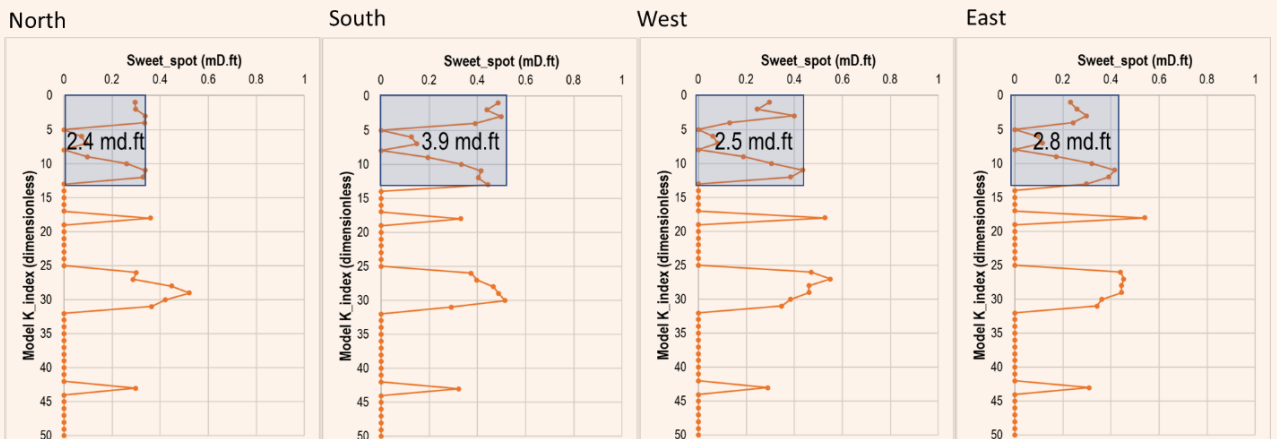
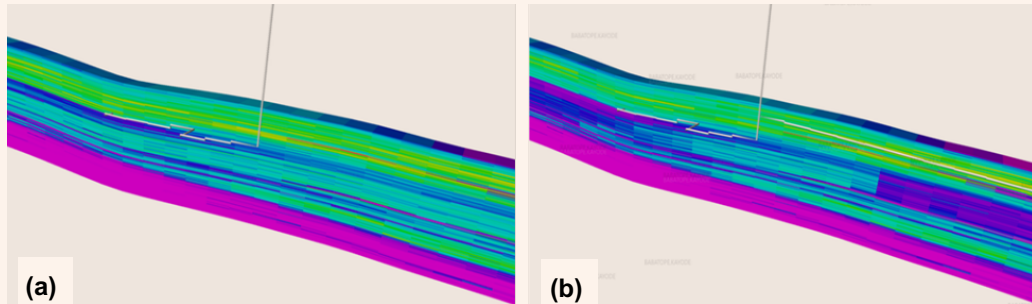


Fig. 8 (a) The historic well trajectory on a background of the initial sweet spot map, and (b) The automatically placed sidetrack well on a background of the sweet spot map at the time the historic well's water cut reaches the $wcut_trigger$.



derived unswept zones. Such a full-field run could also provide insight into the sidetrack wells having the most incremental benefits, thereby ensuring that investments are targeted at the sidetracks with the highest potential.

Discussion of Results

Conventionally, numerical simulators perform calculations related to the physics of fluid flow within a reservoir. Subsequently, they could be coupled with vertical lift performance tables to calculate wellhead pressures. In the same way, the present work couples artificial intelligence with the numerical simulator to help automate the placement of sidetrack wells.

Because the decisions made by the simulator are based on the model properties, the uncertainty of the predicted sidetracks depends on the uncertainty of the static model used. To mitigate this uncertainty, a PNL run on the historic well can be used to verify the sweet spot log of the central observation well.

Designing the sidetrack wells as horizontal, as we have done in this work, is merely for convenience; they could be defined as deviated if required. Moreover, in the author's experience, horizontal and deviated wells of similar length drilled within a given zone perform similarly in cases of large vertical permeability. In certain cases where water injection is taking place at the base of the zone, a horizontal well drilled close to the top of the zone may perform better than a deviated well, the toe of which is closer to the advancing flood front.

Sometimes, multiple sweet spot zones may be detected by the central observation well as previously shown in Fig. 6b. By default, the algorithm selects the zone with the largest cumulative coefficient and discards the other zones. If the user-specified value of $max_re-entry > 1$, then the other zones are not discarded, and they are placed on standby and used to replace the active sidetrack zone once it reaches the $wcut_trigger$ criteria. The idea here is that only a single sidetrack is active for each well at any time, and the total number of sidetracks that can be active on any well must not exceed the $max_re-entry$ specification.

To optimize field development costs, operators strive to maximize oil production and minimize water production. This is because produced water needs to be treated before disposal, and the treatment criteria are becoming more stringent with the development of green economics and reduced tolerance for environmental pollution. We expect this new tool to significantly help to approach the objective of oil production with minimum associated water production.

Conclusions

1. An algorithm has been described to enable a numerical simulator to automatically detect an optimum location and direction to sidetrack a historic well in run time.
2. This methodology assumes that reservoir continuity exists between a historic well and its associated observation wells.
3. In an example application, the automatically generated sidetrack was similar to the result that an expert practitioner would have manually designed, and yielded better performance than other nonselected locations.
4. In an example application involving a few hundred historic wells, bypassed oil identification and planning of sidetrack wells was conducted in eight weeks of engineering working time. Subsequently, the automated approach presented completed the exercise within one day, including several sensitivities to $well_length$, $wcut_trigger$, and so forth.

Nomenclature

Hu:	Net cell thickness (ft)
Phi:	Porosity (fraction)
K:	Permeability (mD)
S_o :	Oil saturation (fraction)
S_{or} :	Residual oil saturation (fraction)

References

1. Zhang, J., Wang, G., He, K. and Ye, C.: "Practice and Understanding of Sidetracking Horizontal Drilling in Old Wells in Sulige Gas Field, NW China," *Petroleum Exploration and Development*, Vol. 46, Issue 2, April 2019, pp. 584-592.
2. Magizov, B., Topalova, T., Loznyuk, O., Simon, E., et al.: "Automated Identification of the Optimal Sidetrack Location by Multivariant Analysis and Numerical Modeling. A Real Case Study on a Gas Field," SPE paper 196922, presented at the SPE Russian Petroleum Technology Conference, Moscow, Russia, October 22-24, 2019.
3. Joshi, S.D.: "Augmentation of Well Productivity with Slant and Horizontal Wells (includes associated papers 24547 and 25508)," *Journal of Petroleum Technology*, Vol. 40, Issue 6, June 1988, pp. 729-739.
4. Joshi, S.D.: *Horizontal Well Technology*, Tulsa: PennWell Books, 1991, 535 p.

About the Authors

Babatope O. Kayode

*M.S. in Petroleum Engineering,
Heriot-Watt University*

Babatope O. Kayode is a Senior Reservoir Engineer working in Saudi Aramco's Reservoir Description & Simulation Department, where he works as a Simulation Engineer.

Babatope has 22 years of oil and gas industry experience. His research interests include the development of workflows for faster and better reservoir characterization and history matching.

Babatope is the author of 17 conference and

journal papers, and has filed 15 U.S. patents.

Babatope received his B.S. degree in Petroleum Engineering from the University of Ibadan, Ibadan, Nigeria, and his M.S. degree in Petroleum Engineering from Heriot-Watt University, Edinburgh, Scotland, U.K. Babatope is in the final stages of obtaining his Ph.D. degree from Heriot-Watt University.

Dr. Karl D. Stephen

*Ph.D. in Physics,
University of Strathclyde*

Dr. Karl D. Stephen is Associate Professor at Heriot-Watt University where he has worked for more than 25 years. Karl served as Visiting Professor for Enhanced Oil Recovery (EOR) at the Universiti Teknologi Petronas, Malaysia, in 2017.

He has taught Reservoir Simulation at Heriot-Watt University since 2000 and is Program Director for the Mature Field Management M.S. program. Karl also teaches CPD courses on reservoir modeling and simulation through industry training companies.

His research interests include history matching, optimization, proxy modeling,

upscaling, geological modeling, and simulation of EOR processes. Karl has authored or coauthored over 70 peer-reviewed papers and more than 90 conference papers.

He is a Technical Editor for the *Society of Petroleum Engineer (SPE) Journal* and *SPE Reservoir Evaluation*. Karl is a recipient of the 2012 Award for Outstanding Service by the SPE.

He received his B.S. degree in Physics from the University of Aberdeen, Aberdeen, Scotland, U.K. and his Ph.D. degree in Physics from the University of Strathclyde, Glasgow, Scotland, U.K.

Dr. Babatunde O. Moriwawon

*Ph.D. in Petroleum Engineering,
The Robert Gordon University*

Dr. Babatunde O. Moriwawon is a Petroleum Specialist working in Saudi Aramco's Reservoir Description and Simulation Department. Babatunde joined Saudi Aramco in 2013. Prior to this, he worked with various international oil companies and national oil companies in Nigeria, the U.K., and South Africa.

Babatunde's experience was garnered through his employment at notable E&P companies such as Eni, Shell, Sasol Petroleum, and the BG Group. Babatunde's research interests include assisted history matching

methodologies, uncertainty identification and quantification, geomechanics, and production optimization.

He is the author of many filed patents. Babatunde has also authored many technical papers.

He received his B.S. degree in Mathematics from the University of Port Harcourt, Choba, Nigeria. Babatunde received his M.S. and Ph.D. degrees in Petroleum Engineering from The Robert Gordon University, Aberdeen, Scotland, U.K.

Real-time Bit Wear Prediction and Deployment Validation in Challenging Hard and Heterogeneous Sandstones Using 3D Detailed and Simplified Physics-Based Progressive Wear Models

Dr. Guodong (David) Zhan, William B. Contreras, Dr. Xu Huang, Reed Spencer and Dr. John Bomidi

Abstract /

Drill bits experience significant cutter wear in hard and abrasive drilling applications, leading to high drilling cost. Therefore, the accurate prediction of bit progressive wear and its influences on drilling performance is crucial for bit design and drilling optimization, e.g., abrasive sandstones. This article presents two high fidelity bit wear models and how these drill bit wear tools were applied and validated in real-time tests in abrasive sandstone drilling.

Two advanced drilling prediction software models were trained on the drilling parameter, bit design, cutter wear, and formation evaluation data from past runs of interest. The models predict forces on both sharp and worn drill bits, and also use these cutting forces, the drilling parameters, and the rock properties to calculate the current wear state while drilling, and predict future wear state of the bit. Cutting force and thermomechanical wear formulas based on decades of drilling mechanics research are implemented.

The detailed physics-based model was used in the design workflow to simulate target drilling. The simplified physics-based wear model was developed based on this detailed model. In the simplified model, the cutting structure is represented by an equivalent single cutting element and validated against both lab and drilling data.

Multiple offset well data is cleaned and processed to build a pre-well training database. The two wear models are first trained using offset bit runs in the database and then tested on another selected target run in pre-well. The training and testing results show both wear models captured the progressive wear and the corresponding drilling responses very well. The pre-trained wear models were then deployed in the real-time trials. The predicted real-time bit wear and drilling performance matches with the well measurement reasonably well. While the detailed model considering the drill bit cutting structure is used in the bit design, the simplified wear model (SWM) implements the equivalent single cutting element and reduces the simulation time by more than 90%. It was observed that the physics and the learning transfer of the lab data improves the generalization capacity of the model and overcomes the overfitting issue, due to the limited scarcity or data bias in the real-time application.

This study presents two high fidelity progressive wear models by combining drilling physics and the data learning approach. The hybrid physics and data learning approach is applicable to the real-time applications in challenging drilling formations. The SWM improves the simulation speed significantly without losing the prediction accuracy, thereby opening new pathways for real-time applications and drilling automations.

Introduction

Drilling optimization is critical in hard rock applications. Polycrystalline diamond compact (PDC) bits experience significant wear in abrasive hard rock applications. When PDC bits wear significantly, it can drastically reduce the rate of penetration (ROP) in harder rock, which adds days for well production, increasing drilling costs. Because of this, it is important to have tools that allow engineers to design wear-resistant PDC bits, plan for drilling parameters before the run, and adjust drilling parameters during the run. PDC bit wear models have existed for a quite some time.

Physics-based wear models¹ and data-driven wear models² for bit wear and ROP predictions have been around for nearly 40 years. Consequently, challenges remain in applying these models to the applications for pre-well planning and real-time operations. The main difficulties are: (1) developing cutting force equations that cover all scenarios, (2) calibrating cutting forces for new drillings, and (3) calibrating wear characteristics for these new and various PDC bits based on their chemical makeup. In recent studies³, 3D drilling models using a hybrid

physics and lab/data learning approach successfully predicted the bit drilling parameters in a test.

In this article, the progressive wear of an individual cutter is included in this 3D drilling model to simulate the evolution of wear flats with the distance drilled. Thermomechanical wear modeling is based on decades of cutting mechanics research and laboratory findings. The progressive wear model was first trained and validated on multiple offset training wells. Then the pre-trained wear model was deployed in real-time tests. The results show the wear model reliably predicted both the progressive drilling response and final wear state in multiple real-time trial tests.

Detailed 3D and Simplified Progressive Wear Model

A detailed 3D progressive wear model is developed to predict the bit wear in real-time. In the detailed model, the 3D geometry of the bit body, cutters, and rock is represented by 3D mesh studies³. The geometric interaction between the cutting elements and the rock is calculated using a Boolean engine, Fig. 1a.

Figure 1b shows the cutting areas of various shaped cutters on the same bit blade. The red arrow indicates the cutting force magnitude and its orientation. In progressive wear simulation, the wear flat is modeled as a planar surface orientated along the local tangent of the drill bit profile. The evolution of the wear flat profile is accomplished by incrementally increasing the wear flat depth. Figure 2 demonstrates the wear evolution from the sharp state at the beginning of a normal run to the final wear state.

The cutting forces are calculated using a unified cutting force model library built on decades of cutting mechanics research studies³. The wear flat cutting force considers the effect of the depth of cut and local confinement due to the wear flat contact⁴. The force model formulas are evaluated against hundreds of controlled full-scale lab drilling tests under the downhole pressurized condition.

The highest ranking force model with the least training error and the least number of model fitting parameters is selected by the ensemble for performance

Fig. 1 (a) A detailed 3D representation of the bit-rock interaction, and (b) the cutting areas of various shaped cutters on the same bit blade.

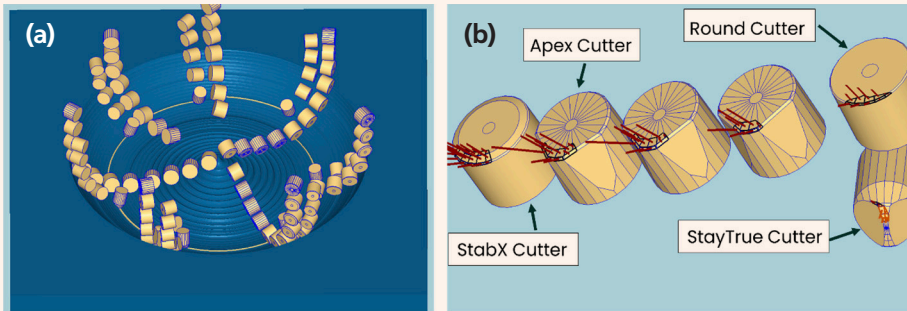
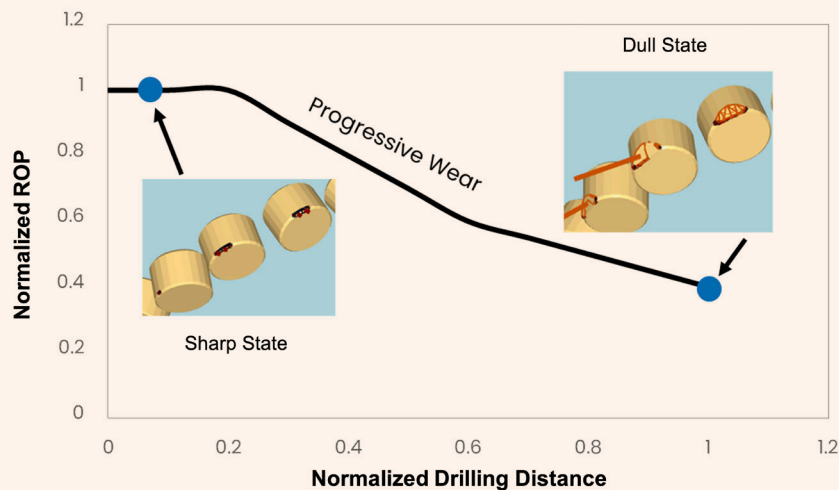


Fig. 2 The wear evolution from sharp state to dull state.



prediction and bit design optimization. The progressive wear rate is calculated at each drilling depth using a thermomechanical wear model⁵. The wear rate is a function of cutting force, cutting velocity, surface friction, cooling rate, and material abrasivity¹. The parameters of the wear rate model are determined by combining the results from finite element analysis, computational fluid dynamics modeling, and lab wear tests. In real-time applications, the wear parameters are further refined by training on the offset well data of the target well.

A robust differential evolution algorithm is employed for the model parameter optimization⁶. The error metric includes both a drilling response error, such as weight on bit (WOB)/torque on bit (TOB), and the final wear area distribution error. During the model training process, it is observed that transferring the lab data learning to the data training is critical for the model generalization capacity⁷.

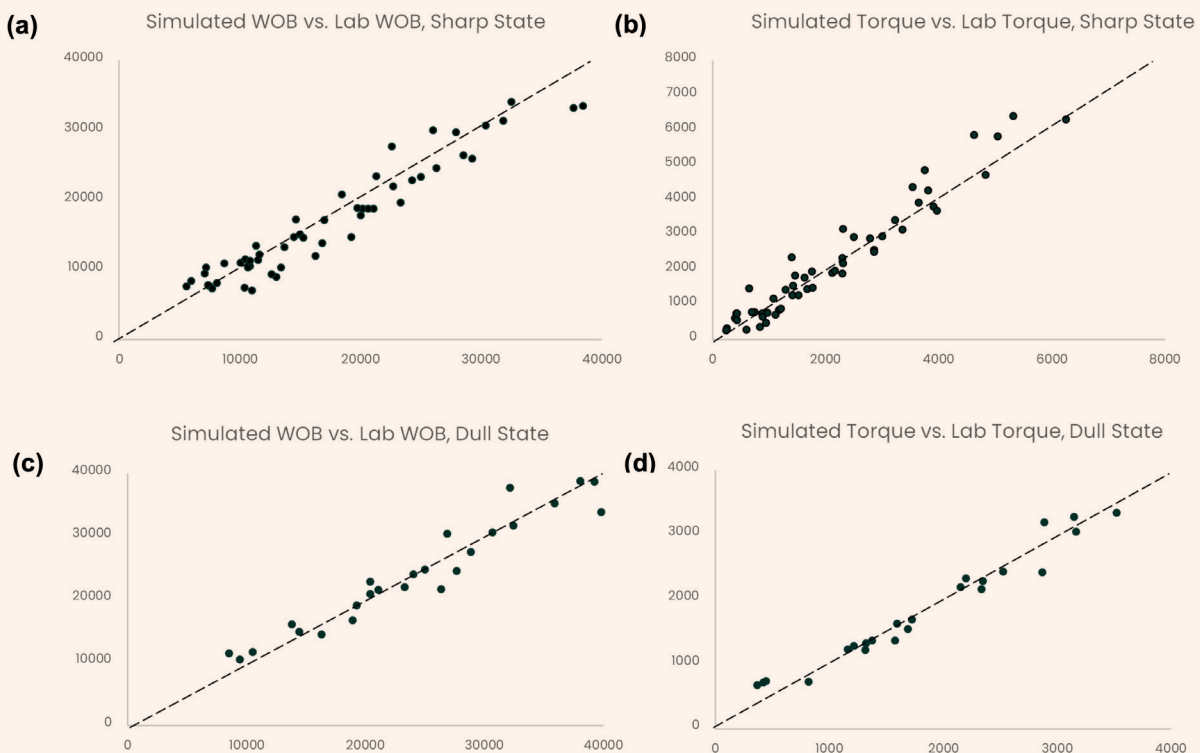
While the 3D mesh model captures the detailed cutting structure and bit-rock interaction, its real-time application is limited by the high computational cost. To improve the model efficiency, a simplified progressive wear model is developed. The simplified wear model (SWM) converts the detailed cutting structure into a simplified equivalent single cutting element. The bit diameter and bit total penetration rate is utilized to calculate the equivalent cutting area of the single

cutting element. An equivalent radial position, averaged back rake angle, and chamfer size is implemented in the SWM to capture the geometry effect on the in situ rock cutting strength⁸. Different from the detailed progressive wear model, the SWM calculates the total wear area on the bit, instead of per cutter wear.

The same unified cutting force model and thermo-mechanical wear model is applied in the SWM. To verify the geometry simplification and assumptions in the SWM, the SWM is trained using the same lab data set as the detailed wear model. Figure 3 shows the lab training results of the SWM on both sharp and dull states. The simulation is performed under a controlled ROP, and the simulated WOB/TOB response is compared with the lab measurements. Each data point in the figure represents one stable drilling state extracted from the full-scale downhole drilling tests. The training results show the SWM can capture the drilling response reasonably well for both the sharp state and dull state.

The training accuracy of the SWM is comparable to the detailed 3D model. It should be noted though, as the SWM improves the simulation speed with a comparable model accuracy, the SWM doesn't consider the detailed cutting structure of the bit. Therefore, the application of the SWM should focus on the real-time bit wear prediction, and the detailed 3D wear model is required for the bit design optimization.

Fig. 3 The simulation results of the SWM vs. lab drilling results after model training at both sharp and dull states: (a) sharp state WOB, (b) sharp state TOB, (c) dull state WOB, and (d) dull state TOB.



Multi-Well Model Training and Validation in Pre-Well

The lab trained detailed 3D and SWM models are re-trained using the offset well data in the target application. It was found that the learning transfer from the lab training to the well is crucial to improve the model generalization capacity and avoid model overfitting.

The lab learning transfer involves two aspects. The first aspect is the model parameter transfer such that the selected model parameters trained using the lab analogy rock remains the same in the application. The second aspect of the learning transfer is to apply the searching boundaries learned from the lab to constrain the parameter optimization in the model training. It not only improves the training speed, but also avoids nonphysical solutions.

This section presents the pre-well training and validation results of the 3D detailed model and the SWM using multiple offset well runs in the target hard and abrasive sandstone application.

Figures 4a to 4c shows the simulated WOB of the detailed wear model vs. the WOB after the model training on three offset bit runs. To improve the training efficiency, a stand-alone parameter optimization engine was developed and coupled with the detailed 3D progressive simulation engine. The progressive wear rate and the cutting force is calculated at every 10 ft, and the wear flat geometry is updated accordingly. The training results show the detailed progressive wear

model captured the WOB response very well for all three offset runs. As expected, the simulated WOB increases gradually as increasing the drilling distance due to the progressive wear effect.

Figures 4d to 4f shows the wear comparison of the detailed model. It was observed that the simulated wear matches with the wear very well in terms of both the distribution shape and the wear magnitude. To validate the model, the pre-trained model is set in the prediction mode and applied to predict another offset run, run 4. The predicted WOB agreed with the WOB reasonably well with an overall error of ~11%.

Figure 5 shows the predicted wear matches with the distribution wear. It was observed that the dull grade of the measurement jumped suddenly from the standards provided by the International Association of Drilling Contractors (IADC) 0.2 to 1.0 from the fourth cutter, indicating a nonabrasive impact damage, probably due to the bit vibration.

The same pre-well training runs (run 1 to run 3) and validation run (run 4) are used to train and test the SWM. Figure 6 shows the simulated WOB of the SWM vs. the WOB on the three training runs, runs 1 to 3. After the model training, the SWM captured the progressive WOB, Figs. 6a to 6c, with a reasonable accuracy. The model training time of the SWM is less than 5% of the time required for the detailed model. Figure 6d shows the total wear area comparison between the SWM and the measurement. Note the

Fig. 4 The detailed model: simulation results vs. results after model training on three offset well runs, runs 1 to 3.

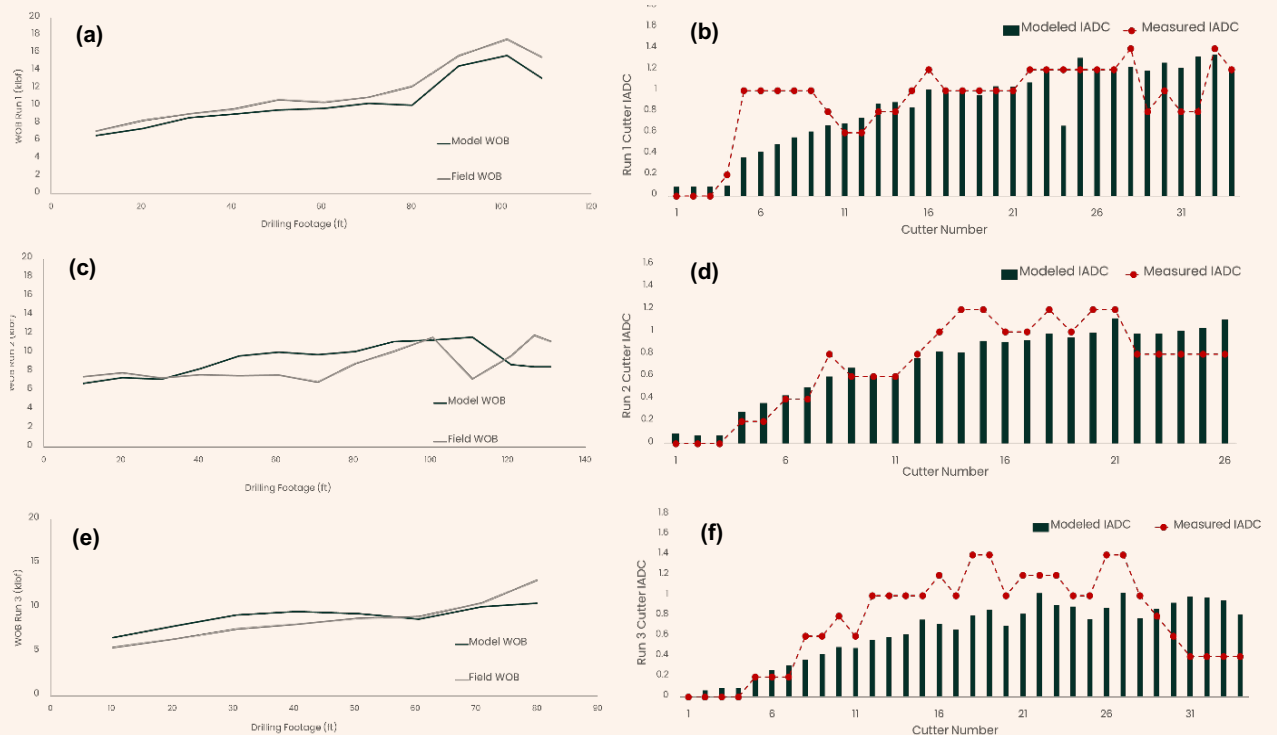
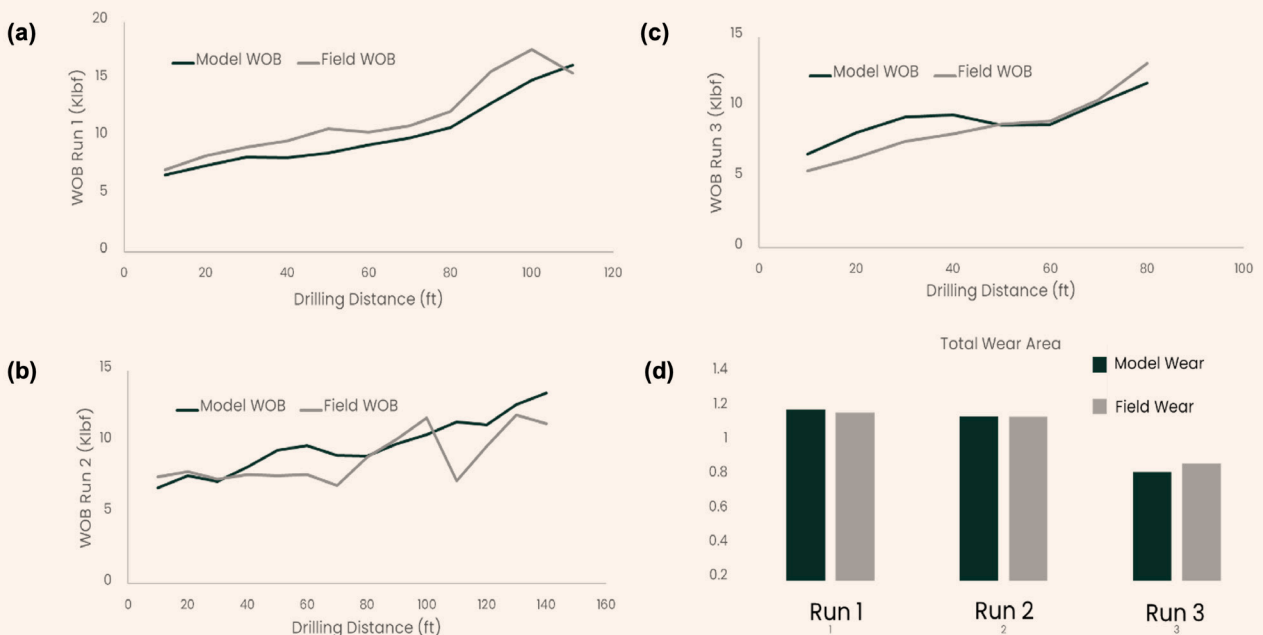


Fig. 5 The detailed model: predicted wear distribution vs. wear distribution on test run 4.



Fig. 6 The SWM: simulation results vs. results after model training on three offset well runs, runs 1 to 3.



SWM approximates the bit cutting structure as an equivalent single cutting element, instead of the detailed 3D cutting geometry. Therefore, only the total wear area is available and outputted for the comparison. The training results show the simulated total wear area agrees with the wear area decently well on all three training runs.

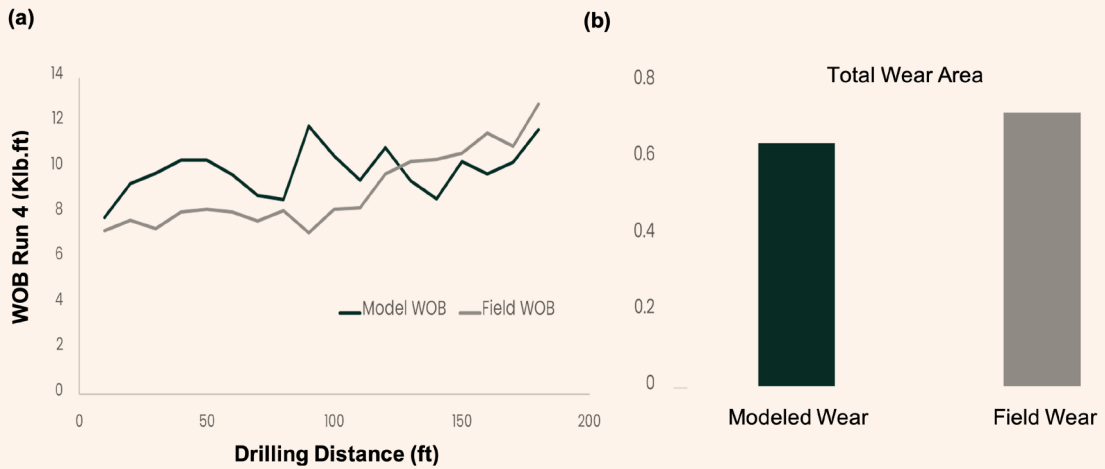
Figure 7 shows the validation results of SWM on run 4. Figure 7a shows the predicted WOB vs. the field WOB. The overall error of the predicted WOB is ~15%. The predicted total wear area matches with

the measurement very well, Fig. 7b. Overall, the SWM captured both the WOB response and the final wear state very well in validation run 4, and the wear model is ready for the real-time trial.

Wear Model Real-Time Trial

The pre-trained detailed 3D wear model and the SWM were tested in real-time for a selected target well. During the real-time trial, the surface drilling data and downhole logging data was cleaned and processed in real-time. The averaged rock properties from

Fig. 7 The SWM: predicted results vs. results on test run 4.



the offset wells are used as the initial input and fine adjusted if needed⁹.

The predicted wear and projected ROP in the next 50 ft were reported daily as a drilling guidance. The simulated WOB was monitored and compared to the WOB to verify the drilling response of the model. Once the bit run was completed, the reported final bit wear before the bit was pulled out of the hole was compared to the measured wear based on the wear photos.

Figure 8 shows the real-time simulated WOB vs. the WOB of the detailed 3D model. The comparison results show the detailed 3D model captured the WOB very well in real-time. Figure 9 shows the final bit wear comparison. The model predicted wear (blue bar) matched with the wear (red dot) excellently. Note, that to improve the comparison accuracy, a refined

IADC grade with a resolution of 0.2 is implemented as shown in the figure, instead of the standard IADC resolution of 1.0. It is observed the wear shows a wear jump at cutter number 7, 10, and 34, probably due to the downhole vibration.

The same run was utilized to test the SWM in real-time. Figure 10 shows the real-time simulated ROP vs. the ROP. It should be noted the ROP, instead of WOB, is used for the drilling response comparison in the real-time SWM. The ROP calculation under the WOB control is usually more time-consuming. Numerical iterations are required to obtain a converged solution and the optimization of the proportional integral derivative parameters are needed. The low computational cost of the SWM enables the real-time ROP calculations.

Fig. 8 The real-time detailed model: modeled WOB vs. WOB on real-time run 6.

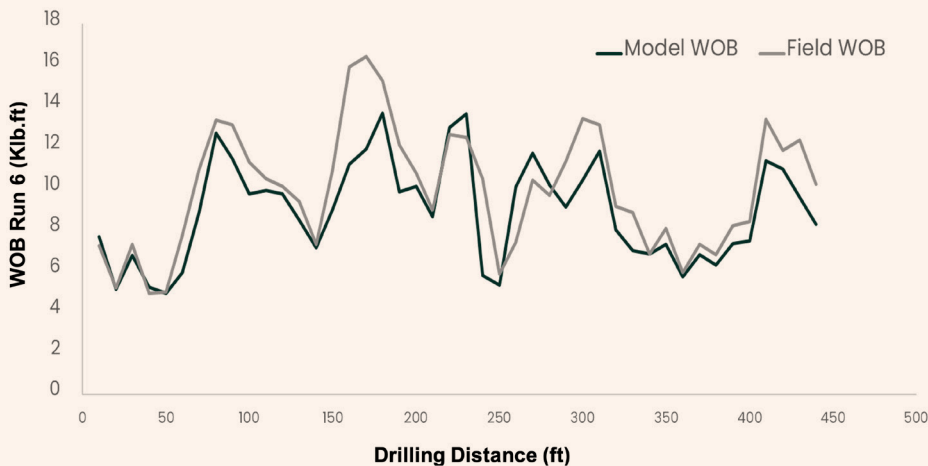


Fig. 9 The real-time detailed model: predicted wear distribution vs. wear distribution on real-time run 6.

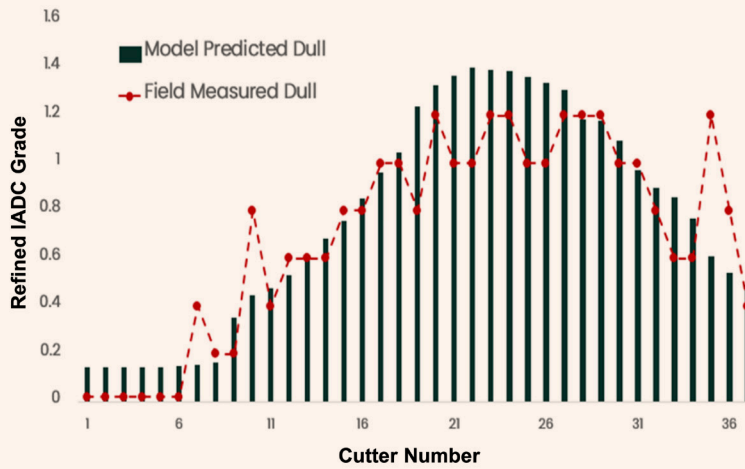


Fig. 10 The real-time SWM: predicted results vs. results on the real-time run 6.

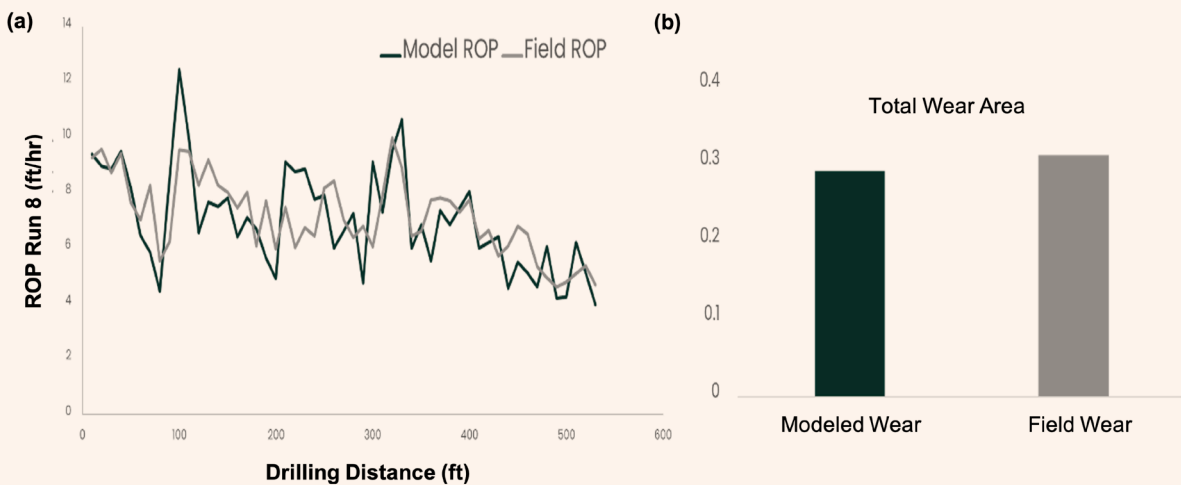


Figure 10a shows the real-time simulated ROP matched with the ROP. The decreasing trend of the ROP due to the progressive wear is captured by the SWM very well. Figure 10b shows the final wear area predicted in real-time vs. the measured final wear area. The prediction error of the total wear area is smaller than 10%. Both the detailed model and the SWM were real-time tested in multiple runs in this well and good matches were observed. Overall, the real-time results validated the real-time application of both the 3D detailed model and the SWM.

Conclusions

This article presents two high fidelity bit wear models and how these drill bit wear tools were applied and validated in real-time tests. The two wear models are first trained using three offset bit runs and then tested

on another selected target run in pre-well environment. The pre-trained wear models were then deployed in real-time trials. The predicted bit wear and drilling performance in real-time matches with the measurement reasonably well for both the detailed 3D model and the SWM. While the detailed wear model considers the bit cutting structure and is used for the bit design, the SWM implements the equivalent single cutting element and reduces the simulation time by more than 90%.

It was observed that the physics and the lab data learning transfer improves the generalization capacity of the model and overcomes the overfitting issue due to the limited scarcity or data bias in the real-time application. The SWM improves the simulation speed significantly without losing the prediction accuracy,

thereby opening new pathways for real-time applications and drilling automations.

Acknowledgments

This article was presented at the Middle East Oil and Gas Show and Geosciences Conference and Exhibition, Manama, Kingdom of Bahrain, February 19-21, 2023.

The authors would like to thank Oliver Matthews III, Mahmoud Alraheb, Ali Al Dhamen, Will Moss, and Trieu Luu for all their respective contributions in model development, rock properties, data evaluation, data cleaning/synchronization, lab data preparation. The exploratory hybrid model work by Jayesh Jain, Richard Borge, Alberto Rivas, and the Baker Hughes authors was a good reference for this study. We also thank the reviewers for valuable input.

References

1. Glowka, D.A. and Stone, C.M.: "Effects of Thermal and Mechanical Loading on PDC Bit Life," *SPE Drilling Engineering*, Vol. 1, Issue 5, June 1986, pp. 201-214.
2. Gooneratne, C.P., Magana-Mora, A., Contreras Ovalvora, W., Affleck, M., et al.: "Drilling in the Fourth Industrial Revolution — Vision and Challenges," *IEEE Engineering Management Review*, Vol. 48, Issue 4, December 2020, pp. 144-159.
3. Zhan, G., Magana-Mora, A., Moellendick, E., Bomidi, J., et al.: "Hybrid Physics — Field Data Approach Improves Prediction of ROP/Drilling Performance of Sharp and Worn PDC Bits," IPTC paper 21457, presented at the International Petroleum Technology Conference, virtual, March 25-April 1, 2021.
4. Zhou, Y. and Detournay, E.: "Analysis of the Contact Forces on a Blunt PDC Bit," paper presented at the 48th U.S. Rock Mechanics/Geomechanics Symposium, Minneapolis, Minnesota, June 1-4, 2014.
5. Archard, J.F.: "Contact and Rubbing of Flat Surface," *Journal of Applied Physics*, Vol. 24, Issue 8, 1953, pp. 981-988.
6. Storn, R. and Price, K.: "Differential Evolution — A Simple and Efficient Heuristic for Global Optimization over Continuous Spaces," *Journal of Global Optimization*, Vol. 11, Issue 4, December 1997, pp. 341-359.
7. Magana-Mora, A. and Bajic, V.B.: "OmniGA: Optimized Omnivariate Decision Trees for Generalizable Classification Models," *Scientific Reports*, Vol. 7, Issue 1, June 2017, pp. 1-11.
8. Detournay, E., Richard, T. and Shepherd, M.: "Drilling Response of Drag Bits: Theory and Experiment," *International Journal of Rock Mechanics and Mining Sciences*, Vol. 45, Issue 8, December 2008, pp. 1547-1560.
9. El Sherbeny, W., Hasan, G., Lindsay, B.W., Madkour, A., et al.: "Role of Wellbore Imaging and Specific Mineralogy Inputs Data in Bit Selection and Design Softwares," SPE paper 182759, presented at the SPE Kingdom of Saudi Arabia Annual Technical Symposium and Exhibition, Dammam, Kingdom of Saudi Arabia, April 25-28, 2016.

About the Authors

Dr. Guodong "David" Zhan

Ph.D. in Metallurgical Engineering,
Huazhong University of Science and Technology

Dr. Guodong "David" Zhan is a Science Specialist and the Team Leader of the Advanced Drilling Tools team in the Drilling Technology Division at Saudi Aramco's Exploration and Petroleum Engineering Center – Advanced Research Center (EXPEC ARC). David is a world-renowned materials scientist and expert in advanced drilling tools/technology. He has over 29 years of experience in industrial R&D and managerial positions, including positions as Chief Engineer and R&D Manager at top oil/gas and semiconductor global companies, such as Schlumberger, NOV, and Applied Materials.

Additionally, David has held academic positions at the University of London and the University of Colorado at Boulder, and staff scientist positions at the Japan National Institute for Materials Science and the Shanghai Institute of Ceramics, Chinese Academy of Sciences.

He is an active member of the Society of Petroleum Engineers (SPE) where he serves on several conferences such as the SPE International Petroleum Technology Conference and the Asia Pacific Drilling Technology Conference/ International Association of Drilling Contractors as co-chair and technical committee member.

David is also serving as an editorial board member and reviewer for a number of international scientific journals published by The Minerals, Metals and Materials Society and the Material Research Society.

He has won many prestigious international awards, such as the 2020 Hart Energy Award, two 2021 World Oil Awards on Best Drilling Technology and the Innovative Thinker Award, the 2022 ADIPEC Award Breakthrough of Research Award, the 2022 Industry of Thing (IoT) World Award, and the 2023 Offshore Technology Conference Distinguished Achievement Special Citation Award.

David has published 104 peer-reviewed articles in journals such as *Nature Materials* and *Nature Scientific Reports*, 115 conference proceedings, and has more than 150 filed/published/granted U.S. patents, with an H-index of 39.

In 1994, he received his Ph.D. in Metallurgical Engineering from Huazhong University of Science and Technology, Wuhan, China, and completed a postdoctoral fellowship in Nanomaterials and Nanotechnology at the University of California at Davis.

About the Authors

William B. Contreras

*M.S. in Petroleum Engineering,
University of Tulsa*

William B. Contreras is a Drilling Engineering Specialist working in the Information Analysis and Integration Unit of Saudi Aramco's Drilling Technical Department. Prior to joining Saudi Aramco in 2009, he worked with several different oil and gas companies, including PDVSA in Venezuela, PEMEX in Mexico, and Halliburton in several countries within Latin America, working in diverse positions, such as Drilling Engineer, Drilling Superintendent, and several management positions.

During William's time at Saudi Aramco, he has been working at multiple development sites, trying to capitalize on the drilling

information assets to generate smart systems based on traditional data, as well as real-time information coming from the surface and down-hole sensors.

William has published more than 20 papers and holds three patents. He is an active member of the Society of Petroleum Engineers (SPE).

In 1990, William received his M.E. degree in Mechanical Engineering from the Universidad de Los Andes, Mérida, Venezuela, and in 2002, he received his M.S. degree in Petroleum Engineering from the University of Tulsa, Tulsa, OK.

Dr. Xu Huang

*Ph.D. in Engineering Mechanics,
Pennsylvania State University*

Dr. Xu Huang is a Senior Research Engineer with Baker Hughes. He is considered the industry expert in drilling mechanics and the advanced modeling of drill bits.

In 2012, Xu received his Ph.D. degree in Engineering Mechanics from the Pennsylvania State University, State College, PA.

Reed Spencer

*B.S. in Mechanical Engineering,
University of Utah*

Reed Spencer is a Research and Development Engineer with Baker Hughes, working in the Measurements, Physics and Sensors R&D Group. He 15 years of experience in the oil and gas industry.

Reed has developed directional drilling modeling software combining the bit, bottom-hole assembly, lithology, and drilling parameter effects.

He has also studied stick-slip, high frequency torsional oscillation, and lateral vibrations of polycrystalline diamond compact (PDC) bits. Reed has developed novel PDC design features for directional and abrasive drilling applications.

He received his B.S. degree in Mechanical Engineering from the University of Utah, Salt Lake City, UT.

Dr. John Bomidi

*Ph.D. in Mechanical Engineering,
Purdue University*

Dr. John Bomidi is the Research Manager for drill bits at Baker Hughes. He leads the Drill Bit R&D on themes of cutting-edge materials, engineering advancements, and artificial

intelligence/physics predictive modeling.

John received his Ph.D. degree in Mechanical Engineering from Purdue University, West Lafayette, IN.

Using Isotope Technology to Identify Oil and Gas Reservoir Sweet Spots

Dr. Feng H. Lu

Abstract /

Porosity and permeability of rocks are crucial parameters utilized to evaluate the quality of oil and gas reservoirs. Diagenesis in carbonate reservoirs commonly results in dissolution, and creates secondary porosity and permeability. At the same time, geochemical records, e.g., isotopes and elements, in the carbonate rocks are diagenetically altered. This study is to utilize the isotope technology to evaluate diagenesis and its impact on oil and gas reservoirs.

Micro-samples were collected from marine carbonate rocks in a studied reservoir for carbon and oxygen isotope analyses, plus analyses of strontium (Sr) isotopes and element concentrations. The analytical results show outstanding negative shifts of oxygen isotopes in some intervals, whereas carbon and Sr isotopes have a minor or little change. These intervals also contain lower elements, including Sr. It is believed that these intervals experienced the dissolution with abundant secondary porosity, and are the best potential for oil and gas reservoirs.

A petrographic study indicates minor cements, but higher porosity developed within these intervals. This is confirmed by high porosity measured within these intervals by using other methods, including gas injection and well logging. Therefore, the isotope technology can be utilized as an effective method to assess reservoir potential and determine reservoir sweet spots. Note that carbonate cementation commonly occurs during diagenesis, and diagenetic calcite cements normally show negative oxygen isotopes. If the samples happen to contain a certain amount of such cements, the analytical results will show lower oxygen isotopes and trace elements than their primary values in the studied marine carbonates.

The petrographic study was also conducted to help micro-sampling, and verify that cements were not collected in the studied carbonate rocks for isotope analysis. Furthermore, the degrees of water-rock interaction were quantitatively assessed by modeling variations of isotope pairs, which can help evaluate the quality of reservoirs relating to the intensity of diagenesis.

The implementation of this study is that the isotope results obtained from one studied well can be applied in the whole field or/and the region, as diagenesis rarely occurs only around one well. This will save the cost for repeated measurements from different wells and fields by using other methods.

Introduction

Characterizing conventional and unconventional oil and gas reservoirs is not only challenging, it is one of the major tasks for reservoir development and management¹. Porosity and permeability are the key parameters to understand reservoir sweet spots. Porosity is defined as a measure of the capacity of reservoir rocks to contain or store fluids, which may be gas, oil, and water stored in the reservoir pore spaces². Obviously, higher porosity indicates more capacities of reservoir rocks to store these fluids, while lower porosity suggests the opposite. The intervals with high porosity contain more hydrocarbons, and are the sweet spots.

Porosity in carbonate rocks includes primary and secondary, and the latter is often more important as carbonates, compared to clastic rocks, are more reactive and prone to be altered physically and chemically during diagenetic and catagenetic processes³. There are numerous methods to directly and indirectly measure porosity in a reservoir, such as fluid/gas injection, image analysis, well logging technique, seismic analysis, and well testing⁴. Many of these methods are time-consuming and expensive, and require cross-checking to validate and calibrate data for one another due to uncertainty and errors.

This article proposes a new isotope technology to evaluate porosity development relating to diagenesis, and quantitatively model the intensity of diagenesis and water-rock interaction to help identify the best reservoir intervals.

Methods

Marine carbonate sediments often contain metastable mineral components, including aragonite and high magnesium (Mg)-calcite, which may be dissolved out and/or replaced by a more stable phase, e.g., low-Mg

calcite, dolomite, in a new regime where either pore fluids have changed, e.g., meteoric water or seawater evaporation, or temperature and pressure have changed in deep burial². For example, dolomitization (dolomite replaces calcite) drastically increases secondary porosity — > 12% — based on the mole-for-mole replacement, as the molar volume of dolomite is much smaller than that of the precursors, the calcium carbonate minerals⁵. More importantly, such diagenetic processes increase not just total porosity, but also effective porosity and permeability when diagenetic fluids pass through and interact with carbonates.

Diagenetic processes alter the geochemistry of carbonate rocks as well. Oxygen isotopes of carbonates are the most sensitive, and therefore, the first to change because oxygen is the major element in both carbonate minerals and water. When water-rock interaction occurs, e.g., between meteoric water and marine carbonate minerals, oxygen isotopes between water and carbonates start to exchange, commonly resulting in negative oxygen isotope shifts in the altered minerals⁶.

The most negative oxygen isotope shifts can be utilized as an indicator for the development of dissolution and secondary porosity during diagenesis, and these intervals are the best reservoir potentials. As water-rock interaction increases intensity, other isotopes in carbonates such as strontium (Sr) and carbon isotopes will be gradually altered as well⁶. In addition, modeling the co-variations of isotope pairs in the process of increasing diagenesis and water-rock interaction can quantify the intensity of diagenesis.

A slab of core carbonate rocks was collected from each foot, and a dental drill was employed to drill into the slab in a matrix area to draw micro-sample powders. Only clean and fresh portions without cements and fragments of clasts and fossils were micro-sampled. The powder samples were weighed, ranging from 200 µg to 400 µg, in reaction vials, which were then flushed with helium to remove the air.

Thereafter, phosphorous acid (H_3PO_4) was added to each of these vials to liberate CO_2 from the carbonates. The samples were analyzed for carbon and oxygen isotopes utilizing a Thermo-Fisher Gasbench coupling with a MAT 253 mass spectrometer. Two laboratory standards, which were previously calibrated with numerous international standards for carbon and oxygen isotopes, were analyzed along with samples at the beginning, middle, and end to calibrate isotope ratios for the samples. In addition, two international carbonate standards were analyzed to check the analytical accuracy. Standard deviations from repeated analyses of standards for carbon and oxygen isotopes are better than 0.10%.

Besides carbon and oxygen isotope analyses, the sampled powders were also utilized for Sr isotope analysis along with the analyses of element concentrations, including Sr. The analysis of Sr concentrations was performed using an Agilent 7500cx quadrupole inductively coupled plasma mass spectrometer. A calibration curve was established using certified element standards.

The range in standard concentration was 50% to 200% of the expected sample concentration. Concentrations in the solution were determined by using the signal intensity relative to the certified standard. In addition, calculation based on the dilution factors was applied for the original samples.

The analyses of the Sr isotope compositions were performed using an IsotopX Phoenix X62 thermal ionization mass spectrometer. The Sr was separated from interfering elements using a Sr specific ion exchange resin. The separation chemistry and dilutions were performed in a class 10 clean room using ultra-pure reagents. Approximately 200 ng of Sr was loaded on zone refined Re filaments with a tantalum “loader” solution for mass spectrometric analysis.

Several standards (NIST SRM 987) were run with every turret. The long-term average was used to correct the sample to the certified National Bureau of Standards and Technology (NIST) value. An in-run mass bias correction was applied for all sample and standard analyses using the in-run measured $^{86}Sr/^{88}Sr$ ratio, which is corrected to the natural abundance ratio of 0.1194 using an exponential relation. Internal precision for a single run was less than 0.0004%, and there was a negligible contribution to the analytical uncertainty. Analytical uncertainty is determined from the 2-sigma uncertainty of repeated analyses of SRM 987 in the laboratory before and during the time of the analyses.

Furthermore, thin sections from the representative lithofacies were prepared for petrographic studies to understand mineral composition and diagenetic processes, e.g., cementation, dissolution and recrystallization, by utilizing instruments, including polarizing microscopes, cathodoluminescence, scanning electron microscopy, and X-ray diffraction. The geochemical data were then processed, including the plots of isotope and element values vs. depth from the core samples.

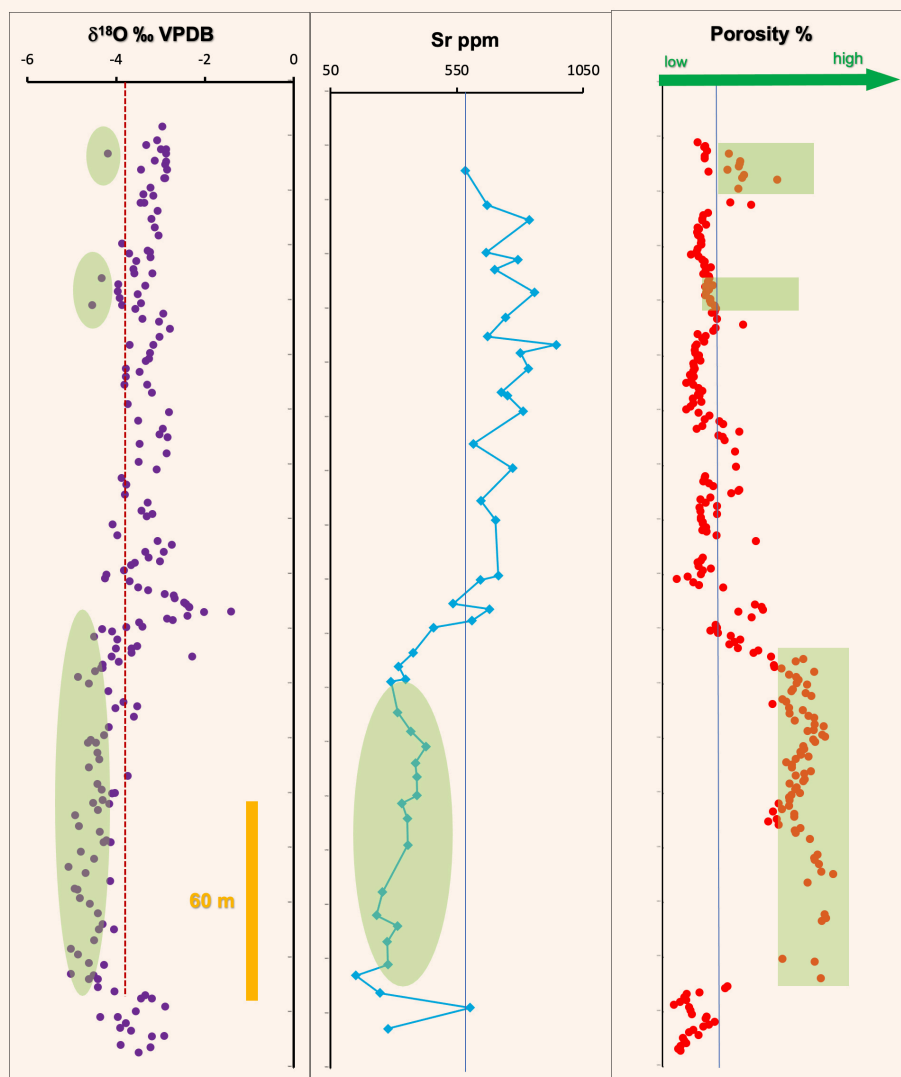
Results and Discussion

Figure 1a shows the oxygen isotope profile of carbonate rocks collected from a studied formation. It appears that outstanding negative shifts of oxygen isotopes occur in two to three intervals, which are identified as the best potential of reservoir sweet spots. Figure 1b shows the profile of the Sr concentrations from the core samples taken from the same well, and the lower Sr contents are consistent with the negative oxygen isotopes in the same interval. Porosity from these core samples was measured by using other methods (well logging and gas injection), Fig. 1c.

As demonstrated in Fig. 1, the highest porosity is consistent with the outstanding negative oxygen isotopes and lower Sr contents in these intervals. It is noteworthy that the petrographic study on these core samples indicates that there are multiple diagenetic events, including compaction, dissolution and cementation, which occurred during the relatively early diagenesis, perhaps in a shallow burial environment where meteoric water intruded in the marine carbonate rocks.

The petrographic study also indicates that cements are

Fig. 1 The profiles of the parameters in a studied well. (a) The profile of oxygen isotopes; (b) The profile of Sr contents, consistent with the oxygen isotope data; and (c) the profile of porosity, measured by using well logging calibrated by the gas injection. The shaded intervals are the sweet spots.



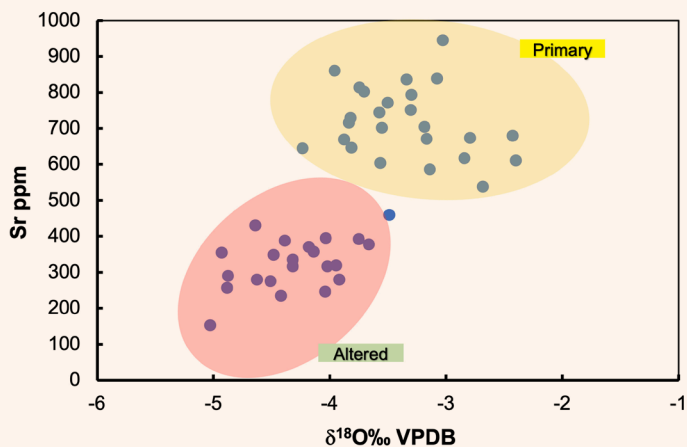
insignificant in these carbonate rocks. While contacting with meteoric water, metastable minerals in the marine carbonates such as aragonite and high-Mg calcite would experience dissolution and conversion to a more stable mineral phase such as calcite or dolomite¹.

Figure 2 shows the cross-plot of oxygen isotopes and Sr content, and there are two distinguishable groups. The lower group has a positive correlation between the depleted Sr content and the low oxygen isotope values, suggesting that the two parameters were likely altered by a similar process, i.e., meteoric water diagenesis. In contrast, the upper group with relatively higher Sr and oxygen isotopes — representing the ranges of primary marine carbonates — shows no trend or correlation. Note that the values of the two parameters (Sr and oxygen isotopes) in carbonate minerals are controlled by completely different factors during the deposition

of marine carbonate minerals. For example, the Sr content in carbonate minerals is mainly controlled by several factors, including the Sr content in seawater, the mineral phase, e.g., high in aragonite, and the rate of mineral growth⁷. Whereas the oxygen isotope values of carbonate minerals are controlled mainly by factors that include temperature, seawater, and salinity⁸.

The degree of physical and chemical change in marine carbonate rocks by diagenesis depends on the intensity of water-rock interaction. For instance, progressive water-rock interaction may result in dissolution, porosity development, and high potential for petroleum reservoirs. Moreover, a highly intensive water-rock interaction in a closed system may cause recrystallization, crystal overgrowth, and widespread cementation, which would decrease porosity and permeability, and have a negative impact on the quality of reservoirs⁹.

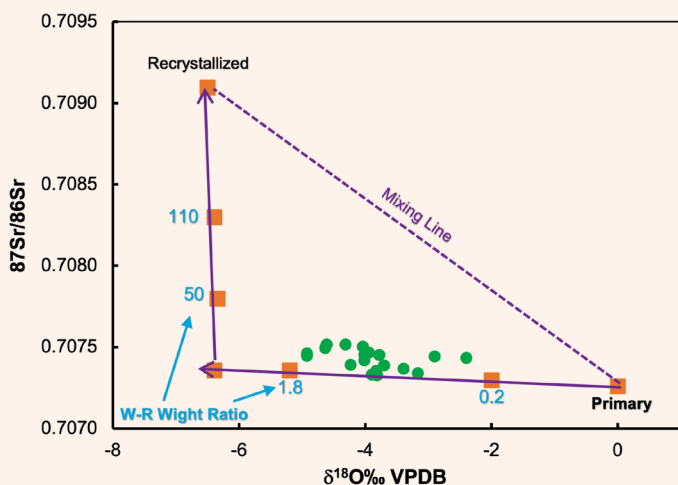
Fig. 2 The cross plot of Sr content and oxygen isotopes (two groups). The upper group mainly represents primary marine carbonates, and the lower group represents altered carbonates, which experience water-rock rock interaction.



Therefore, it is important to understand the degree of diagenesis and water-rock interaction.

Figure 3 shows that the modeling covariations of the Sr and oxygen isotope pairs are utilized to track and assess the process and intensity of water-rock interactions. As previously mentioned, because oxygen is a major element in both water and carbonate minerals, oxygen is perhaps the first geochemical parameter to change when a water-rock reaction occurs. In contrast, carbon is a major element in carbonate minerals, but a trace element in formation water. In addition, Sr is a trace element in carbonate minerals and diagenetic fluids, so the exchange of Sr isotopes and carbon

Fig. 3 Modeling oxygen and Sr isotopes tracking the water-rock interaction in marine carbonates during meteoric water diagenesis. The mixing line represents a mixture between the two end members (the primary marine carbonates and cements or completely recrystallized carbonates).



isotopes between mineral and water is much lower than that for oxygen⁶.

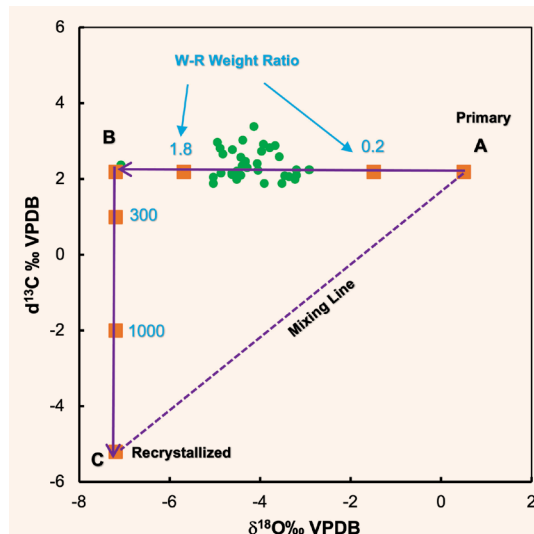
The pathway is marked with water-rock weight ratios. The modeling results show that the degree of water-rock interaction in the studied rocks is not high, because little change has occurred to the Sr isotopes.

Figure 4 shows variations of modeling carbon and oxygen isotopes during the water-rock interaction. It appears the impact of water-rock interaction is significant on oxygen isotopes, but little on carbon isotopes. As carbon is a major element in carbonate minerals, e.g., calcite, and diagenetic waters normally contain little carbon, the water-rock weight ratios have to be high, e.g., hundreds to thousands, to change carbon isotopes in the minerals¹⁰. Note that if sampling contains a certain amount of recrystallized portion plus an unaltered portion of the primary marine carbonates, the data will fall along the dashed mixing line.

As previously mentioned, a mild water-rock interaction may help improve the quality of reservoirs. In contrast, highly intensive water-rock interaction and significant cementation in a relative closed system may reduce porosity and permeability. As previously shown in Fig. 1a and Fig. 4, the intervals with the outstanding negative isotope shifts shall have experienced a mild diagenesis/dissolution, and contain abundant secondary porosity.

These intervals are the best reservoir potential, as confirmed by the high porosity data measured by using other methods, Fig. 1c. Therefore, it appears that the isotope technology can be utilized as one of the effective methods to evaluate reservoir potential and determine reservoir sweet spots.

Fig. 4 The modeling of oxygen and carbon isotopes tracking the water-rock interaction in carbonate rocks during meteoric water diagenesis. The mixing line represents a mixture between the two end members (the primary marine carbonates and cements or completely recrystallized carbonates).



Conclusions and Implementations

The porosity and permeability of rocks are crucial parameters utilized to assess the quality of oil and gas reservoirs. Diagenesis — meteoric water diagenesis in particular — in carbonate reservoirs commonly results in dissolution, and creates secondary porosity and permeability, which are often more important for carbonate rocks. Isotope technology can be utilized to evaluate diagenesis and the reservoir's potential, and also identify sweet spots. In addition, modeling covariations of isotope pairs can help quantify the degree of water-rock interaction.

Highly intensive water-rock interaction, particularly in a closed system, may result in additional cementation, alteration of most geochemical parameters, and a negative impact on the quality of reservoirs. It is important to note that a petrographic study is needed to help with the micro-sampling, and verify whether or not the outstanding negative oxygen isotopes were derived from carbonate cements or recrystallization.

The implementation of this methodology is that the results from one studied well can be applied in the whole field/region, as diagenesis rarely occurs only in a small area near one well. This will save on the expense for repeated measurements from different wells and fields by using other methods.

References

1. Moore, C.H. and Wade, W.J.: *Carbonate Reservoirs: Porosity, Evolution and Diagenesis in a Sequence Stratigraphic Framework*, 2nd edition, Amsterdam: Elsevier Science, 2015, 392 p.
2. Morse, J.W.: "Formation and Diagenesis of Carbonate Sediments," Chapter 5 in *Sediments, Diagenesis and Sedimentary Rocks: Treatise on Geochemistry*, Vol. 7, Mackenzie, F.T. (ed.), Elsevier, 2005, pp. 67-85.
3. Choquette, P.W. and Pray, L.C.: "Geologic Nomenclature and Classification of Porosity in Sedimentary Carbonates," *AAPG Bulletin*, Vol. 54, February 1970, pp. 207-250.
4. Elkatatny, S., Tariq, Z., Mahmoud, M. and Abdulraheem, A.: "New Insights into Porosity Determination Using Artificial Intelligence Techniques for Carbonate Reservoirs," *Petroleum*, Vol. 4, Issue 4, December 2018, pp. 408-418.
5. Al-Aasm, I.S. and Lu, F.H.: "Multistage Dolomitization of Mississippian Turner Valley Formation, Quirk Creek Field, Alberta: Chemical and Petrologic Evidence," *Canadian Society of Petroleum Geologists Memoir*, Vol. 17, 1994, pp. 657-675.
6. Meyers, J.W., Lu, F.H. and Zachariah, J.K.: "Dolomitization by Mixed Evaporative Brines and Freshwater, Upper Miocene Carbonates, Nijar, Spain," *Journal of Sedimentary Research*, Vol. 67, Issue 5, September 1997, pp. 898-912.
7. Dietzel, M., Gussone, N. and Eisenhauer, A.: "Co-Precipitation of Sr²⁺ and Ba²⁺ with Aragonite by Membrane Diffusion of CO₂ between 10 and 50 °C," *Chemical Geology*, Vol. 205, Issues 1-2, January 2004, pp. 159-151.
8. Kubota, K., Shirai, K., Tomihiko, H. and Toshihiro, M.: "Oxygen and Hydrogen Isotope Characteristics of Seawater in Otsuchi Bay and Meteoric Water of Inflowing Rivers," *Coastal Marine Science*, Vol. 41, Issue 1, January 2018, pp. 1-6.
9. Luan, G., Azmy, K., Chunmei, D., Lin, C., et al.: "Carbonate Cements in Eocene Turbidite Sandstones, Dongying Depression, Bohai Bay Basin: Origin, Distribution, and Effect on Reservoir Properties," *AAPG Bulletin*, Vol. 106, Issue 1, January 2022, pp. 209-240.
10. Lu, F.H. and Meyers, W.J.: "Massive Dolomitization of a Late Miocene Carbonate Platform: A Case of Mixed Evaporative Brines with Meteoric Water, Nijar, Spain," *Sedimentology*, Vol. 45, Issue 2, March 1998, pp. 265-277.

About the Authors

Dr. Feng H. Lu

Ph.D. in Geochemistry,
Stony Brook University

Dr. Feng H. Lu is a Geological Consultant and the isotope application group leader, working in the Geochemistry Unit of Saudi Aramco's Exploration and Petroleum Engineering Center – Advanced Research Center (EXPEC ARC).

He has 30 years of experience in the oil and gas industry and academic research, involving environmental/ecological issues, paleoclimate change, and energy resources.

Feng's areas of expertise include isotope and element applications in source rock and reservoir characterization, the studies of source, maturation, and the migration of oil and natural

gas, chemostratigraphy, H₂S origin, and formation water characterization.

He has numerous granted patents and journal papers to his credit, and has been serving as a manuscript peer reviewer for multiple journals.

Feng received his B.S. degree in Structural Geology from the China University of Geosciences, Beijing, China, and his M.S. degree in Sedimentology from the University of Windsor, Windsor, Ontario, Canada. Feng received his Ph.D. degree in Geochemistry from Stony Brook University, Stony Brook, NY.

Thermal Impact on Sandstone's Physical and Mechanical Properties

Qasim A. Sahu, Ayman R. Al-Nakhli and Dr. Rajendra A. Kalgaonkar

Abstract /

Many processes in subsurface applications result in heating or cooling operations. Processes such as steam flooding, thermally induced fracturing, perforation, deep disposal of nuclear waste, and extraction of energy from geothermal reservoirs can impose a thermal field in geological reservoirs. That is, heat flux can induce stress in the rock and can have a pronounced effect on the physical and mechanical properties of rock bodies. Many researchers are exploring this method for fracturing applications; either by applying a thermal shock due to cooling the formation or imposing an instantaneous heating using plasma jet technology.

In this study, data were collected from the literature for physical and mechanical properties of sandstones that were subjected to different modes of thermal treatment. The objective is to investigate the impact of different thermal fields on sandstone properties. The main properties that were considered under this study were permeability, Young's modulus, and unconfined compressive strength (UCS).

The data was normalized to obtain a fair comparison and to understand the general trend at which those properties change as a function of temperature. Overall, the data shows that the permeability of sandstone increases when a cooling mode of treatment is imposed. Furthermore, the sandstone subjected to thermal shock with nitrogen shows a higher rate of increase in permeability. On the other hand, heating decreases the permeability of sandstone. Cooling reduces the UCS and Young's modulus, while heating, resulted in inconclusive results.

Introduction

Hydraulic fracturing in recent years has unlocked the potential from unconventional and tight reservoirs. These reservoirs cannot produce a commercial quantity of hydrocarbon because of very low matrix reservoir permeability in the range of milliDarcy to microDarcies. It is a revolutionary technology that connects the reservoir rock to the wellbore, through a highly conductive channel that helps in oil and gas production.

In a typical fracturing job, a water-based fluid (at surface temperature) is injected at a pressure above the breakdown pressure of the rock to initiate and propagate a fracture inside the reservoir rock. Even though fracturing technologies are advancing dramatically, there is still a remaining potential to further improve the efficiency of hydraulic fracturing. The main reason is that researchers in rock geomechanics are focused on hydraulic fracturing, and that other options are not seriously considered. Moreover, there are still some challenges associated with the currently available technologies such as high breakdown pressure, excessive use of freshwater, and residual damage from current fracturing fluids.

One phenomena that is not yet fully understood and addressed is the effect of thermal treatment in reservoir rock and how it affects, for example, hydraulic fracturing treatments. Researchers are exploring alternative ways to improve fracturing treatment, such as the thermal shocking technique. Conceptually, the unconstrained rock will expand and undergo a volumetric strain if a heat treatment is applied and the temperature of the rock is increased. The opposite is also true when the rock is cooled down. In constrained rock, like hydrocarbon reservoirs, the stress regime will change as a result of thermal alteration.

The thermo-elasticity theory implies that stress is induced in the formation as a result of thermal effects. The induced stress may result in a tensile or shear failure of the reservoir rock. An injectivity increase was observed in the field after the injection of a cold fluid. The increase in injectivity is attributed to induced stress, which resulted from the change in the reservoir temperature. The in situ stress was reduced to the point that the injection pressure is higher than the minimum in situ stress, which opens cracks that enhanced the well injectivity. In that context, applying a sudden thermal treatment can have a pronounced effect on the physical, mechanical, and thermal properties of the rock.

Some researchers have reported that heating the rock under confining pressure may reduce the overall rock permeability¹. On the other hand, cooling the rock can increase the permeability due to crack generation or opening of existing cracks. The reaction of rocks and their effect on the physical and mechanical properties to

a thermal treatment depend on many parameters, such as the heating/cooling rate, rock structure, mineralogy, thermal properties, and experimental procedures.

Therefore, it is crucial to understand the effect of the thermal treatment on rock properties when considering this mode of fracturing. Also, many processes in the subsurface application impose cyclic heating and cooling to rock.

This article presents the result of previous studies that were focused on the effect of thermal treatment on sandstone's physical and mechanical properties. It is essential to consider the change in the rock's mechanical and physical properties if thermally induced fracturing is implemented, as the modeling and design of the method are profoundly affected by the change in rock properties.

Previous Studies

Applying a sudden thermal gradient can induce thermal stress in reservoir rock and open cracks in the formation. Rock as other material will experience a volumetric strain as a result of heating/cooling, Fig. 1. Several studies were performed to evaluate the effect of thermal treatment in rock properties. An essential step before applying thermally induced fracturing is to study the effect of heat on basic rock mechanical properties.

Usually, the temperature effect is ignored in the analysis of hydraulic fracturing, but if the induced thermal gradient is large, then this effect has to be considered with respect to the mechanical and physical properties. The constitutive equations governing the thermal effect in elastic material can be represented in the following form:

$$\sigma = E\alpha (T - T_0) \quad 1$$

where σ is the stress induced by a thermal gradient, α is the rock's linear thermal expansion coefficient, E is Young's modulus, T is the new temperature, and T_0 is the reference temperature.

The heat flow in the rock is governed by Fourier's law, which relates the heat flux to the rock's thermal conductivity as follows:

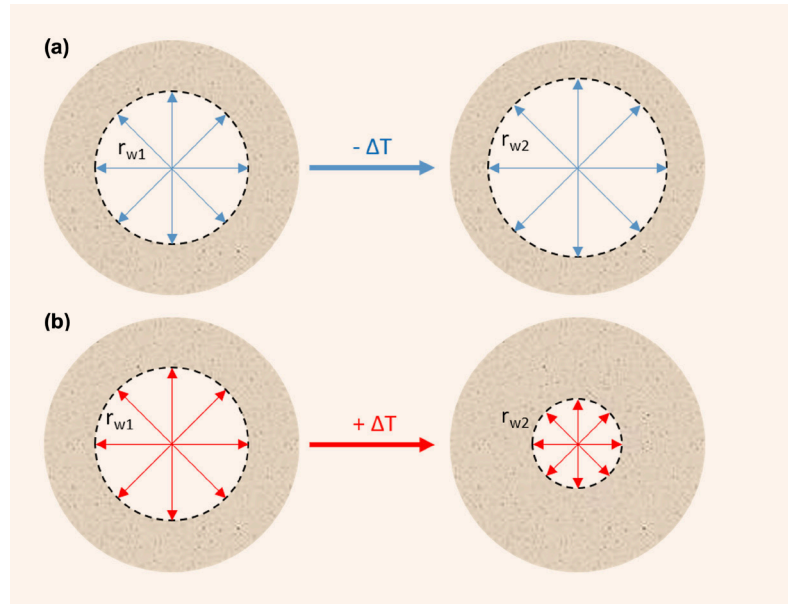
$$q_T = k_T \nabla T \quad 2$$

where q_T is the heat flux, k_T is the thermal conductivity, and ∇T is the thermal gradient.

The heat front propagates in the reservoir rock based on thermal diffusivity and permeability. If the rock has high permeability, then heat transport is mainly controlled by convection, and if the rock permeability is low, then heat transfer is controlled by conduction.

Stephens and Voight (1982)² studied the conditions at which thermal stresses can induce fracturing. They concluded that rock with higher Young's modulus can experience higher thermal stresses. Thermal cracking in the laboratory was evaluated using both cooling and heating methods. In the experimental study, crack generation was observed due to the injection of liquid

Fig. 1 The contraction of rock around a wellbore due to cooling (a), and the expansion of rock around a wellbore, due to heating (b).



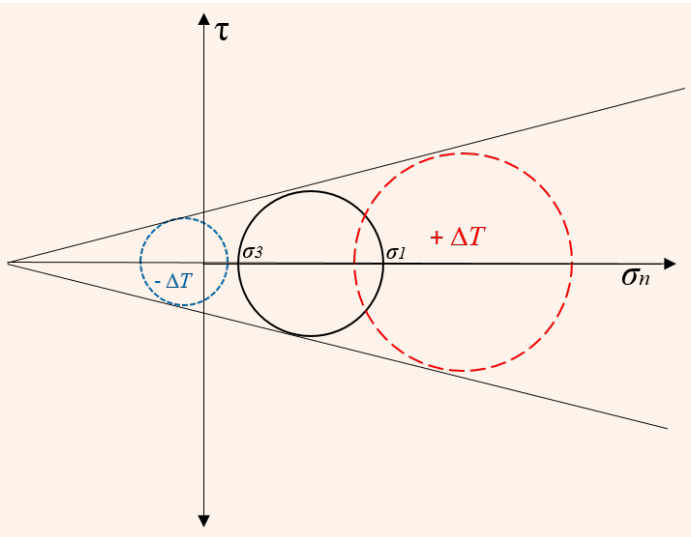
nitrogen, and it was shown that the surface heat transfer coefficient is the limiting factor for thermal cracking³.

Another experimental study carried out on a tight sandstone and shale using liquid nitrogen under a true triaxial test proved that thermal fracturing has a positive impact on permeability and it also decreases the fracturing initiation pressure by almost 65%⁴. The in situ state of stress in hydrocarbon and the geothermal reservoir is greatly influenced by thermal treatment. Cooling can decrease the in situ stresses, which facilitate fracture initiation and propagation. On the other hand, heating can heal or inhibit fracture propagation.

McDaniel et al. (1997)⁵ performs a simple experiment where rock samples were inserted in liquid nitrogen under atmospheric conditions. Extensive microfractures were generated as a result of rock contraction. The thermal effect on the principal stresses can be represented by Mohr-Coulomb failure criteria, Fig. 2. Moreover, heating and cooling can alter rock physical properties, i.e., porosity and permeability. Several studies have been conducted to investigate the impact of temperature in permeability. Contradicting results have been reported showing that permeability can increase/decrease or remain unchanged for thermal treatments up to 200 °C, where the heating was conducted at atmospheric pressure⁶.

The previously mentioned studies were undertaken under ambient conditions, which does not represent the actual reservoir condition of the rock, which leads to different inconsistent results. Experimental studies where heating was conducted under confinement conditions found that the permeability decreases by 0.5% per degree over the tested temperature range of 20 °C to 60 °C.

Fig. 2 The change in state of stress induced by temperature change. The blue circle shows that the temperature reduction causes the effective stress in reservoir rock to decrease, which might induce fractures. The red circle shows that an increase in temperature increases the effective stress in reservoir rock.



Like stress and pressure, the temperature has a significant effect on the measured geomechanical properties of rock, such as unconfined compressive strength (UCS), per Young's modulus and Poisson's ratio. Thermal treatment can also alter the elastic and mechanical properties of the rock. A nonuniform trend in strength properties was observed in sandstone after subjecting the rock specimen to a high temperature, up to 800 °C⁷. It was observed that the UCS and Young's modulus fluctuate below a critical temperature, from 500 °C to 600 °C. After this temperature range, a sharp decrease was observed indicating a shift from the elastic regime to the plastic region. Triaxial tests were conducted to investigate the effect of temperature on rock properties under simulated reservoir conditions as this setup allows for more realistic stress conditions⁸.

Sandstone core samples were taken from an oil reservoir in Brazil and loaded in the triaxial equipment. The samples were heated at 1.5 °C/min before applying confining and axial pressure. The study found that the Young's modulus decreased by 23% when the temperature is raised from 25 °C to 80 °C. Agar et al. (1987)⁹ characterized the strength of sandstone cores obtained from Athabasca oil sand at a temperature range from 20 °C to 200 °C.

A series of triaxial tests were conducted in the samples and it was observed that heating in particular increases the initial Young's modulus of the tested specimen. The sandstone samples from Flechtinger shows that heating can have permanent deformation in the rock, depending on the applied confining stress¹⁰. Tests performed at low confining pressure shows a decrease in bulk modulus, while the opposite trend was observed at high confining pressure. The author attributed this

response to the generation of microfractures.

In another study performed under triaxial test conditions, samples were subjected to a wide temperature range from 50 °C to 180 °C under different confining pressure from 60 psi to 1,190 psi. Arias Buitrago et al. (2016)¹¹ concluded that heating the samples at high confining pressure might decrease the porosity and Young's modulus of the rock. The reason behind this change is the alteration to rock structure after thermal heating. Several studies were performed where the specimen was heated to a very high temperature range under atmospheric conditions, and then loaded in the triaxial cell. Although the experimental procedure might not fully represent the actual reservoir simulation, useful information was extracted from those tests.

Yu et al. (2015)¹² conducted triaxial tests on sandstone samples at a very high temperature range from 25 °C to 800 °C, but the samples were heated in the furnace at ambient conditions. In this study, it was observed that Young's modulus of the tested samples increases from 25 °C to 200 °C, while after reaching that temperature, it was observed that Young's modulus started to decrease. The explanation given to the increase in rock stiffness was due to the closure of fractures and some pores, where at high temperatures, the samples started to degrade. Visual inspection of the samples reveals that the color of the sample has changed from gray to brownish red with an increase in temperature.

In a study conducted at a microscale level, Liu et al. (2019)¹³ reported that some of the minerals in sandstone start to decompose as a result of excessive heating after 500 °C, which eventually leads to the development of microcracks. Moreover, rocks are composed of different minerals, and the thermal expansion of those minerals is different, and that differential expansion during the heating process alters the rock structure.

Sengun (2014)¹⁴ studied the impact of temperature (105 °C to 600 °C) in the elastic properties of carbonate rocks. Based on the results, he concluded that the tensile strength, Young's modulus, and UCS decreases by an average of 50%, 40%, and 52%, respectively. The rapid thermal cooling impact on the mechanical properties of sandstone was also investigated by Kim et al. (2014)¹⁵. The specimens were heated first in a furnace until the target temperature is reached, followed by rapid cooling with a fan. The development of microfractures and crack healing was observed as a result of multiple thermal cycles. Rock with a coarse grain texture experienced a growth of cracks while fine-grained specimens undergo crack healing.

A study performed on granite to investigate the effect of thermal shock by water in multiple heated samples shows that stiffness of granite increase below a temperature of 200 °C, while no obvious change was observed between 200 °C to 500 °C¹⁶. The effect of the cooling rate on preheated sandstone was studied by Rathnaweera et al. (2018)¹⁷. The study shows that a high cooling rate reduces the elastic properties more than a low cooling rate.

This study collected a database of permeability,

Young’s modulus, and UCS values of sandstone from published data^{18–21}. The data were compiled based on similar experimental protocols and testing conditions to investigate the effect of thermal treatment on the previously mentioned properties.

In this work, the objective was to study the difference between the effect of heating and cooling in permeability, Young’s modulus, and UCS. In the reviewed publications, three main methods were followed to impose a thermal field on the tested sandstone samples. First, the samples were heated under atmospheric pressure where it was maintained at the target temperature for a certain period, and then, it was loaded in the testing cell. The second method, heating or heating/cooling, was performed under confinement conditions in the same equipment where the properties are measured. Third, heating and cooling of the specimen were performed under atmospheric conditions and loaded in the cell for testing of physical and mechanical properties. Figure 3 illustrates this methodology used on the third procedure.

The limitation in the first and third experimental procedure is that it does not simulate the real reservoir conditions, and therefore may lead to unreliable results; but it is still useful to gain the wide variation of the measured parameters with temperature.

Data Analysis

Permeability Variation

Permeability is one of the most important parameters in the geotechnical engineering application, and its variation with a thermal field has to be considered. Permeability is defined as the ability of the rock to transport fluid through the connect pores network. Data was collected from various temperature ranges and different conditions to understand the general permeability response to a temperature field. The values were normalized to obtain a fair comparison between data, as different rocks with different permeability were used. The normalized permeability is defined as:

$$k_n = k/k_j \tag{3}$$

where k_n is the normalized permeability, k is the permeability after thermal treatment, and k_j is the permeability at a reference temperature, which is usually taken at room temperature.

Figure 4 shows the change of permeability as a function of temperature for a heating rate and cooling rate of 2 °C per min and -3 °C per min, respectively, except for the N₂ cooling case where the heating rate was 6 °C per min. The same general direction is seen for sandstones cooled without confining pressure, Fig. 5. Each marker type indicates a different data source. All samples were cooled down at a similar cooling rate — 3 °C per minute.

The permeability of the sandstone shows up to a 100% increase in effective permeability below 400 °C. After that temperature, the permeability increases at a much higher rate. On the other hand, heating has a reverse effect when it is applied at a confining

Fig. 3 The methodology for the heating/cooling process under atmospheric conditions.

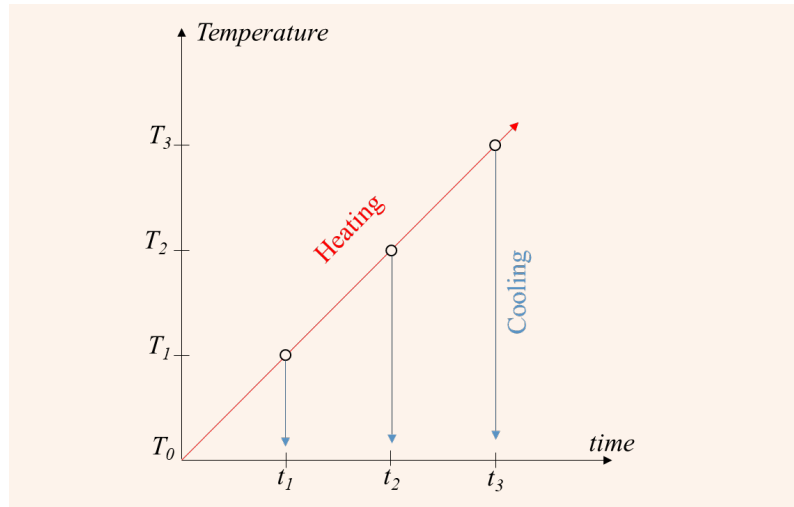
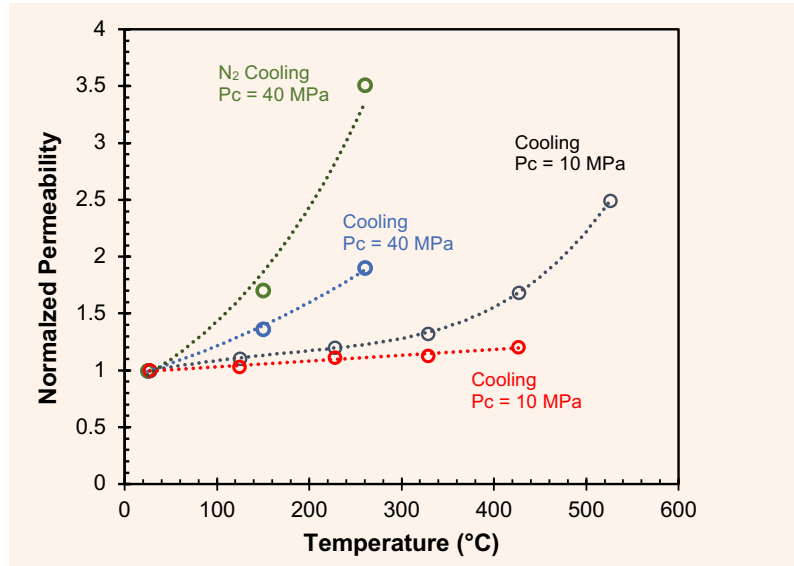


Fig. 4 The variation of normalized permeability vs. the temperature for samples subjected to different cooling rates. The heating and cooling was conducted at confining conditions.



pressure, Fig. 6. Although various studies show that permeability can increase with heating, that could be correct if heating is performed at ambient conditions, and the rock specimen is not constrained, which means it can expand freely.

The results in Fig. 6 shows that permeability decreases at a linear rate with thermal heating (3 °C per minute) below 250 °C. There is a clear distinction between the responses of sandstone to heating compared to cooling. That is an indication that the sandstones are a thermally sensitive medium. This thermal impact is mainly attributed to the geometry of the matrix and

Fig. 5 The variation of normalized permeability vs. the temperature for samples subjected to a similar cooling rate. The heating and cooling was performed at atmospheric conditions.

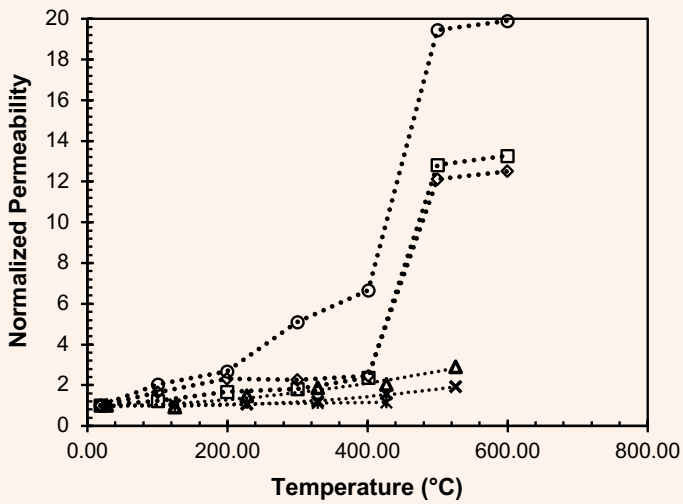
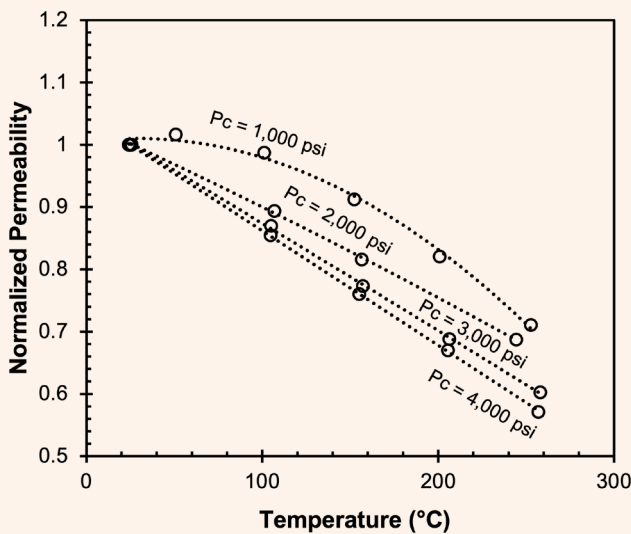


Fig. 6 The variation of normalized permeability vs. the temperature for samples subjected to similar heating rate. The heating was performed at confining conditions



the microcracks. Almost 50% decrease in permeability occurs at a 4,000 psi confining pressure. The alteration to permeability experienced by the sandstone was happening at a higher rate as the confining pressure increases.

Young's Modulus Variation

The elastic modulus of sandstones and other rock types is temperature dependent. Young's modulus represents the stiffness of solid material and its ability to undergo deformation. Data was collected from various temperature ranges and at different conditions

to understand the general Young's modulus response to a temperature field. The values were normalized to obtain a fair comparison between data, as different rocks with different stiffness were used. The normalized Young's modulus is defined as:

$$E_n = E/E_i \quad 4$$

where E_n is the normalized Young's modulus, E is Young's modulus after thermal treatment, and E_i is Young's modulus at a reference temperature, which is usually room temperature.

Thermal flux can change the elastic properties of the rock. When rock is exposed to a high temperature field, the change can be beyond just a volumetric strain and it can extend to chemical reaction and melting some of the present minerals in the rocks. Eventually, that can lead to an unexpected change in elastic properties because of the interaction of many processes at the microscale.

The normalized elastic modulus of the sandstone samples that were heated to a certain temperature and then cooled down either by air or water is presented in Fig. 7.

The stiffness of sandstone decreases at a small rate below 400 °C, after this temperature, the stiffness of sandstone decreases at a faster rate. The sandstone samples that were cooled down with water exhibits a smaller reduction in stiffness. On the other hand, it is difficult to predict the stiffness of sandstone when thermal heating only is imposed, Fig. 8.

As can be seen in Fig. 8, the stiffness fluctuates between rising and falling trends below a specific temperature range (400 °C to 500 °C). After that temperature, the stiffness of sandstone decreases. That turning point is different for the various sandstones presented. Three out of the four curves for the different sandstones presented shows an increase in the stiffness of the samples before the turning point, while one sample shows a

Fig. 7 The variation of normalized Young's modulus vs. the temperature for samples subjected to a similar heating rate and cooled down. The heating and cooling was performed at atmospheric conditions

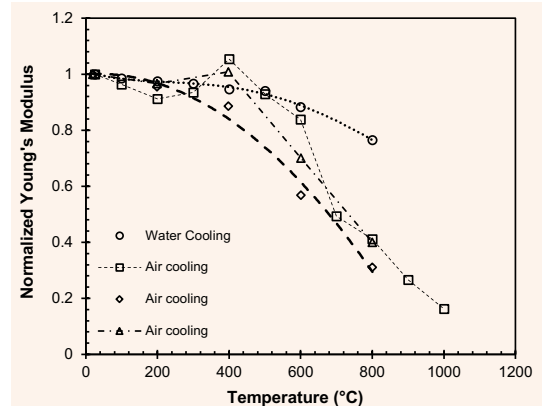
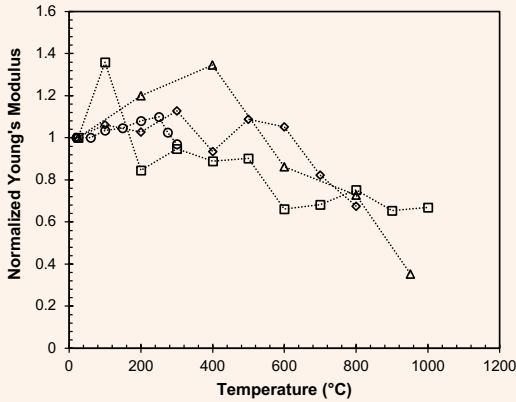


Fig. 8 The variation of normalized Young's modulus vs. the temperature for samples subjected to a similar heating rate. The heating was performed under atmospheric conditions.



fluctuating trend.

The change in elastic modulus is attributed to many reasons, such as the development of microcracks, and relative expansion of the grains. The variation of rock stiffness is case dependent and cannot be generalized for the same rock, as the pore network, mineral compositions, and the presence of cracks are not identical from one rock to another. As such, there is enormous heterogeneity among the same rock type, which makes it challenging to obtain a general trend for the elastic modulus. Specifically, when the thermal field is imposed into the rock under atmospheric conditions.

Variation of UCS

UCS is an important material property that reflects the strength of the rock when an axial load is applied to a cylindrical rock specimen. This property is widely used in various engineering applications. It is vital to estimate the change in UCS when exposed to the thermal field. Data was collected from various temperature ranges and at different conditions to understand the general strength response to a temperature field.

The values were normalized to obtain a fair comparison between data, as different sandstones with different strengths were used. The normalized UCS is defined as:

$$C_n = C/C_i \tag{5}$$

where C_n is the normalized UCS, C is the UCS after thermal treatment, and C_i is the UCS at a reference temperature, which is usually room temperature.

The UCS values for sandstones presented here were obtained from a static loading UCS test where the samples were thermally treated before testing. The impact of a thermal field into the rock strength is tricky, Fig. 9.

In general, there is a decreasing trend of the strength of the sandstone when exposed to a thermal field and cooled down. That decrease is even clearer after

reaching a critical temperature, which ranges from 300 °C to 400 °C for the selected sandstones.

In the presented data (Fig. 9), the curve with a circular marker shows a different trend compared to other tests. The strength of the samples increases until the critical temperature of 400 °C, after which the samples lose 50% of the original strength. On the other hand, the remaining sandstones almost reveal a similar decreasing trend. There was no significant difference in the effect of the cooling rate on sandstone. As can be seen in Fig. 9, the sandstone that was cooled with water almost shows a similar rate of change compared to other samples that were air cooled.

Figure 10 shows the evolution of the sandstone's strength, subjected to heating. It appears that heating is hardening the sandstone as the trend of strength reveals an increase in the UCS, up to a certain temperature threshold. There is a minor change in the strength of sandstone represented by the gray curve sample. As in previous geomechanical properties, there is a threshold temperature at which the strength of sandstone decreases. The presented data for the UCS data suggests that heating might increase the strength of the sandstone.

Discussion

The presented data for the sandstone shows a significant variation with temperature. There is a clear distinction between the effect of heating and cooling in the permeability, UCS, and Young's modulus. The thermal alteration of sandstone strongly depends on the experimental procedure conducted to measure the specific property.

The permeability increases when sandstone is cooled down. Furthermore, a higher cooling rate with nitrogen

Fig. 9 The variation of normalized UCS vs. the temperature for samples subjected to a similar heating rate and then cooled down. The heating and cooling was performed at atmospheric conditions.

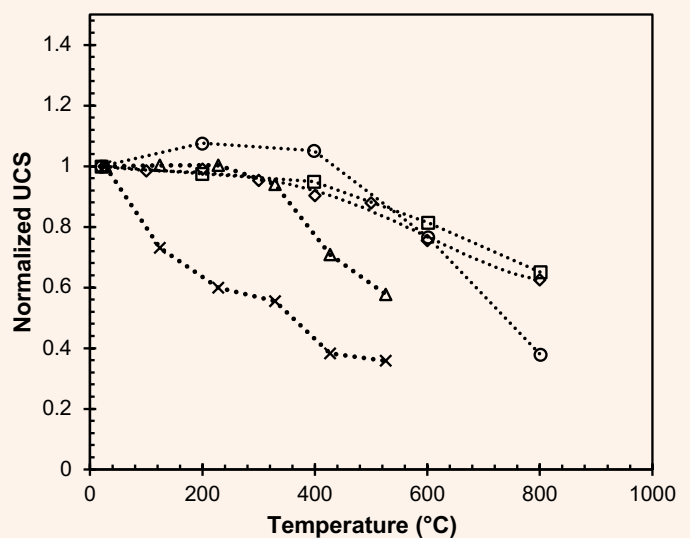
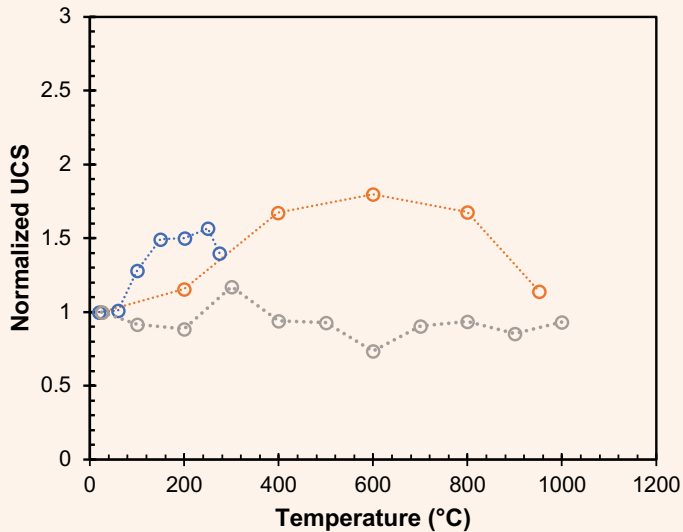


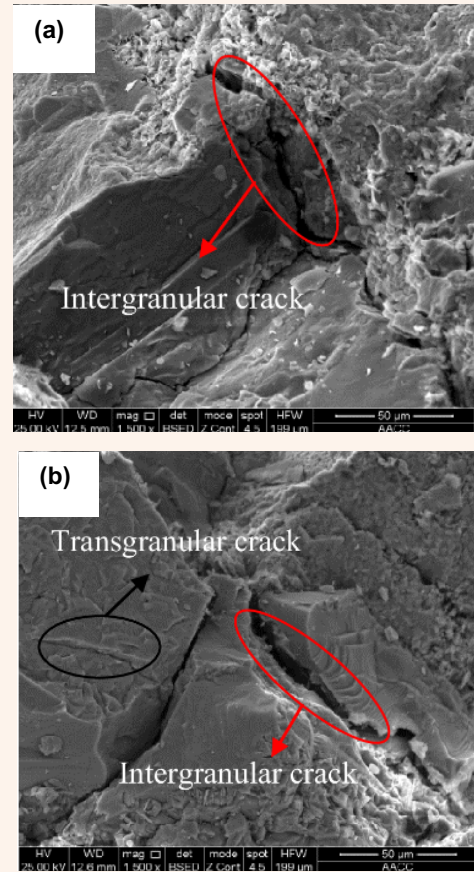
Fig. 10 The variation of normalized UCS vs. the temperature for samples subjected to a similar heating rate. The heating was performed at atmospheric conditions. The three colors correspond to different data sources.



shows more improvement in permeability. Heating sandstone under confinement pressure reduces the permeability of the sandstone. In terms of mechanical properties, the prediction of thermal is more challenging, especially since the thermal treatment in all the experiments reported in the literature reviewed were performed at atmospheric conditions. In general, the stiffness and strength of sandstone decrease when a cooling thermal gradient is applied, while the unclear trend is observed when the measurement was taken after imposing a heating thermal gradient.

A possible reason for the thermal effect on sandstone is the development of microcracks. The scanning electron microscope (SEM) image, Fig. 11, shows the development of a microcrack on sandstone. The sandstone was heated first to the target temperature and then subjected to thermal shock by water; however, it is not clear whether this crack is a result of heating or the imposed thermal shock. The other reason is the different thermal expansion and thermal properties

Fig. 11 The SEM image of the sandstone that was subjected to (a) 500 °C, and (b) 800 °C, and then cooled down with water²².



of minerals composing sandstone, Table 1.

It can be seen that the thermal properties are different for the minerals, which affect the heat flow and how different minerals react to a thermal field. The other important factor affecting the response of sandstone to a thermal field is the experimental protocol. Most of the data used in this study were obtained from sandstone that was subjected to thermal treatment under atmospheric conditions.

Table 1 The typical thermal properties of sandstone constituting minerals²³.

Mineral	Linear Thermal Expansion Coefficient (1/K)	Thermal Conductivity (W/m K)	Specific Heat Capacity (kJ/kg K)
Quartz	18×10^{-5}	6.5	0.72
Calcite	24×10^{-6}	3.6	0.8
Kaolinite	18.6×10^{-6}	2.6	0.93
Smectite	9×10^{-6}	1.9	0.93

Subsequently, it is challenging to control the thermal treatment under confining pressure either due to the equipment limitation or minimizing the heat loss during the experiment.

Conclusions

An extensive review was conducted to understand the response of sandstone to a thermal field. This article studied the differences between the effect of heating and cooling on sandstone permeability, UCS, and Young's modulus. The main conclusions drawn from this study are:

- There is an evident change in the sandstone's physical and mechanical properties when subjected to a thermal treatment.
- The sandstone's permeability decreases with heating and increases with cooling.
- High cooling with liquid nitrogen improves the permeability further compared to a low cooling rate.
- The stiffness of sandstone is greatly impacted by a thermal treatment, where cooling decreases the overall stiffness of sandstone. A similar trend was observed for the UCS.
- There was no clear trend in a variation of Young's modulus and UCS when subjected to heating.

Acknowledgments

This article was prepared for presentation at the International Geomechanics Symposium, al-Khobar, Kingdom of Saudi Arabia, October 30-November 2, 2023.

References

1. Palciauskas, V.V. and Domenico, P.A.: "Characterization of Drained and Undrained Response of Thermally Loaded Repository Rocks," *Water Resources Research*, Vol. 18, Issue 2, April 1982, pp. 281-290.
2. Stephens, G. and Voight, B.: "Hydraulic Fracturing Theory for Conditions of Thermal Stress," *International Journal of Rock Mechanics and Mining Sciences and Geomechanics Abstracts*, Vol. 19, Issue 6, December 1982, pp. 279-284.
3. Finnie, I., Cooper, G.A. and Berlie, J.: "Fracture Propagation in Rock by Transient Cooling," *International Journal of Rock Mechanics and Mining Sciences & Geomechanics Abstracts*, Vol. 16, Issue 1, February 1979, pp. 11-21.
4. Alqahtani, N.B.: "Experimental Study and Finite Element Modeling of Cryogenic Fracturing in Unconventional Reservoirs," Ph.D. thesis, Colorado School of Mines, Golden, Colorado, 2015, 264 p.
5. McDaniel, B.W., Grundmann, S.R., Kendrick, W.D., Wilson, D.R., et al.: "Field Applications of Cryogenic Nitrogen as a Hydraulic Fracturing Fluid," SPE paper 38623, presented at the SPE Annual Technical Conference and Exhibition, San Antonio, Texas, October 5-8, 1997.
6. You, L.J. and Kang, Y.L.: "Effects of Thermal Treatment on Physical Property of Tight Rocks," *Progress in Geophysics*, Vol. 24, 2009, pp. 1850-1854.
7. Zhang, L.-Y., Mao, X.-B. and Lu, A.-H.: "Experimental Study on the Mechanical Properties of Rocks at High Temperature," *Science in China Series E: Technological Sciences*, Vol. 52, 2009, pp. 641-646.
8. Araújo, R.G.S., Sousa, J.L.A.O. and Bloch, M.: "Experimental Investigation on the Influence of Temperature on the Mechanical Properties of Reservoir Rocks," *International Journal of Rock Mechanics and Mining Sciences*, Vol. 34, Issues 3-4, April-June 1997, pp. 298.e1-298.e16.
9. Agar, J.G., Morgenstern, N.R. and Scott, J.D.: "Shear Strength and Stress-Strain Behavior of Athabasca Oil Sand at Elevated Temperatures and Pressures," *Canadian Geotechnical Journal*, Vol 24, Issue 1, February 1987, pp. 1-10.
10. Hassanzadegan, A., Blöcher, G., Milsch, H., Urpi, L., et al.: "The Effects of Temperature and Pressure on the Porosity Evolution of Flechtinger Sandstone," *Rock Mechanics and Rock Engineering*, Vol. 47, 2014, pp. 421-454.
11. Arias Buitrago, J.A., Alzate-Espinosa, G.A., Arbelaez-Londono, A., Morales, C.B., et al.: "Influence of Confining Stress in Petrophysical Properties Changes during Thermal Recovery in Silty Sands Colombia," SPE paper 181197, presented at the SPE Latin America and Caribbean Heavy and Extra Heavy Oil Conference, Lima, Peru, October 19-20, 2016.
12. Yu, J., Chen, S.-J., Chen, X., Zhang, Y.-Z., et al.: "Experimental Investigation on Mechanical Properties and Permeability Evolution of Red Sandstone after Heat Treatments," *Journal of Zhejiang University — Science A: Applied Physics and Engineering*, Vol. 16, Issue 9, September 2015, pp. 749-759.
13. Liu, Q., Qian, Z. and Wu, Z.: "Micro/Macro Physical and Mechanical Variation of Red Sandstone Subjected to Cyclic Heating and Cooling: An Experimental Study," *Bulletin of Engineering Geology and the Environment*, Vol. 78, 2019, pp. 1485-1499.
14. Sengun, N.: "Influence of Thermal Damage on the Physical and Mechanical Properties of Carbonate Rocks," *Arabian Journal of Geosciences*, Vol. 7, 2014, pp. 5543-5551.
15. Kim, K., Kemeny, J. and Nickerson, M.: "Effect of Rapid Thermal Cooling on Mechanical Rock Properties," *Rock Mechanics and Rock Engineering*, Vol. 47, 2014, pp. 2005-2019.
16. Zhang, F., Zhao, J., Hu, D., Skoczylas, F., et al.: "Laboratory Investigation on Physical and Mechanical Properties of Granite after Heating and Water-Cooling Treatment," *Rock Mechanics and Rock Engineering*, Vol. 51, 2018, pp. 677-694.
17. Rathnaweera, T.D., Ranjith, P.G., Gu, X., Perera, M.S.A., et al.: "Experimental Investigation of Thermo-mechanical Behavior of Clay-Rich Sandstone at Extreme Temperatures Followed by Cooling Treatments," *International Journal of Rock Mechanics and Mining Sciences*, Vol. 107, July 2018, pp. 208-225.
18. Greenberg, D.B., Cresap, R.S. and Malone, T.A.: "Intrinsic Permeability of Hydrological Porous Mediums: Variation with Temperature," *Water Resources Research*, Vol. 4, Issue 4, August 1968, pp. 791-800.
19. Rao, Q.-H., Wang, Z., Xie, H.-F. and Xie, Q.: "Experimental Study of Mechanical Properties of Sandstone at High Temperature," *Journal of Central South University of Technology*, Vol. 14, February 2007, pp. 478-485.
20. Sirdesai, N.N., Mahanta, B., Ranjith, P.G. and Singh, T.N.: "Effects of Thermal Treatment on Physico-Morphological Properties of Indian Fine-Grained Sandstone," *Bulletin of Engineering Geology and the Environment*, Vol. 78, 2019, pp. 885-897.

21. Somerton, W.H., Mehta, M.M. and Dean, G.W.:
“Thermal Alteration of Sandstones,” *Journal of Petroleum Technology*, Vol. 17, Issue 5, May 1965, pp. 589-595.
22. Han, G., Jing, H., Su, H., Liu, R., et al.: “Effects of Thermal Shock due to Rapid Cooling on the Mechanical Properties of Sandstone,” *Environmental Earth Sciences*, Vol. 78, Issue 3, February 2019.
25. Clark Jr., S.P.: *Handbook of Physical Constants*, Geological Society of America, 1966, 587 p.

About the Authors

Qasim A. Sahu

M.S. in Energy Resources and Petroleum Engineering, King Fahd University of Petroleum and Minerals

Qasim A. Sahu is a Petroleum Engineer working with the Production Technology Division of Saudi Aramco's Exploration and Petroleum Engineering Center – Advanced Research Center (EXPEC ARC). Since joining Saudi Aramco in 2013, he has worked in a portfolio of projects leading the development of new technologies in hydraulic fracturing and carbonate stimulation. In less than 8 years, Qasim played a critical role in delivering and implementing sustainable cost-effective solutions to boost the gas production where circular water economy and water sustainability is at heart of those technologies.

He developed and implemented novel engineered acidizing technology that improves operational efficiency, increases stimulation effectiveness, and overcomes pressing field challenges.

Qasim has authored and coauthored more than 15 publications, including peer-reviewed journals, conference papers, granted patent,

and invention disclosures. He and his team were shortlisted as a finalist for the Best Oil Field Chemical Award in the 2020 World Oil awards. Also, Qasim received the Saudi Aramco Vice President award in 2015 as a distinguished Society of Petroleum Engineers (SPE) member. He has represented the company in numerous regional and international events promoting knowledge sharing and knowledge transfer across the industry.

Qasim is a member of the SPE and the European Association of Geologists and Engineers (EAGE).

He received his B.S. degree (with first honors) in Petroleum Engineering from King Fahd University of Petroleum and Minerals (KFUPM), Dhahran, Saudi Arabia. Qasim received his M.S. degree in Energy Resources and Petroleum Engineering from King Abdullah University of Science and Technology (KAUST), Thuwal, Saudi Arabia.

Ayman R. Al-Nakhli

M.S. in Entrepreneurship for New Business Development, Open University Malaysia

Ayman R. Al-Nakhli is a Petroleum Scientist in Saudi Aramco's Exploration and Petroleum Engineering Center – Advanced Research Center (EXPEC ARC), where he leads the research program on thermochemicals and develops technologies related to conventional and unconventional reservoirs such as pulse fracturing, stimulation, diverting agents, and heavy oil.

Ayman has developed and field deployed several novel technologies, with four of them being commercialized with international service

companies. He received the World Oil Award for Best Production Chemical in 2015.

Ayman has filed more than 20 patents, published 35 journal papers, and 40 conference papers.

He received his B.S. degree in Industrial Chemistry from King Fahd University of Petroleum and Minerals (KFUPM), Dhahran, Saudi Arabia, and an M.S. degree in Entrepreneurship for New Business Development from Open University Malaysia, Bahrain.

Dr. Rajendra A. Kalgaonkar

Ph.D. in Polymer Chemistry and Nanotechnology, University of Pune

Dr. Rajendra A. Kalgaonkar is a Petroleum Scientist in the Productivity Enhancement Focus Area of the Production Technology Team at Saudi Aramco's Exploration and Petroleum Engineering Center – Advanced Research Center (EXPEC ARC). He has over 19 years of experience in Research and Development, out of which he spent 11 years in the upstream oil and gas industry.

Prior to joining Saudi Aramco in May 2015, Rajendra worked as a Technology Leader with Halliburton. He has rich experience in areas of nanotechnology; polymer blends and composites while being associated with the National Chemical Laboratory, India, and the University of Western Sydney, Australia.

Rajendra's research is focused on developing new fluids technologies for enhancing

hydrocarbon production, including fracturing, sand control, conformance control and acidizing. He has successfully developed new chemistries based on nanomaterials for enhancing hydrocarbon production as well as for drilling fluids.

Rajendra has published 25 patents and patent applications, and 35 peer-reviewed articles, invited book chapters and conference proceedings. He has delivered presentations at Society of Petroleum Engineers (SPE) key advanced technology workshops and forums.

Rajendra received his B.S. degree in Chemistry, an M.S. degree in Polymer Science, and his Ph.D. degree in Polymer Chemistry and Nanotechnology, all from the University of Pune, Pune, India.

Another Record Year for Patents

Michael Ives

In 2022, Aramco was granted 966 patents — the company’s highest number ever.

This success reflects our track record of innovation and technology development and is clear evidence of our commitment to innovating across our value chain, and leveraging our investment in the 12 R&D centers we run across the globe.

In an era where an energy transition is underway, a significant driver of our investment in innovation is ensuring we retain our position as one of the lowest carbon and energy intensive producers among the major oil companies. In addition, we are working to help our customers and consumers to secure their own aspirations for a lower carbon future.

Fundamentally, as reflected in our high patent numbers, Aramco is leveraging technology and innovation toward a low carbon future and driving sustainable energy solutions across our business and the industries we supply. We are innovating toward more sustainable solutions to help drive our positive impact on society and boost the quality of life for future generations — and ensure the efficiency of our own business.

While patents are a leading indicator of innovation, the ultimate goal is to create value through the development of solutions that help to address a particular need. Such results are often only possible with significant upfront investments, and patents make it possible to recoup these costs and potentially generate additional revenue through commercialization.

A stable energy transition driven by innovation

Through our extensive R&D, we are investing in the technology needed for a stable energy transition that utilizes all sources of energy to meet the world’s growing energy demand while reducing greenhouse gas emissions. Our focus is on leading in low carbon intensity energy production and supporting the development of nonfuel applications for crude oil, targeting the highest impact solutions across our value chain. The challenge is to develop and deploy technology solutions at speed and scale, to provide the benefits of oil and gas for future generations, while minimizing emissions. This is where our investment in research truly comes to the fore.

Overall, we remain focused on leading in low carbon intensity and abatement technologies and supporting

the development of nonfuel applications for crude oil, while we continue to invest in the ability to meet the world’s need for energy sourced from hydrocarbons. With innovation and technology, we seek to reduce our energy and carbon footprint and enhance our operations, from well to wheel — and beyond.

2022 Patent/IP Achievements

1. Ranked 31st in the top 50 U.S. patent assignees and first among oil and gas companies by ifi Claims.
2. Ranked in the top 100 Global Innovators by Clarivate.
3. Ranked in the Global Top 100 Innovation Momentum by LexisNexis.
4. Ranked in Top 50 Most Innovative Companies by BCG.

Table 1 Saudi Aramco’s granted U.S. patents from 2017 to 2022.

Saudi Aramco’s U.S. Granted Patents	2017	2018	2019	2020	2021	2022
	261	338	527	683	864	966

Have an article you would like to publish? Here are our guidelines.

These guidelines are designed to simplify and help standardize submissions. They need not be followed rigorously. If you have any questions, please call us.

Length

Average of 2,500-4,000 words, plus illustrations/photos and captions. Maximum length should be 5,000 words. Articles in excess will be shortened.

What to send

Send text in Microsoft Word format via email. Illustrations/photos should be clear and sharp. Editable files are requested for graphs, i.e., editable in Excel.

Procedure

Notification of acceptance is usually within three weeks after the submission deadline. The article will be edited for style and clarity and returned to the author for review. All articles are subject to the company's normal review. No paper can be published without a signature at the manager level or above.

Format

No single article need include all of the following parts. The type of article and subject covered will determine which parts to include.

Working Title

Lorem Ipsum here.

Abstract

Usually 150-300 words to summarize the main points.

Introduction

Different from the abstract in that it sets the stage for the content of the article, rather than telling the reader what it is about.

Main body

May incorporate subtitles, artwork, photos, etc.

Conclusion/Summary

Assessment of results or restatement of points in introduction.

Endnotes/References/Bibliography

Use only when essential. Use author/date citation method in the main body. Numbered footnotes or endnotes will be converted. Include complete publication information. Standard is *The Associated Press Stylebook*, 52nd ed. and *Webster's New World College Dictionary*, 5th ed.

Acknowledgments

Use to thank those who helped make the article possible.

Illustration/Tables/Photos and explanatory text

If the files are large, these can be submitted separately, due to email size limits. Initial submission may include copies of originals; however, publication will require the originals. When possible, submit original images. Color is preferable.

File Format

Illustration files with .EPS extensions work best. Other acceptable extensions are .TIFF/.JPEG/.PICT.

Permission(s) to reprint, if appropriate

Previously published articles are acceptable but can be published only with written permission from the copyright holder.

Author(s)/Contributor(s)

Please include a brief biographical statement.

Submission/Acceptance Procedures

Papers are submitted on a competitive basis and are evaluated by an editorial review board comprised of various department managers and subject matter experts. Following initial selection, authors whose papers have been accepted for publication will be notified by email.

Papers submitted for a particular issue but not accepted for that issue may be carried forward as submissions for subsequent issues, unless the author specifically requests in writing that there be no further consideration.

Submit articles to:

Editor

The Saudi Aramco Journal of Technology

C-10B, Room AN-1080

North Admin Building #175

Dhahran 31311, Saudi Arabia

Tel: +966-013-876-0498

Email: william.bradshaw.1@aramco.com.sa

Submission deadlines

Issue	Paper submission deadline	Release date
Winter 2023	August 3, 2023	December 31, 2023
Spring 2024	November 5, 2023	March 31, 2024
Summer 2024	February 11, 2024	June 30, 2024
Fall 2024	May 22, 2024	September 30, 2024

There is more.

Expandable Resin for Countering Severe Loss of Circulation

Dr. Vikrant B. Wagle, Dr. Jothibas Ramasamy, Khawlah A. Alanqari and Dr. Abdullah S. Al-Yami

Abstract / One of the main reasons why loss of circulation is difficult to remedy is the lack of knowledge about accurate fracture width and depth encountered while drilling, leading to an improper selection of suitable plugging materials that can adapt — in both volume and shape — to effectively plug a wide range of fractures with unknown dimensions.

Mixed Preformed Particle Gel System for Water Shutoff in Fractured Carbonate Reservoir

Dongqing Cao, Dr. Ayman M. Almohsin, Dr. Ming Han and Dr. Bader G. Alharbi

Abstract / Water shutoff from a production well using particle type material is a great challenge, due to the complex pressure and flow distributions near the wellbore. A mixed preformed particle gel (ppg) system was developed to enhance the performance for water shutoff in fractured carbonate reservoirs. The ppg blocking behaviors in fractures and methods to improve the water flush tolerance were investigated. Effects of the ppg strength dominated the water shutoff performances in the fractures.

A Method for EUR Forecasting in Unconventional Reservoirs Using Early Flow Back Data

Ihab S. Mahmoud and Nouf M. Alsulaiman

Abstract / Evaluating the estimated ultimate recovery (EUR) and production forecasting in multi-fractured horizontal wells completed in unconventional shale reservoirs during early exploration and appraisal stages is very challenging. With the absence of suitable production facilities to handle produced fluids, production data are limited to short flow backs and extended production for some key wells to the early production facility.

Calcium Sulfate Risk Assessment throughout the Injection and Production System

Dr. Tao Chen, Dr. Qiwei Wang, Faisal A. Alrasheed and Norah A. Aljeaban

Abstract / The formation of calcium sulfate (CaSO_4) mineral scale is a persistent flow assurance problem in the oil and gas industry. To establish an effective mitigation strategy, it is essential to understand the scaling potential and severity at different production units. In this work, the CaSO_4 scaling risk is assessed for the entire production system, all along the seawater injection unit, production well, surface flow line, separator, and disposal well.



Aramco
Journal
of Technology

Liked this issue? Sign up. It's free.

To begin receiving the *Aramco Journal of Technology* please complete this form, scan and send by email to william.bradshaw.1@aramco.com.

Got questions?

Just give us a call at +966-013-876-0498 and we'll be happy to help!



Scan the QR code to go straight to your email and attach the form!

Subscription Form

